


2019

Chemical Vapor Deposition Growth of Large Area 2D MoS₂ Layers: Layer Orientation Control, Heterostructure Integration, And Applications for Stretchable Sensors.

Md. Ashraful Islam
University of Central Florida

 Part of the [Electrical and Computer Engineering Commons](#)
Find similar works at: <https://stars.library.ucf.edu/etd>
University of Central Florida Libraries <http://library.ucf.edu>

This Doctoral Dissertation (Open Access) is brought to you for free and open access by STARS. It has been accepted for inclusion in Electronic Theses and Dissertations by an authorized administrator of STARS. For more information, please contact STARS@ucf.edu.

STARS Citation

Islam, Md. Ashraful, "Chemical Vapor Deposition Growth of Large Area 2D MoS₂ Layers: Layer Orientation Control, Heterostructure Integration, And Applications for Stretchable Sensors." (2019). *Electronic Theses and Dissertations*. 6780.
<https://stars.library.ucf.edu/etd/6780>



CHEMICAL VAPOR DEPOSITION GROWTH OF LARGE AREA 2D MoS₂ LAYERS:
LAYER ORIENTATION CONTROL, HETEROSTRUCTURE INTEGRATION, AND
APPLICATIONS FOR STRETCHABLE SENSORS

by

MD ASHRAFUL ISLAM

M.Eng., University of Tulsa, Oklahoma, 2015

B.S. and MS Islamic University, Kushtia, Bangladesh, 2006 & 2008

A dissertation submitted in partial fulfillment of the requirements
for the degree of Doctor of Philosophy
in the Department of Electrical and Computer Engineering
in the College of Engineering and Computer Science
at the University of Central Florida
Orlando, Florida

Fall Term
2019

Major Professor: Yeonwoong Jung

© 2019 Md Ashraful Islam

ABSTRACT

Two-dimensional (2D)-layered MoS₂ layers have exhibited a broad set of unusual and superior material properties unattainable in any traditional bulk materials, drawing significant research interests nowadays. For instance, they present excellent semiconducting properties accompanying high carrier mobility and large current ON/OFF ratio as well as extensive in-plane strain limit and thickness, projecting high suitability for emerging flexible and stretchable electronics. Such properties and applications strongly depend on the physical orientation and chemical composition of constituent 2D layers. 2D MoS₂ layers chemically grown in two distinct orientations, e.g., horizontal alignment for electronics and optoelectronics, and vertical alignment for electrochemical and sensing applications. Moreover, 2D heterostructure layers composed of vertically stacked dissimilar 2D TMDs held via weak van der Waals (vdW) attractions offer unique 2D/2D interfaces, envisioned to display exotic material properties, unattainable in their monocomponent counterparts. However, the underlying principle of their layer orientation-controlled growth and integrations are not well suited for scalable production, leaving their projected technological opportunities far from being realized for various novel applications. Herein, I study various aspects of 2D MoS₂ layers that were studied from their large-area layer-orientation controlled growth and heterostructures integration to applications in stretchable electronic devices. I developed a chemical vapor deposition (CVD) synthesis, which can grow large-area ($> \text{cm}^2$) 2D MoS₂ layers in a layer-controlled manner and investigated their underlying growth mechanism. I then developed a viable transfer approach of the as-grown 2D layers and integrated them into secondary target substrates to realize a new type of 2D MoS₂-layers based heterostructures. To further extend their layer-controlled CVD growth and integration approach, a

high-performance stretchable 2D MoS₂-based electrical sensors were demonstrated on the elastomeric substrates with unconventional structural layouts. This study paves the way to explore this emerging atomically-thin material in realizing a wide range of unusual device and technologies which have been foreseen to be impossible otherwise.

To my family

ACKNOWLEDGMENTS

First and foremost, I would like to thank my advisor Professor Yeonwoong (Eric) Jung, for the continuous guidance, support, and encouragement throughout my research. I am indebted to his constructive criticism and strong professionalism, which helped me to become a competent researcher in the field of study. I could not have imagined having a better advisor and mentor for my doctoral research.

My sincere thanks go to Professor Kalpathy Sundaram, for collaborating and supporting me with the Teaching Assistantship opportunities. I am also thankful to Professor Parveen Wahid to allow me to teach courses at UCF.

I want to thank my fellow lab mates in the Jung Research Group, Dr. Nitin Chowdhary, Dylan, Anthonny, Luis, Dr. Jung Han Kim, Dr. Tae Jun Ko, Emmanuel, Mashiyat, Kaium, and Sang-Sab. My sincere thanks also go to our collaborator, Professor Woo Hyoung Lee, Professor Hee-Suk Chung, Professor Lei Zhai, and Professor Tania Roy for the stimulating discussions we have had in the last few years and support for various characterizations, including TEM, SEM, electrical measurements, and water contact angle measurements.

Last but not least, I would like to thank my parents, Jebunnahar and Md Iqbal Hossain, and my former mentor Late. Professor Zahid Hasan Mahmood. I am especially thankful to my lovely wife, Sajia, and our son Adyan who always encouraged me throughout my Ph.D. work over the last few years.

TABLE OF CONTENTS

LIST OF FIGURES	x
LIST OF ACRONYMS (or) ABBREVIATIONS	xvii
CHAPTER-1: INTRODUCTION.....	1
1.1 Motivation and Background.....	1
1.2 Thesis Statement and Organization.....	7
CHAPTER-2: THEORETICAL BACKGROUND	10
2.1 Crystal Structure of 2D MoS ₂	10
2.2 Properties of 2D MoS ₂	11
2.2.1 Electronic and Optical Properties of 2D MoS ₂	11
2.2.2 Mechanical Properties	14
2.2.3 Chemical and Sensing Properties	14
2.3 Synthesis Methods of 2D MoS ₂	15
2.3.1 Mechanical Exfoliation Method	15
2.3.2 Liquid Exfoliation Method	16
2.3.3 Chemical Vapor Deposition Method	17
CHAPTER-3: EXPERIMENTAL DETAILS.....	20
3.1 Experimental Methods for the Layer Orientation Control Growth.....	20
3.1.1 Fabrication of WO ₃ nanowires	20
3.1.2 Growth of 2D MoS ₂ /WS ₂ Vertical Stacks	20
3.1.3 TEM Characterizations	21
3.2 Experimental Methods for the Heterostructure Integration	22
3.2.1 CVD Growth.....	22
3.2.2 Lift-off and Transfer	22
3.2.3 Raman and TEM Characterizations.....	23
3.2.4 Electrical and Photoresponse Characterizations.....	23
3.3 Experimental Methods for the Flexible Humidity Sensor	24
3.3.1 Growth of 2D MoS ₂ With Vertically-aligned Layers.....	24
3.3.2 2D Layer Transfer and Integration	25
3.3.3 Raman, SEM, TEM, and Optical Characterization	25

3.3.4 Humidity Sensing Characterization	25
3.3.5 DFT Calculation	26
3.4 Experimental Methods for the Stretchable Gas Sensing	26
3.4.1 Growth of 2D MoS ₂ With Vertically-aligned Layers	26
3.4.2 Transfer and Integration Process	27
3.4.3 Raman, TEM, and Optical Characterization	27
3.4.4 Gas Sensing Characterization	27
CHAPTER-4: LAYER ORIENTATION CONTROL GROWTH	29
4.1 Introduction	29
4.2 Results and Discussions	31
4.2.1 Steps in Growth Process	31
4.2.2 Morphology of the as Grown 2DWS ₂ /WO ₃ Nanowires	32
4.2.3 Morphology of the MOS ₂ /WS ₂ Heterostructure	33
4.2.4 Growth Mechanism	35
4.3 Conclusion	39
CHAPTER-5: HETEROSTRUCTURES INTEGRATION	40
5.1 Introduction	40
5.2 Results and Discussions	41
5.2.1 Growth and Gold Assisted Transfer Approach	42
5.2.2 Morphology of the as-grown 2D MOS ₂ /WS ₂ heterostructures	43
5.2.3 Structural and Electrical Characterizations	45
5.2.4 Feasibility of Gold (Au) as a Growth Substrate	48
5.2.5 Flexible MoS ₂ /CNT Device Integration	50
5.3 Conclusions	54
CHAPTER-6: VERTICALLY-ALINGED 2D MoS ₂ FOR HUMIDITY SENSING	55
6.1 Introduction	55
6.2 Results and Discussions	57
6.2.1 Growth and Water Assisted Transfer Process	57
6.2.2 Morphology of the as-grown 2D MoS ₂	59
6.2.3 Structural and Optical Characterizations	60
6.2.4 Stretch-Tunable Mechanical Properties	64

6.2.5 Flexible Humidity Sensing Properties	64
6.3 Conclusions	68
CHAPTER-7: VERTICALLY-ALIGNED 2D MoS ₂ FOR GAS SENSOR.....	69
7.1 Introduction	69
7.2 Results and Discussions	71
7.2.1 Sensor Fabrication Steps	71
7.2.2 Chemical/Structural Morphology	73
7.2.3 Mechanically Stretchable Functionalities.....	75
7.2.4 Stretchable Gas Sensing	76
7.3 Conclusion.....	78
CHAPTER-8: SUMMARY AND FUTURE PERSPECTIVES.....	79
APPENDIX: COPYRIGHT PERMISSIONS.....	81
LIST OF REFERENCES	97

LIST OF FIGURES

Figure 1: Number of publications per year of various 2D materials from 2009 to 2019[Extracted from Web of Science. Available at: http://apps.webofknowledge.com [Accessed 19 Jul. 2019], searching keywords are Mxene, Black Phosphorus, and MoS ₂	1
Figure 2: Schematics representation for the concept of the horizontal and vertical growth of 2D TMDs. The horizontal layers; (a) Side-view, (b) projected-view, (c) High-resolution transmission electron microscopy (TEM) image. The vertical layers; (d) Side-view, (e) projected-view, (e) Top view of the high-resolution TEM image. Figure (c,e) adapted with permission from references[5,6].	2
Figure 3: (a-c) 2D TMDs heterostructures are analogous to Lego blocks. Here, different layered TMDs are considered as atomically thin Legos. The construction of a wide variety of layered structures becomes possible with this concept, adapted with permission from reference [13]. (d-e) Schematic representation of the layer orientation with (d)both horizontal and (e) horizontal to vertical heterostructure.	3
Figure 4: Schematics for the overview of chemical vapor deposition (CVD) grown 2D TMDs heterostructure displaying from single crystal and continuous films to device applications, adapted with permission from reference [2].	4
Figure 5: The periodic table of the elements, more than 80 members of the 2D TMDs compound exist by combining transition metal with the chalcogen atoms, adapted with permission from reference [3].	10
Figure 6: Schematics of the crystal structure of single-layer MoS ₂ (a) trigonal prismatic (b) and octahedral structure adapted from reference [45].	11

Figure 7: (a-b) The lattice structure of 2D MoS₂ in both the in-plane and out-of-plane directions. (c) A band diagram of bulk MoS₂, showing the lowest conduction band c_1 and the highest split valence bands v_1 and v_2 . A and B are the direct-gap transitions, and I is the indirect-gap transition where E'_g and E_g are the bandgap of the bulk and monolayer, adapted with permission from reference[48]. 12

Figure 8: The optical transition of at the K-point in the monolayer, bilayer, and bulk 2D MoS₂ layers, the A excitonic peak shift originated from the 1st exciton level. The reduction in the exciton levels offset with increasing valence band splitting energy; hence, the B-exciton peak did not change. Adapted with permission from reference [50]. 13

Figure 9: (a-b) The mechanical exfoliation of 2D MoS₂ layers with scotch tape; (a) Camera image. (b) Optical image of the single-layer MoS₂ transfer with random flakes with irregular shape and size. (c-d) Schematic representations of the of the liquid-mediated exfoliation process; () Adapted with permission from reference[63,64]. 15

Figure 10: An overview of the conventional 2D TMDs synthesis approaches, adapted with permission from reference [66]. 17

Figure 11: The metal seed layer-based one-step CVD growth process. (a) Schematic diagram of the CVD growth process. (b) A large-area growth process. (c) A patternable growth process. (d) A controllable layer thicknesses. Figure (b-d) adapted with permission from reference[12,68,69]. 18

Figure 12: A picture of the CVD furnace used to grow 2D MoS₂ and heterostructures in this study. 21

Figure 13: (a) Schematic for 2D MoS₂/WS₂ vdW vertical heterostructure growth experiments. (b) As fabricated 2D WS₂/WO₃ nanowires. (c) Low-magnification TEM image of an isolated nanowire. (d) Magnified view of the red box in (c). (e) ADF STEM image of a 2D WS₂/WO₃ interface. (f) ADF STEM image of a cross-sectioned nanowire. (g) Magnified view of the red box in (f), revealing a 2D WS₂/WO₃ interface. 31

Figure 14: (a) Raman spectroscopy profile obtained from 2D MoS₂/WS₂-grown nanowires. (b–e) TEM characterization of 2D MoS₂/WS₂ vdW vertical stacks obtained by sulfurizing ≈ 3 nm Mo. (b) ADF STEM image of an isolated nanowire. (c) Magnified view of the blue box in (b), revealing 2D MoS₂/WS₂ vertical stacks. (d) ADF STEM image of a 2D MoS₂/WS₂/WO₃ interface. (e) Detailed crystalline structure of the 2D MoS₂/WS₂ interface. (f–i) TEM characterization of 2D MoS₂/WS₂ vdW vertical heterostructures obtained by sulfurizing ≈ 12 nm Mo. (f) ADF STEM image of an isolated nanowire, revealing vertically reoriented 2D MoS₂ layers. (g) Top-down plane-view of high-resolution TEM (HRTEM) image revealing the edges of vertical 2D MoS₂ layers. (h,i) Redirection of horizontal 2D MoS₂ layer orientation interfered by impeaching layers. 34

Figure 15: Schematics for the initial growth stage of 2D MoS₂ layers on 2D WS₂ layers. (a) Mo nanoparticles exposing the S–S (Mo–WS₂ basal plane) interface, which provides preferred nucleation sites. (b) Growth of a 2D MoS₂ layer on the interface, exposing another S–S interface for subsequent layer-by-layer growth. Schematics for the distinguishable growth characteristics obtained by sulfurizing Mo of different thicknesses. (c) Layer-by-layer growth of horizontal 2D MoS₂ layers on 2D WS₂ layers achieved by sulfurizing thin Mo. The insets are representative ADF STEM (top) and TEM (bottom) images to show disconnected nanoparticles on the surface of a 2D WS₂/WO₃ nanowire in a top/side view, respectively. (d) SK-like growth of vertically reoriented 2D MoS₂ layers on 2D WS₂ layers, achieved by sulfurizing thick Mo. The inset is a representative TEM image to show the side view of a continuous Mo (≈ 9 nm thickness) on the surface of a 2D WS₂/WO₃ nanowire. 36

Figure 16: Illustration for the large-area growth of vertically stacked 2D MoS₂/WS₂ heterostructure layers on a SiO₂/Au-based substrate and their subsequent transfer and integration in two different ways..... 42

Figure 17: Morphology of the as-grown 2D MoS₂/WS₂. (a) Image of as-grown 2D MoS₂/WS₂ heterostructure layers on a SiO₂/Au/SiO₂/Si substrate. (b) Raman spectrum obtained from the sample, revealing the presence of both MoS₂ and WS₂. Low-magnification TEM (c) and a HRTEM (d) micrographs of the 2D MoS₂/WS₂ heterostructure layers in plain view. (e) STEM-EDS elemental mapping images revealing the uniform spatial distribution of constituent elements. The scale bar is 50 nm. (f) Cross-section TEM characterizations of 2D MoS₂/WS₂ heterostructure layers on a SiO₂ (left) and their detailed crystalline structures (right). (g) ADF-TEM image of the corresponding MoS₂/WS₂ interface, revealing a distinct image contrast. (h) STEM-EDS elemental map to show the spatial localization of Mo and W at the interface..... 44

Figure 18: Sequential procedures for the transfer of 2D MoS₂/WS₂ heterostructure layers using the water-assisted Au-SiO₂ separation (a-h). (g) PDMS-coated 2D WS₂/MoS₂ heterostructure layers integrated on the surface of a cup. (h) 2D MoS₂/WS₂ heterostructure layers on a PDMS transferred from a thermal release tape. (i) Raman spectrum from 2D MoS₂/WS₂ heterostructure layers in comparison to the Raman spectra from individual 2D MoS₂ and 2D WS₂. (j) Transport characteristics of transferred 2D MoS₂/WS₂ heterostructure layers. 47

Figure 19: (a) Illustration for the direct growth of 2D MoS₂ layers on Au-deposited substrates and their subsequent transfers. (b) Images of 2D MoS₂-grown on Au/SiO₂/Si substrates. 2D MoS₂ are selectively grown with Mo of different thicknesses (left: 3 nm, right: 10 nm). (c) Raman spectrum obtained from the 2D MoS₂ layers grown on in panel b. (d) Cross-sectional ADF-TEM micrographs of 2D MoS₂ grown on an Au/SiO₂/Si substrate. The zoom-in image (red box) reveals the growth of continuous 2D MoS₂ layers. (e) ADF-TEM

micrograph revealing the sharp 2D MoS₂/Au interface. (f) A plane-view of an HRTEM micrograph of few-layer 2D MoS₂ layers revealing Moiré patterns. (g) 2D MoS₂/Au before (left) and after (right) integration to a supporting tape. (h) Large-area 2D MoS₂ layers attached to a supporting tape. (i) Patterned 2D MoS₂ layers attached to a supporting tape. 49

Figure 20: Flexible device integration process. (a) Schematic for the fabrication of a vertically stacked SWNT/2D MoS₂ heterojunction integrated on a flexible Cu foil. (b) Side-view illustration of a vertically stacked SWNT/2D MoS₂ heterojunction configured for electrical characterizations. (c) Image of 2D MoS₂ /Au layers integrated on a Cu foil. (d) The J–V characteristics from an SWNT/2D MoS₂ heterojunction showing current rectification and the corresponding semilogarithmic presentation (inset). (e) Photoresponse characteristics from an SWNT/2D MoS₂ heterojunction. (f) Energy band diagram of SWNT/2D MoS₂ heterojunction depicting the separation/diffusion of photocarriers generated under light illumination (purple arrow). CB, VB, and E_f represent the conduction band, valence band, and Fermi energy, respectively. 52

Figure 21: Comparison of growth approaches. (a) BOE-based separation of 2D MoS₂-PMMA layer, which took ~51 min (left), resulting in partially peeled-off 2D MoS₂ layers (right). (b) Water-based separation of 2D MoS₂/Au-PMMA layer, which took ~3 min (left), resulting in clean transfer (right). Both of the samples were prepared under identical experimental conditions. 53

Figure 22: Schematic illustration of the large-area integration of three-dimensionally ordered 2D MoS₂ vertical layers onto a flexible PDMS substrate enabled by a water-assisted layer transfer method. 57

Figure 23: Growth morphology of the 2D MoS₂. (a) An SEM image of the 2D MoS₂ layer coated SiO₂/Si pillars. The scale bar in the inset is two μm. (b) SEM-EDS elemental maps showing

the spatial distribution of Si, O, Mo, and S atoms in the pillars. (c) Side-view an SEM image of 2D MoS₂ layer-coated SiO₂/Si pillars. (d) Cross-sectional TEM image of the red box in (c), showing the growth of 2D MoS₂ layers on SiO₂. (e)–(g) Cross-sectional HRTEM images of the A–C regions in (d), respectively. All the images show vertically-aligned 2D MoS₂ layers irrespective of the probed locations. (h) Plane-view HRTEM image of vertically-aligned 2D MoS₂ layers revealing their 2D layer edge sites. 59

Figure 24: Optical microscopy images: (a) large-area vertical 2D MoS₂ layer-coated SiO₂/Si pillars, and (b) color variation of the corresponding pillar patterned area. (c) Optical microscopy image of vertically-aligned 2D MoS₂ layers integrated on PDMS transferred from the same sample in (a). (d) An SEM image of the corresponding vertically-aligned 2D MoS₂ layers integrated on PDMS. (e) SEM-EDS elemental map showing the spatial distribution of Mo and S in the same sample. (f) Raman spectroscopy profiles of the same sample before and after transfer. 61

Figure 25: Camera and optical microscope images of vertically-aligned 2D MoS₂ layers/PDMS under uniaxial tensile strains of (a) 0% and (b) 30%. (c) Optical absorbance of the same sample with varying strain levels. (d) Variation of A excitonic peak energy with varying strain levels. (e) Optical images of the water contact angle (WCA) with varying strain levels from 0% to 30% strain, exhibiting decreasing water contact angle with increasing surface roughness owing to the flattening of the sample substrate by applying tensile strain. 63

Figure 26: (a) *I*–*V* characteristics of patterned vertically-aligned 2D MoS₂ layers/PDMS upon water molecule absorption in the relative humidity range of 30% to 90%. (b) Comparison of the relative resistance change with varying relative humidity for patterned vertical 2D MoS₂/PDMS (black), patterned vertical 2D MoS₂/PDMS under bending (red), vertical 2D MoS₂/PDMS without patterns (blue), and horizontal 2D MoS₂/PDMS without patterns (pink). (c) Schematic illustration of electron transfer in vertically-aligned 2D MoS₂ layers

upon water molecule absorption. (d)–(f) DFT calculation snapshots of adsorbed water molecules on the (d) basal plane, (e) Mo edge, and (f) S edge in 2D MoS₂ layers. 67

Figure 27: Schematic diagram of the stretchable gas sensor fabrication process. (a) Metal Mo deposition. (b) Thermal sulfurization. (c) Spin-coating with PMMA. (d-e) Water immersion and lift-off. (f-g) Mechanically cut the serpentine pattern and remove the extraneous/un-patterned area. (h) Gold electrode deposition with a shadow mask..... 71

Figure 28: Optical, structural, and chemical morphology of the vertically-aligned 2D MoS₂ stretchable sensor by AFM, Transmittance, Raman, and XPS analysis. (a) The HRTEM image is exhibiting all vertically-aligned 2D MoS₂ layers of the entire sample. (b) AFM height profile measurement of the 2D MoS₂/PMMA. (c) Optical transmittance spectra of bare PMMA and MoS₂/PMMA. (d) Raman spectra obtained from as-grown and transferred 2D MoS₂ layers. (e-f) The XPS scans for the Mo and S binding energies of the 2D MoS₂ layers. (e) The XPS spectra (Mo3d core level) of the as-grown 2D MoS₂/SiO₂/Si (black) substrate and transferred MoS₂ film on the PMMA (red) substrate. (f) XPS spectra of the S2p core level of the as-grown and transferred sample 73

Figure 29: Mechanically stretchable performance of the device, (a) Camera image under stretching from 0 to 70%. (b) Two-terminal electrical (I-V) characterization of the sensor from 0 to 50% strain. (c, f) Raman-strain and photocurrent measurement from 0 to 40% strain. (d-e) The real-time gas response at 5 ppm, 10 ppm, 20 ppm, and 30 ppm and gas sensing performance at 40% strain. 77

LIST OF ACRONYMS (or) ABBREVIATIONS

2D TMD	Two-Dimensional Transition Metal Dichalcogenide
ADF STEM	Annular Dark-Field Scanning Transmission Electron Microscopy
CVD	Chemical Vapor Deposition
DFT	Density Functional Theory
EDS	Energy Dispersive X-ray Spectroscopy
FEM	Finite Element Method
HRTEM	High-Resolution Transmission Electron Microscopy
PDMS	Polydimethylsiloxane
PMMA	Poly (methyl methacrylate)
SEM	Scanning Electron Microscopy
TEM	Transmission Electron Microscopy
XPS	X-ray Photoelectron Spectroscopy

CHAPTER-1: INTRODUCTION

1.1 Motivation and Background

Recently, two-dimensional (2D) transition metal dichalcogenides (TMDs), such as molybdenum (or tungsten) disulfides (MoS_2 or WS_2), have attracted unprecedented scientific and technological interests owing to their extraordinary physical, chemical, electronic, and mechanical properties. In particular, their unique combination of anisotropic crystal structure, atomic-scale thickness, tunable bandgap ($\sim 1.2\text{--}1.8$ eV), and very high in-plane strain limit ($>30\%$) make them interesting for fundamental studies and applications in high-end flexible electronics, optoelectronics, electrochemical, sensing, and environmental applications [1-3].

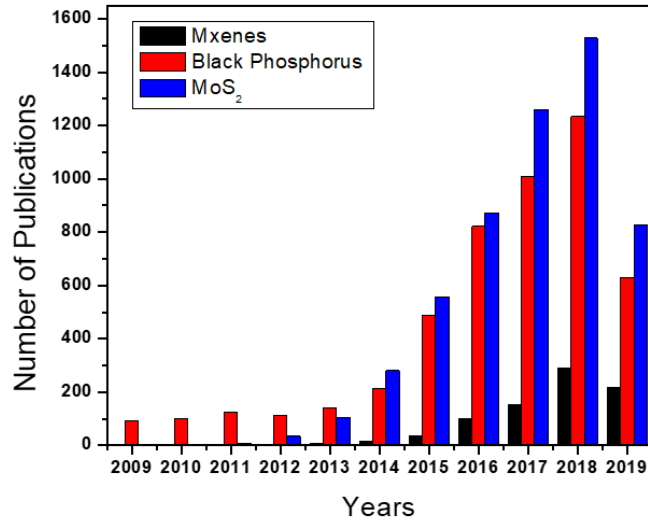


Figure 1: Number of publications per year of various 2D materials from 2009 to 2019[Extracted from Web of Science. Available at: <http://apps.webofknowledge.com> [Accessed 19 Jul. 2019], searching keywords are Mxene, Black Phosphorus, and MoS_2 .

2D MoS_2 is one of the most widely studied materials in the TMDs family, owing to its indirect to direct bandgap transition, robustness, non-toxicity as compared to their selenide and

telluride, ease of fabrication, and abundance of constituent elements [4]. Figure 1 is a year-wise publication list of 2D materials; Mxene, Black Phosphorus, and MoS₂, clearly indicate a rising trend of 2D MoS₂ research as rapidly growing attention to the scientists as compared to other 2D materials from 2009 to 2019.

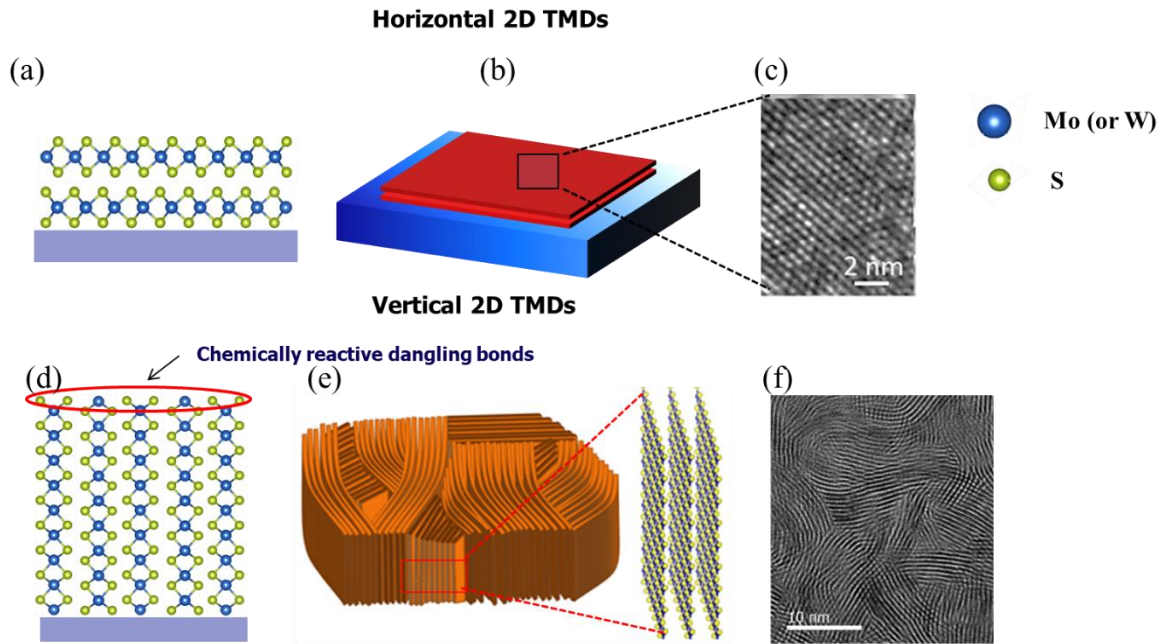


Figure 2: Schematics representation for the concept of the horizontal and vertical growth of 2D TMDs. The horizontal layers; (a) Side-view, (b) projected-view, (c) High-resolution transmission electron microscopy (TEM) image. The vertical layers; (d) Side-view, (e) projected-view, (e) Top view of the high-resolution TEM image. Figure (c,e) adapted with permission from references[5,6].

Intriguingly, the captivating physical and chemical properties of the 2D MoS₂ depend on the terrace and edge sites, which is attributed to their horizontal and vertical orientation, respectively (in figure 2). For instance, the exposed terrace sites of their horizontal layers have been demonstrated for electronics and optoelectronics devices owing to its indirect-to-direct bandgap transition and high on/off ratios ($>10^5$). In contrast, the vertically-aligned 2D MoS₂ exhibits a rich set of dangling bonds on their chemically reactive 2D edges, which have very high

adsorption energy as compared to their chemically inert basal plane. Moreover, the edges of this vertically-aligned 2D MoS₂ contain high d-orbital electron density, which provides strong binding interactions with outside environment/molecules[7]. Because of this high chemical/physical adsorption on the surface, there is a dramatic change in electrical properties when interacting with analytes. Hence, the vertically-aligned 2D MoS₂ layers are ideal for detecting chemical or biological molecule sensing via storing or transferring charges. Thus, we can take advantage of the exquisite sensitivity of the 2D MoS₂ by controlling the physicochemical variables of the surroundings to open new technological breakthroughs to enable cutting edge and transformative advances beyond existing materials[5,8-12].

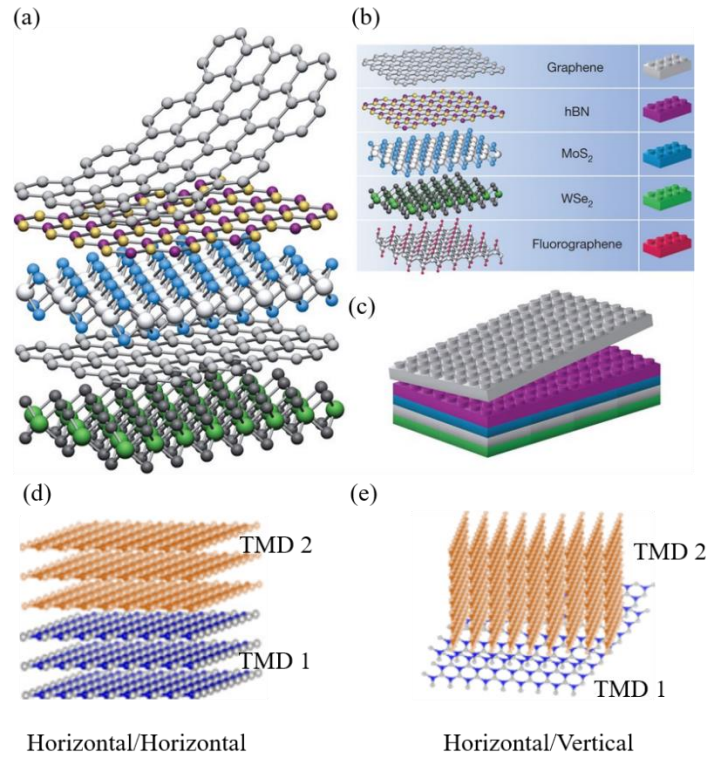


Figure 3: (a-c) 2D TMDs heterostructures are analogous to Lego blocks. Here, different layered TMDs are considered as atomically thin Legos. The construction of a wide variety of layered structures becomes possible with this concept, adapted with permission from reference [13]. (d-e) Schematic representation of the layer orientation with (d) both horizontal and (e) horizontal to vertical heterostructure.

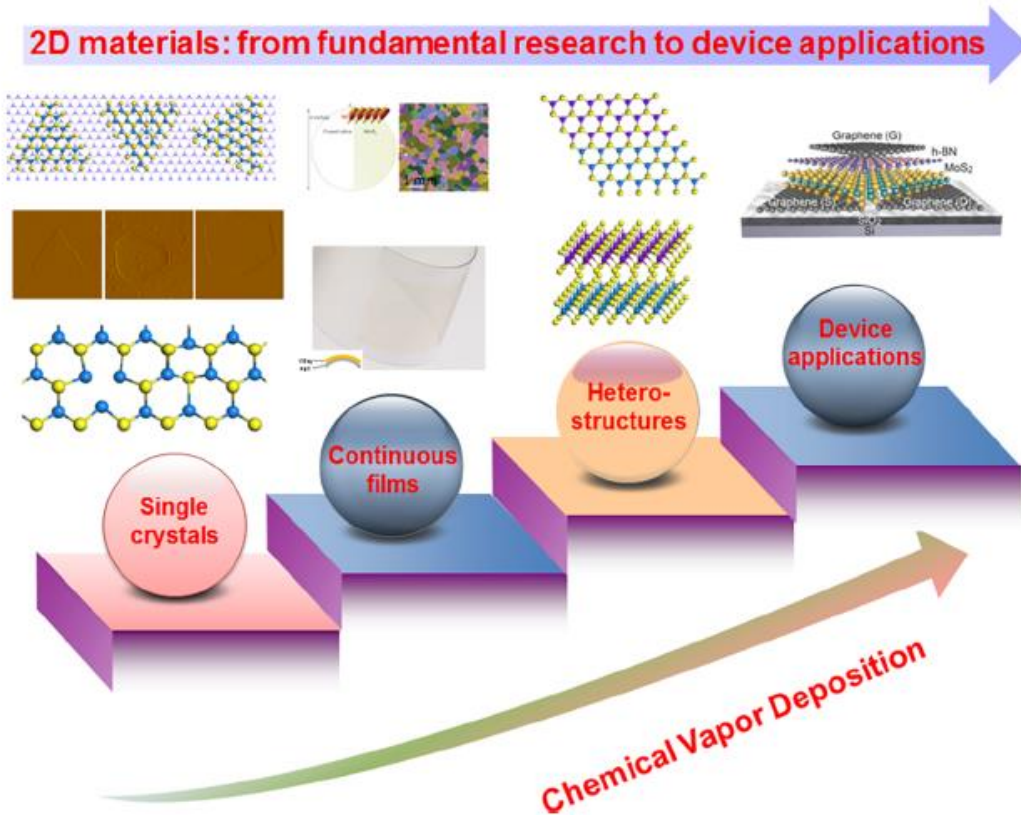


Figure 4: Schematics for the overview of chemical vapor deposition (CVD) grown 2D TMDs heterostructure displaying from single crystal and continuous films to device applications, adapted with permission from reference [2].

2D heterostructures are composed of vertically stacked dissimilar materials on top of each other similar to the Lego blocks, as depicted in figure 3(a-c). They provide a unique platform to create an almost unlimited number of elements with novel properties and applications [14]. A distinct feature attributed to 2D TMDs is the weak van der Waals (vdW) interactions between consecutive layers without lattice match constraints, which allows significant freedom in growth and heterogeneous integration at the atomic level. This groundbreaking opportunity for the flexible integration of different materials has been widely used as the essential building blocks to explore new electronics and optoelectronic devices with unprecedented speed and flexibility [15,16]. The performance of the heterostructure devices mostly depends on the 2D material

quality, including defect, grain boundaries, and significant scattering across vdW gaps. 2D MoS₂-based heterostructures have mainly been produced by mechanical exfoliation and CVD co-evaporation methods. These approaches were unsuccessful in addressing the issues mentioned above. Moreover, the dangling bond free atomically sharp heterointerface is critically important to realize unique carrier transfer behaviors (e.g., interlayer quantum coupling effect).

The crystallographic orientation (i.e., relative alignment of the lattice) of 2D MoS₂ and their heterostructures has a significant impact on their material properties. Although traditional exfoliation and restacking methods offer atomic-level integration, their intrinsic non-scalability hindered their applications for practical devices. Furthermore, the fixed orientation 2D layers achieved by the conventional layer-by-layer stacking usually hindered their diverse applications[15,17-19]. Therefore, a viable growth strategy of the large-area 2D TMDs heterostructures is demanded for an in-depth understanding of their hetero-interface at the atomic level, layer orientation control, and interlayer interaction to leverage their true potentials in electronics/optoelectronics applications. For the potential applications of 2D TMDs vdW heterostructures, one of the top challenges is how to produce wafer-scale thin films with controlled layers and spatial homogeneity. There have been considerable efforts employed to develop various synthetic approaches for the preparation of various 2D TMDs, including vapor-phase chemical reactions, wet-chemical synthesis, and liquid exfoliations. The most common synthesis method, the CVD co-evaporation method, yields 2D TMDs with limited spatial homogeneity and uncontrolled morphologies owing to uncontrollable growth variables. Moreover, mechanical exfoliations were used for initial fundamental studies, which resulted in low yields and poor uniformity in the film. Hence, this method is impractical for scalable fabrication. Considerable efforts have also been devoted to developing a novel synthetic strategy

for 2D vdW heterostructures growth to overcome the bottlenecks of previously explored mechanically assembled complex vdW heterostructures. Remarkably, the layer orientation-controlled growth of the subsequent 2D layers on to the pre-existing 2D layers is quite challenging and unexplored in the previous studies. Therefore, it is essential to develop a scalable synthesis approach to grow 2D TMDs heterostructure with precisely controlled chemical composition, physical dimensions, and layer orientation [13,15,20-27]. The CVD based on the predisposition of metal seed layers is the most effective method for the controllable synthesis of atomically thin 2D TMDs layers [28,29]. Both vertically and horizontally-aligned 2D MoS₂ layers can be fabricated with this method [30]. Since the thickness of the pre-deposited Mo film determines the thickness and size of the obtained MoS₂ thin film, it is projected that high quality, controllable orientation/thickness, and large-scale production can be obtained from this CVD process[5,31].

CVD growth of 2D MoS₂ layers usually depends on high temperature processes (~800 °C) with robust growth substrates (e.g. SiO₂) and is not compatible with soft/flexible substrates (e.g. plastics). In order to realize the aforementioned promise of 2D MoS₂ for emerging flexible electronics, it is critically demanded to develop a reliable and deterministic transfer approach which can separate as-grown 2D MoS₂ from their original growth substrates maintaining both morphological and physicochemical properties intact.

However, this transfer and integration of as-synthesized 2D MoS₂ is also challenging owing to the extreme mechanical delicacy of their atomically thin structure. The most commonly used method relied on the sacrificial polymethyl methacrylate (PMMA) layer and wet etching of the growth substrate, which leads to degrading film quality. Moreover, undissolved PMMA residue trapped and surface got contaminated, which leads to deteriorating intrinsic material properties and unreliable device fabrication [8,32,33]. In another study, polylactic acid (PLLA)

has been used, which involves additional fabrication steps (including deposition, dissolving, and washing). This method is even more complicated and tedious for heterogeneously stacking up multiple 2D layers to a variety of unconventional substrates [34-37]. Moreover, integration of 2D TMDs heterostructure layers mainly involves strong chemical etchant, buffered oxide etchant (BOE) or potassium hydroxide (KOH), which significantly degrade material quality at the 2D MoS₂/SiO₂ interface. Therefore, a deterministic transfer/integration of 2D TMDs heterostructure is necessary for their scalable device fabrication. Furthermore, the transfer/integration of vertically-aligned 2D MoS₂ layers onto flexible substrates was mainly unexplored before this study [31,34,38]. The higher in-plane strain limit of 2D MoS₂ (>4× than silicon) and diverse functionalities offer new venues for 2D flexible technologies, which explores a wide range of applications impossible with conventional electronic materials and/or rigid devices based on them[39]. In addition to mechanical flexibility, stretchable characteristic provides a further level of distinction for reliable and conformal integration of 2D MoS₂ layers into wearable devices, which can tolerate large deformation without compromising device performance. Therefore, it is essential to develop a reliable strategy to explore an unconventional structural layout of 2D MoS₂ for a high-performance stretchable/wearable optoelectronics and sensor devices [40-44].

1.2 Thesis Statement and Organization

Chapter two starts with a background discussion of 2D MoS₂, including crystal structure, electronic, optical, mechanical, and chemical properties. Various synthesis methods of the 2D MoS₂ will be discussed in this chapter.

After the background information, the experimental methodologies are presented in chapter 3. In this chapter, the experimental procedure for the CVD growth of 2D MoS₂/WS₂ heterostructures and the horizontal and vertical growth methods of 2D MoS₂ will be explained. Moreover, all characterization techniques used in this dissertation, including Raman, electrical measurement, photocurrent measurement, scanning electron microscopy (SEM), and TEM analysis, will be addressed. Furthermore, gas and humidity sensing measurement techniques are to be explained in this chapter.

Followed by the experimental procedures, a novel growth strategy of 2D MoS₂-based vertical heterostructures is presented in chapter 4. This chapter reveals their underlying growth mechanism in both experimental and theoretical aspects.

In chapter 5, transfer and integration methods for 2D MoS₂ layers and their heterostructures are presented. In particular, Gold (Au) assisted growth, transfer, and integration of these materials have been demonstrated. Moreover, photoresponse and rectification properties are to be presented to verify the effectiveness of the transfer and integration approach.

Chapter 6 presents the growth, transfer, and integration of vertically aligned 2D MoS₂ for improved sensing applications and their tunable mechanical properties. Here, water-assisted transfer of vertically grown 2D MoS₂ on flexible substrate will be demonstrated. The 3-D patterned pillars were used as a growth template to enhance the edge density of vertically aligned 2D MoS₂.

Chapter 7 demonstrates stretchable gas sensors with vertically aligned 2D MoS₂ layers of serpentine geometry. A facile water-assisted layer transfer method was used to integrate

vertically aligned 2D MoS₂ layers on elastomeric PMMA substrates. Electrical, Raman, and photoresponse characterizations were performed combined with tensile strain to study their mechanically-modulated material properties. Moreover, real-time gas sensing measurements will be explained before and after a 40% tensile strain.

Chapter 8 concludes this dissertation and projects possible future directions.

CHAPTER-2: THEORETICAL BACKGROUND

2.1 Crystal Structure of 2D MoS₂

A large family of 2D TMDs exhibit diverse carrier transport properties such as semiconducting, metallic, insulating, and superconducting. These properties are depending on their crystal structure, phases, size, doping, and defects. Figure 5 showed a large family of 2D TMDs which can be obtained by transition metals with the chalcogen atoms. Among these family members, MoS₂ is one of the most widely studied materials owing to its superior material properties.

H	MX_2 M = Transition metal X = Chalcogen																He
Li	Be											B	C	N	O	F	Ne
Na	Mg	3	4	5	6	7	8	9	10	11	12	Al	Si	P	S	Cl	Ar
K	Ca	Sc	Ti	V	Cr	Mn	Fe	Co	Ni	Cu	Zn	Ga	Ge	As	Se	Br	Kr
Rb	Sr	Y	Zr	Nb	Mo	Tc	Ru	Rh	Pd	Ag	Cd	In	Sn	Sb	Te	I	Xe
Cs	Ba	La-Lu	Hf	Ta	W	Re	Os	Ir	Pt	Au	Hg	Tl	Pb	Bi	Po	At	Rn
Fr	Ra	Ac-Lr	Rf	Db	Sg	Bh	Hs	Mt	Ds	Rg	Cn	Uut	Fl	Uup	Lv	Uus	Uuo

Figure 5: The periodic table of the elements, more than 80 members of the 2D TMDs compound exist by combining transition metal with the chalcogen atoms, adapted with permission from reference [3].

2D MoS₂ layers mainly consist of two different crystalline phases, as shown in figure 6, the hexagonal (2H) and octahedral (1T). The 2H phase is semiconducting and

thermodynamically more stable, hence extensively used for electronic applications. The 1T phase is metallic, obtained through intercalating 2H-MoS₂ with alkali metals that are in a tetragonal symmetry[45]. In a general form, a metal atom(M) is sandwiched between two chalcogen atoms in each unit cell of the 2D layer.

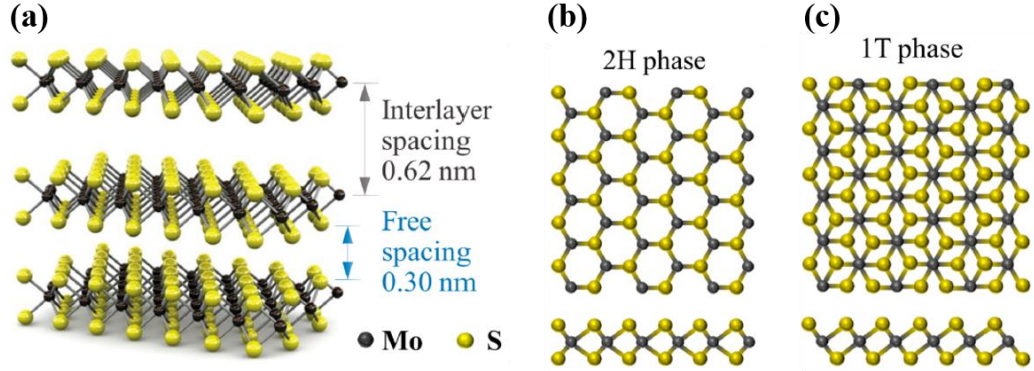


Figure 6: Schematics of the crystal structure of single-layer MoS₂ (a) trigonal prismatic (b) and octahedral structure adapted from reference [45].

Bulk MoS₂ consists of a large number of vertically stacked monolayers which are linked via vdW forces while there is a strong covalent bonding their in-plane between Mo and S atoms. The monolayer of MoS₂ consists of a single sheet of Mo atoms sandwiched in between two S atoms, forming a 2D hexagonal crystal structure. The thickness of each 2D layer is ≈ 6.5 Å, the S-S distance is ≈ 3.2 Å, the covalent bond length of Mo-S is 2.43 Å, and the S-Mo-S bond angle is $\approx 80.56^\circ$ [45].

2.2 Properties of 2D MoS₂

2.2.1 Electronic and Optical Properties of 2D MoS₂

One of the most exciting electronic properties of 2D MoS₂ is that its indirect-to-direct bandgap change with reducing 2D layer number. The direct bandgap depends on the localized d orbital of the

transition metal (e.g., Mo, W), which is minimally affected by the interlayer coupling owing to its location in the unit cell and the quantum confinement effect. On the other hand, the indirect bandgap of this material depends on the overlap of the d-orbital of transition metal and p-orbital of chalcogen atoms, which strongly depends on the interlayer coupling[46]. Bulk MoS₂ is an indirect-gap semiconductor with a bandgap of 1.29 eV, and monolayer 2D MoS₂ presents a bandgap of 1.9 eV. The bottom of the conduction band and the top of the valence band of bulk MoS₂ are located in between the K and Γ points and at the Γ point in the Brillion zone, respectively. The unit cell of individual 2D layers consists of two hexagonal planes of S atoms and a Mo atom in between with covalently bonded S atoms in a trigonal prismatic arrangement, as shown in figure 7 [47].

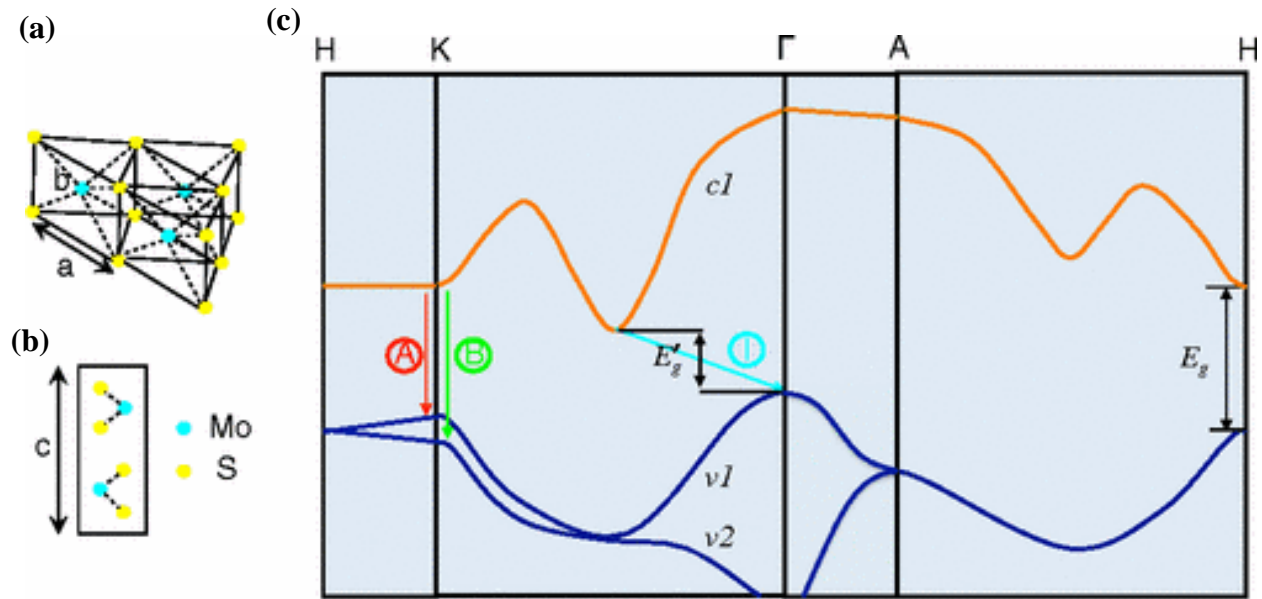


Figure 7: (a-b) The lattice structure of 2D MoS₂ in both the in-plane and out-of-plane directions. (c) A band diagram of bulk MoS₂, showing the lowest conduction band c_1 and the highest split valence bands v_1 and v_2 . A and B are the direct-gap transitions, and I is the indirect-gap transition where E'_g and E_g are the bandgap of the bulk and monolayer, adapted with permission from reference[48].

2D MoS₂ layers have high promise for potential applications in various optoelectronic devices, including light-emitting diodes, transistors, photovoltaic devices, photodetectors, and lasers. In

particular, the optical and electronic properties are extremely sensitive to 2D MoS₂ layer thicknesses owing to inter-layer coupling and quantum confinement effects [49].

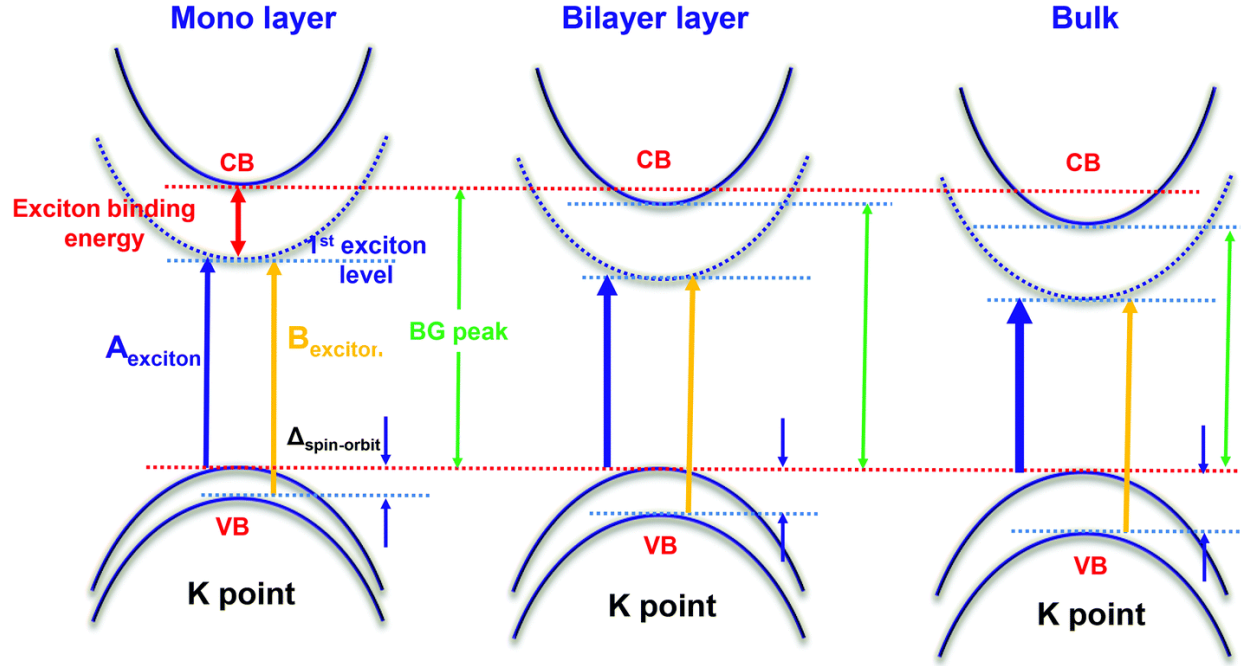


Figure 8: The optical transition of at the K-point in the monolayer, bilayer, and bulk 2D MoS₂ layers, the A excitonic peak shift originated from the 1st exciton level. The reduction in the exciton levels offset with increasing valence band splitting energy; hence, the B-exciton peak did not change. Adapted with permission from reference [50].

Figure 8 shows the optical absorption properties of 2D MoS₂ with varying 2D layer number explained by a simplified band transition model [50]. Two excitonic peaks are observed corresponding to A and B from the K-point of the Brillouin zone. The peak A is shifted due to the change of exciton binding energy or the gap between the lowest conduction band and the highest valence band at the K-point or a combination of both effects. However, the excitonic peak B does not change noticeably as a function of 2D layer number as the decrease in exciton level was offset owing to the valence band splitting.

The bandgap transition of 2D MoS₂ layers manifested by optical absorption is can be confirmed by photoluminescence spectroscopy as well. Owing to the spin-orbit-coupling, the photoluminescence spectra of 2D MoS₂ exhibit two excitonic peaks corresponding to A and B direct exciton transition. The photoluminescence studies reveal that 2D MoS₂ exhibit increasing bandgap energy with decreasing 2D layer number accompanying indirect-to-direct bandgap transition [51-53].

2.2.2 Mechanical Properties

Unique mechanical properties of 2D MoS₂ layers result from their intrinsically large in-plane strain limit coupled with atomic-level thickness. Moreover, the vdW attraction responsible for the molecular binding of individual 2D layers also determines their shear, friction, and fracture behaviors. 2D MoS₂ layers exhibit superior mechanical properties as compared to conventional bulk semiconductors owing to their strong in-plane covalent bonding. Both monolayer and bulk MoS₂ possess higher in-plane stiffness than steel; i.e., Young's modulus of monolayer and bulk MoS₂ are 270 ± 100 GPa and ≈ 240 GPa, respectively, whereas this value is ≈ 205 GPa for steel. This exceptional mechanical stiffness, combined with a large in-plane strain limit, makes them suitable for stretchable and flexible device applications [4,29]. Electronic structures of 2D MoS₂ layers are also affected by their mechanical deformation; e.g., their bandgap is known to decrease with increasing tensile strain [54-57]. This mechanically tunable electronic properties project great promise for emerging stretchable and wearable electronic and optoelectronic technologies[58,59].

2.2.3 Chemical and Sensing Properties

2D MoS₂ layers possess intrinsic structural advantages such as very high surface-to-volume ratio and ample dangling bonds-exposed on their 2D edge sites for highly sensitive gas or humidity sensing applications. These property advantages become further pronounced with vertically aligned 2D MoS₂ layers, which predominantly expose 2D edges and enriched unsaturated dangling

bonds on the surface. These surface-exposed 2D edges offer very high physical or chemical adsorption as compared to the chemically inert basal planes of horizontally aligned 2D layers. For instance, the interaction between 2D MoS₂ layers and analytes occurs via the physical adsorption through non-covalent interactions on their surface, which is desirable for quick response, recovery, and repeatability [31,60-62].

2.3 Synthesis Methods of 2D MoS₂

Large-area, spatially continuous, and chemically homogenous 2D MoS₂ layers with uniform properties are the essential prerequisite for practical device applications. Several challenges are needed to be addressed for exploiting their technological potentials, including (i) preparation of high-quality wafer-scale samples, (ii) their reliable transfer and integration onto secondary substrates, (iii) retention of intrinsic structural morphology and chemistry. Figure 8 shows an overview of various conventional approaches for the synthesis of single-layer material.

2.3.1 Mechanical Exfoliation Method

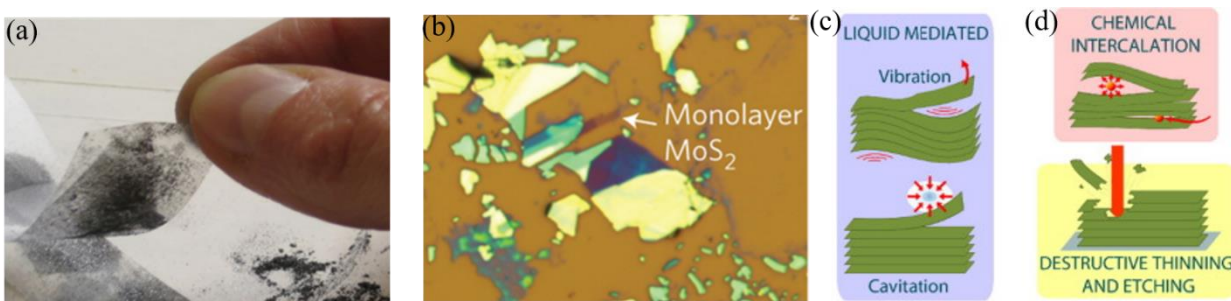


Figure 9: (a-b) The mechanical exfoliation of 2D MoS₂ layers with scotch tape; (a) Camera image. (b) Optical image of the single-layer MoS₂ transfer with random flakes with irregular shape and size. (c-d) Schematic representations of the of the liquid-mediated exfoliation process; () Adapted with permission from reference[63,64].

The mechanical exfoliation method originates from the manual peel-off of graphene using a scotch-tape and still being used to prepare for MoS₂ and other 2D materials. Figure 9 shows mechanically exfoliated 2D MoS₂ transfer processes and their individually isolated monolayer flakes. This method can usually isolate monolayers of relatively small size (~5 μm) from their bulk crystals and transfer them to secondary substrates. This approach has been mainly utilized for the proof-of-concept demonstration and investigation of their materials properties for fundamental sciences. However, this exfoliation method cannot produce large-area 2D layers of controlled layer numbers, size, orientation, and phase; therefore it remains impractical for industrial-scale production [45,65].

2.3.2 Liquid Exfoliation Method

Ultrasonication-mediated liquid-phase exfoliation has been used to separate 2D MoS₂ layers from the bulk. This process is schematically shown in figure 9(c). In this method, the waves from the ultrasonication can propagate through the organic solvents. Therefore, vibration and cavitation energy inputs are generated due to the alternating high and low pressure. The process is continued until dispersed 2D layers are separated. A large quantity of 2D layers can be yielded from this method with irregular shapes and random orientations. As we need to add chemicals to prevent the recombination of 2D materials, their material quality is lower[45,66]. Moreover, a destructive chemical etching is required for thinning 2D layers to produce a mono or few-layered MoS₂. As an alternative strategy, the chemical intercalation process has been developed based on inserting a small atom within the interlayer space of the bulk MoS₂. 2D MoS₂ loss its semiconducting properties with this process as the structural/phase changes in 2D crystals [45,64,67].

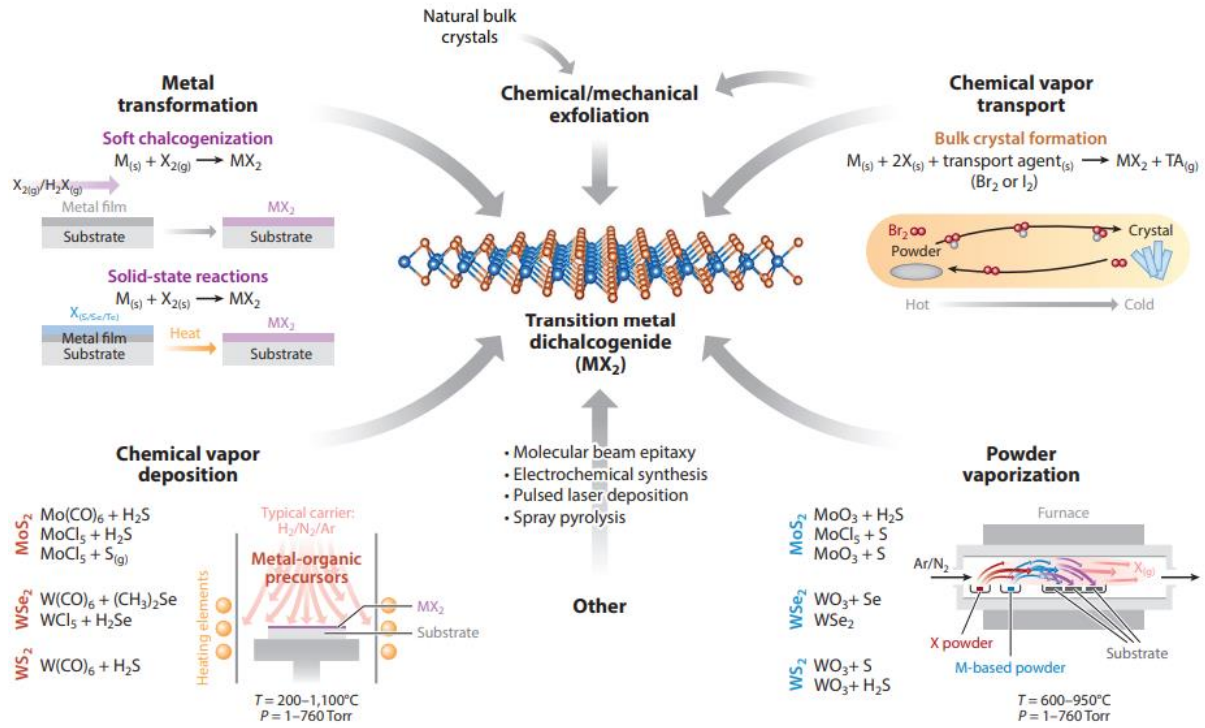


Figure 10: An overview of the conventional 2D TMDs synthesis approaches, adapted with permission from reference [66].

2.3.3 Chemical Vapor Deposition Method

Controllable synthesis of large-area 2D MoS₂ layers with a high level of uniformity and efficiency is a prerequisite for their scalable device applications. However, as above verified, the conventional methods based on mechanical or chemical exfoliations produce 2D layers of high inhomogeneity, i.e., uncontrolled 2D layer size, thickness, and areal coverage, etc. CVD is a viable method for the synthesis of high-quality 2D MoS₂ layers of controlled morphology. This method has been widely used for the synthesis of graphene, hexagonal boron nitride (h-BN), and other 2D TMDs [67].

In the CVD process, a chemical reaction of vaporized precursors containing chalcogen (e.g., S) and transition metals (e.g., Mo) happens, which leads to that solid-phase 2D layers (e.g., MoS₂)

condensates on the surface of a growth substrate [21]. For a large-area growth of 2D TMDs, CVD has been considered as one of the most successful routes. A variety of CVD methods and relevant approaches (e.g., powder vaporization, chemical vapor transport, etc.) have been developed, as illustrated in figure 10. CVD growth of 2D MoS₂ layers has been mostly performed by the co-evaporation of solid-state precursors (e.g., MoO₃ and S powders), which generally yield 2D flakes of uncontrolled structural morphology and incomplete surface coverage.

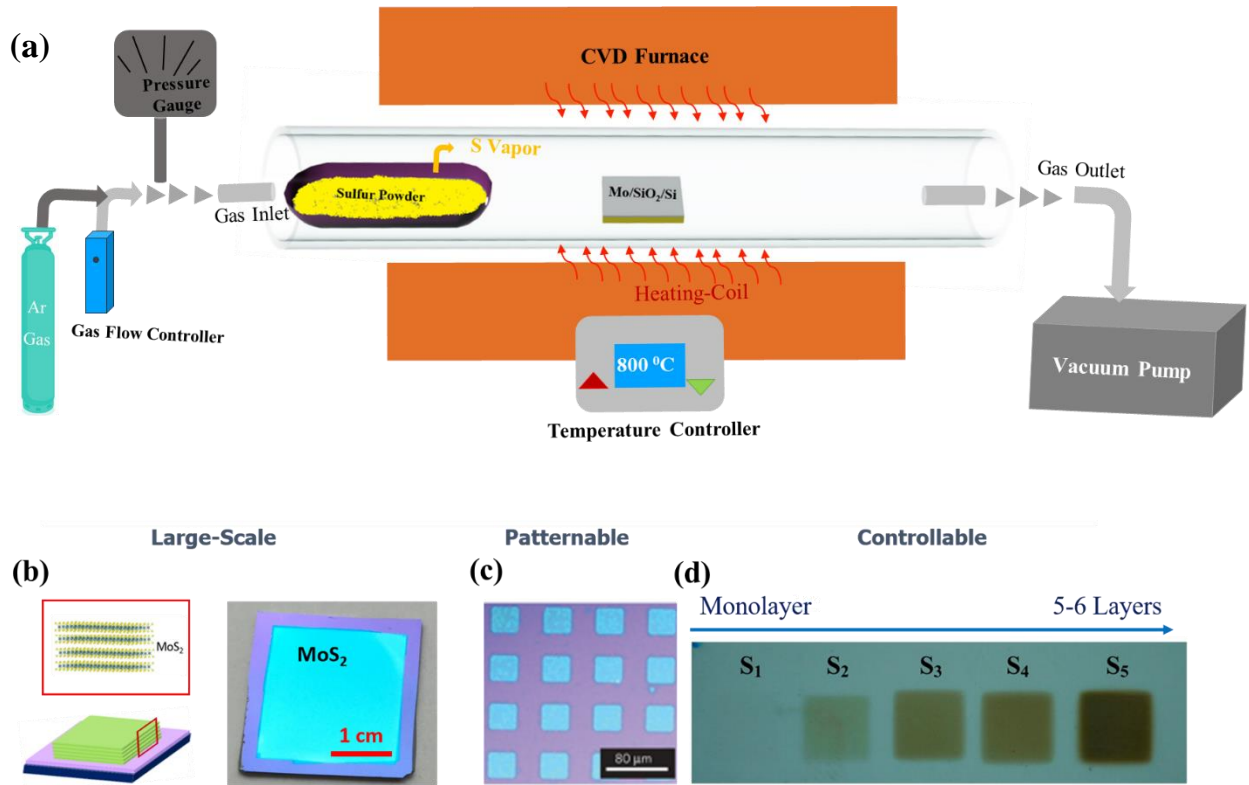


Figure 11: The metal seed layer-based one-step CVD growth process. (a) Schematic diagram of the CVD growth process. (b) A large-area growth process. (c) A patternable growth process. (d) A controllable layer thicknesses. Figure (b-d) adapted with permission from reference[12,68,69].

We developed a one-step CVD growth process which employs the chemical reaction of pre-deposited metal seed layers (e.g., elemental Mo thin films), offering distinct advantages of improved structural homogeneity and uniformity. Figure 11(a) illustrates the schematic of this

CVD process, and figure 11(b-d) demonstrates its large-area scalability, patternability, and layer number controllability. Details for the CVD growth process will be presented in the next section.

CHAPTER-3: EXPERIMENTAL DETAILS

3.1 Experimental Methods for the Layer Orientation Control Growth

The contents of this section have been published in: Choudhary, N., Chung, H., Kim, J., Noh, C., Islam, M., Oh, K., Coffey, K., Jung, Y. & Jung, Y. "Strain-Driven and Layer-Number-Dependent Crossover of Growth Mode in van der Waals Heterostructures: 2D/2D Layer-By-Layer Horizontal Epitaxy to 2D/3D Vertical Reorientation," Advanced Materials Interfaces 5, 1800382 (2018).

3.1.1 Fabrication of WO₃ nanowires

Single crystalline faceted WO₃ nanowires were fabricated by the thermal oxidation of a thin W foil. In a typical fabrication process, ten wt.% potassium hydroxide (KOH) solution was drop-casted on the surface of a W foil, followed by a spin coating at 2000 rpm for 15 seconds. The KOH deposited W foil was subsequently heated at 650°C for 2 hours inside a quartz tube furnace in an ambient condition. Hereafter, the sample was naturally cooled down to room temperature, followed by rinsing with deionized (DI) water and drying overnight at room temperature.

3.1.2 Growth of 2D MoS₂/WS₂ Vertical Stacks

As-prepared WO₃ nanowires were placed at the center of a quartz tube furnace with an alumina boat containing sulfur powder (99.99% purity, Sigma-Aldrich) located at the upstream. The quartz tube was subsequently evacuated to a base pressure of $\sim 10^{-3}$ m Torr and flushed several times with argon (Ar) gas. The sulfurization was performed by heating the furnace ~ 850 °C (ramp rate: ~ 20 °C/min, dwell time: 40 min) under a flow of Ar (200 standard cubic centimeters per minute (sccm)), followed by natural cooling in an inert environment. The layer number of 2D WS₂ layers was controlled by varying the sulfurization dwell time under a continuous supply of

vaporized sulfur. Subsequently, Mo films of controlled thickness were deposited on the surfaces of 2D WS_2 layers-grown WO_3 nanowires via e-beam evaporation. The nanowires were subsequently sulfurized following the identical experimental procedure as above.

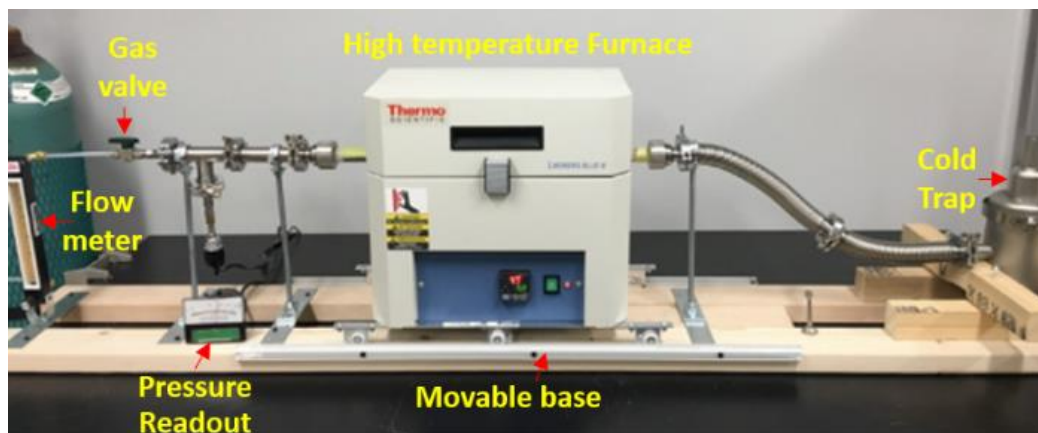


Figure 12: A picture of the CVD furnace used to grow 2D MoS_2 and heterostructures in this study.

3.1.3 TEM Characterizations

All TEM and scanning transmission electron microscopy (STEM) characterizations were performed using a Cs-corrected TEM (JEOL-ARM200F) at an accelerating voltage of 200kV. Annular dark-field (ADF), ADF STEM analysis, was conducted under the following conditions; probe current: $\sim 20\text{pA}$, condenser aperture: $30\mu\text{m}$, and camera length: 6cm. An energy dispersive X-ray spectroscopy (EDS) in STEM (STEM-EDS) analysis was performed using an EDAX detector (SDD type 80T) and analysis software (AZtecTEM, Oxford). Cross-sectional TEM samples were prepared by focused ion beam (FIB; Quanta 2D FEG, FEI) milling/lift-out techniques. As-prepared nanowires were deposited with a $\sim 100\text{ nm}$ thick carbon (C) and platinum (Pt) layers and were subsequently cross-sectioned via FIB gallium (Ga) ion milling at 30keV. The prepared TEM sample was transferred onto a copper (Cu) TEM grid using a micromanipulator (Omniprobe) inside the FIB.

3.2 Experimental Methods for the Heterostructure Integration

The contents of this section have been published in: M. A. Islam, J. H. Kim, A. Schropp, H. Kalita, N. Choudhary, D. Weitzman, S. I. Khondaker, K. H. Oh, T. Roy, H.-S. Chung, and Y. Jung, Centimeter-Scale 2D van der Waals Vertical Heterostructures Integrated on Deformable Substrates Enabled by Gold Sacrificial Layer-Assisted Growth. Nano Letters, 2017, 17, 6157–6165.

3.2.1 CVD Growth

A commercial SiO₂/Si wafer is cut into $\sim 2 \times 2$ cm² pieces followed by sequential cleaning with acetone and methanol. The wafer pieces are sequentially deposited with Au (~ 50 – 100 nm), SiO₂ (~ 300 – 450 nm), and metals (Mo and W: ~ 4 – 6 nm) by electron beam evaporation (Temescal FC-2000 evaporator). The prepared substrates are loaded into a quartz tube CVD furnace which is pumped down to <1 mTorr. After purging with argon (Ar) gas, the furnace is heated up to ~ 650 – 700 °C with a flow of Ar [100 standard cubic centimeters per minute (SCCM)] at an operating pressure of ~ 100 mTorr. After ~ 30 min reaction, the furnace is naturally cooled down, and the substrate is taken out of the furnace. It is observed that the color of the substrate changes from silver to dark green, which indicates the sulfurization of Mo and W. Growth conditions for 2D MoS₂/WS₂ on SiO₂/Au substrates are identical for those for 2D MoS₂ on Au.

3.2.2 Lift-off and Transfer

2D MoS₂/WS₂ layers were grown on SiO₂/Au-based substrates with or without PL are immersed in water. Prior to the immersion, small areas on the corners of the samples are exposed by mechanical scratch, which is to facilitate the water penetration into the Au/SiO₂ interface. After the water immersion, the samples are taken out of the water bath, and the samples are mechanically separated by using a tweezer. Before the 2D layer integrations, the exposed SiO₂ on the samples

is removed by BOE. A thermal release tape (Semiconductor Equipment Corp.) is directly attached to as-grown 2D MoS₂ layers on Au-deposited substrates following water immersion. The tape with the 2D MoS₂/Au layers is manually detached from the growth substrate upon heating at 130 °C at a hot plate. Au residuals on the backside of the MoS₂ can be removed by Au etchant (iron chloride, FeCl₃).

3.2.3 Raman and TEM Characterizations

Raman spectra were collected using the Almega XR Raman spectrometer equipped with an Olympus BX51 microscope at a laser wavelength of 532 nm. The crystalline structure and the chemical composition of as-grown 2D layers were characterized using a JEOL ARM200F FEG-TEM/STEM with a Cs-corrector. STEM-EDS analysis was carried out using an EDAX detector (SDD type 80T) and analysis software (AZtecTEM, Oxford). All TEM/STEM operations were performed at an accelerating voltage of 200 kV. Cross-sectional TEM samples were prepared by focused ion beam (FIB; Quanta 2D FEG, FEI) based milling and lift-out techniques. As-grown 2D TMDs were deposited with ~100 nm thick carbon (C) and platinum (Pt) layers and were subsequently cross-sectioned inside a FIB via gallium (Ga) ion milling at 30 keV. The prepared TEM specimen was placed onto a Cu TEM grid with a micromanipulator (Omniprobe) inside the FIB.

3.2.4 Electrical and Photoresponse Characterizations

2D MoS₂/Au layers transferred to a Cu foil were selectively covered with a polydimethylsiloxane (PDMS) window. Diluted p-type SWNTs in solution were deposited on the exposed 2D MoS₂ extending to the surface of the PDMS window. Silver (Ag) paste is directly applied to the SWNT on PDMS for a top contact, and the bottom contact is connected to the backside of Cu foil. Electrical and photoresponse characterizations were performed at room

temperature in Micromanipulator 6200 probe station using a semiconductor parameter analyzer (KEYSIGHT B1500A). The device is globally illuminated with a white light source (intensity: 20 W/m²), and output characteristics were obtained before and after illumination.

3.3 Experimental Methods for the Flexible Humidity Sensor

The contents of this section have been published in: Islam, M., Kim, J., Ko, T., Noh, C., Nehate, S., Kaium, M., Ko, M., Fox, D., Zhai, L., Cho, C., Sundaram, K., Bae, T., Jung, Y., Chung, H. and Jung, Y. (2018). Three-dimensionally ordered 2D MoS₂ vertical layers integrated on flexible substrates with stretch-tunable functionality and improved sensing capability. Nanoscale, 10(37), pp.17525-17533

3.3.1 Growth of 2D MoS₂ With Vertically-aligned Layers

Ultra-high purity (99.99%) molybdenum (Mo) was deposited (thickness; typically, >8 nm) onto three-dimensionally ordered SiO₂/Si pillars prepared by a standard photolithography process. The Mo deposition was carried out by using an electron beam evaporator (Thermionics VE-100) at a deposition rate of 0.15 Å s⁻¹. MoS₂ growth was carried out with a single-zone horizontal tube furnace (Lindberg/Blue M) equipped with a 1-inch diameter quartz tube. The Mo-deposited pillar substrate was placed at the center of the heating zone with 100 mg of sulfur (S) powder (99.5%, Sigma Aldrich) separately placed at the upstream side. The tube was then pumped down to 1 mTorr base pressure followed by heating up to 650 °C for 30 minutes at a ramping rate of 43 °C min⁻¹. Ultra-high purity argon (Ar) gas (flow rate: 100 SCCM) was supplied throughout the CVD reaction, and the furnace was naturally cooled down to room temperature. The Ar gas was provided all the time until a room temperature reach. The sample is then taken out from the quartz tube very carefully for subsequent fabrication processes.

3.3.2 2D Layer Transfer and Integration

PDMS was spin-coated onto the 2D MoS₂/SiO₂/Si pillar substrate and was subsequently dried at room temperature for one day. The completely cured PDMS-coated sample was then immersed in water for a few hours. Before the water immersion, a corner of the sample was scratched and opened with a sharp object, which is to facilitate the penetration of water into the sample. The 2D MoS₂/PMMA film was then manually peeled off from the SiO₂/Si pillar template substrate and dried by blowing air.

3.3.3 Raman, SEM, TEM, and Optical Characterization

Raman characterization was performed using a Renishaw RM 1000B Micro-Raman Spectrometer with a laser wavelength of 514 nm and a spot size of 1 μ m. The SEM characterization was performed with a field-emission SEM (SU 8230, Hitachi) equipped with an X-ray energy dispersive spectrometer. TEM characterization was performed with a probe-corrected TEM (ARM200F, JEOL) operating at 200 kV. The optical absorbance of 2D MoS₂ layers/PDMS at varying stretch levels was characterized by UV-Vis spectroscopy (Cary WinUV spectrometer) in the wavelength range of 200–800 nm.

3.3.4 Humidity Sensing Characterization

The humidity sensing performance was evaluated by the two-terminal current-voltage (I–V) characterization of gold (Au) electrode-deposited samples using a home-built humidity chamber. The level of relative humidity inside the chamber was controlled by gradually introducing vaporized water and nitrogen (N₂) gas, inspected by using a commercial humidity monitor. I–V characteristics were recorded with a semiconductor parameter analyzer (HP 4156A) connected with a home-built probe station. The mechanical bending of the sample was ensured by employing a circular object underneath the backside of the sample while the metal contacts on the

sample are extended to copper wires. All the humidity sensing tests were performed at room temperature at an applied voltage of -5 V to +5 V. The relative humidity was precisely monitored with the commercial humidity monitor, which was placed inside the humidity chamber.

3.3.5 DFT Calculation

Density functional theory (DFT) calculations were conducted using the Vienna ab initio simulation package (VASP). The projector represents interactions between electrons and nuclei augmented wave (PAW) pseudopotentials with generalized gradient approximation (GGA) of the Perdew–Burke–Ernzerhof (PBE) formulation. The Brillouin zone was sampled using a Monkhorst–Pack grid of $7 \times 7 \times 3$ k points and cut-off energy of 400 eV was used. Besides, DFT-d3 correction was applied to account for the vdW interactions [70-73].

3.4 Experimental Methods for the Stretchable Gas Sensing

3.4.1 Growth of 2D MoS₂ With Vertically-aligned Layers

Ultra-high purity (99.99%) molybdenum (Mo) was deposited (thickness; typically, >8 nm) onto three-dimensionally ordered SiO₂/Si pillars prepared by a standard photolithography process. The Mo deposition was carried out by using an electron beam evaporator (Thermionics VE-100) at a deposition rate of 0.15 \AA s^{-1} . MoS₂ growth was carried out with a single-zone horizontal tube furnace (Lindberg/Blue M) equipped with a one inch-diameter quartz tube. The Mo-deposited pillar substrate was placed at the center of the heating zone with 100 mg of sulfur (S) powder (99.5%, Sigma Aldrich) separately placed at the upstream side. The tube was then pumped down to 1 mTorr base pressure followed by heating up to 650 °C for 30 minutes at a ramping rate of 43 °C min^{-1} . Ultra-high purity argon (Ar) gas (flow rate: 100 SCCM) was supplied throughout the CVD reaction, and the furnace was naturally cooled down to room temperature.

3.4.2 Transfer and Integration Process

A thin layer of PMMA was spin-coated onto the as-grown 2D MoS₂/SiO₂/Si substrate. The PMMA/MoS₂/SiO₂ stack is then cured with normal air at room temperature for one day. The sample is then immersed in water and scratched with a sharp object on the corner edge to facilitate the penetration of water into the sample. The top side of the sample looks different color when water penetrates MoS₂ and SiO₂ interface. The 2D MoS₂/PMMA film was then manually peeled off from the SiO₂/Si substrate and dried by blowing air. The serpentine pattern was made by cutting with a mechanical cutter plotter with the specified dimension to get desired stretchability.

3.4.3 Raman, TEM, and Optical Characterization

Raman characterization was performed using a Renishaw RM 1000B Micro-Raman Spectrometer with a laser wavelength of 514 nm and a spot size of 1 μ m. SEM characterization was performed with a field-emission SEM (SU 8230, Hitachi) equipped with an X-ray energy dispersive spectrometer. TEM characterization was performed with a probe-corrected TEM (ARM200F, JEOL) operating at 200 kV. The optical absorbance of 2D MoS₂ layers/PDMS at varying stretch levels was characterized by UV-Vis spectroscopy (Cary WinUV spectrometer) in the wavelength range of 200–800 nm.

3.4.4 Gas Sensing Characterization

The Gold (Au) electrodes were deposited on the as-patterned 2D MoS₂/PMMA with a serpentine designed shadow mask (0.4 mm width and 0.8 mm gap) with laser cutting. The real-time gas sensing performance was done inside a sealed Acrylic Vacuum Chamber (Sanatron LLC.) with an electrical feed-through as well as a gas inlet and outlet was installed in the chamber. The NO₂ gas was injected inside the gas chamber with a precisely measured syringe injection pump. A commercial NO₂ gas sensor

(DGS Spec Sensor, Part#DGS-NO₂ 968-043) was placed inside the chamber for monitoring precise gas concentration from 5 ppm to 30 ppm. The current(I) vs. time(T) was recorded at a constant voltage of 0-7 volts. The NO₂ gas exposure time was every ten minutes and degassing with N₂ gas connected with the fume hood.

CHAPTER-4: LAYER ORIENTATION CONTROL GROWTH

The contents of this chapter have been published in: Choudhary, N., Chung, H., Kim, J., Noh, C., Islam, M., Oh, K., Coffey, K., Jung, Y. & Jung, Y. “Strain-Driven and Layer-Number-Dependent Crossover of Growth Mode in van der Waals Heterostructures: 2D/2D Layer-By-Layer Horizontal Epitaxy to 2D/3D Vertical Reorientation,” Advanced Materials Interfaces 5, 1800382 (2018).

4.1 Introduction

A large family of 2D vdW heterostructures has recently been developed through various chemical routes [17,74-76] and one of the most explored material systems is 2D molybdenum/tungsten disulfides (MoS_2/WS_2) in vertical stacks [68,77-81]. In order to leverage their desired functionalities, it is essential to tailor the morphological variables of 2D layers during their growth stages, which would only be possible once their underlying growth mechanism is clarified. A large set of parameters that govern the thermodynamic and crystallographic conditions for 2D vdW heterostructure growths remains unclear, [82] leaving following questions to be answered; “How do the subsequent 2D layers grow on top of pre-existing 2D layers, and would it be possible to engineer their crystallographic orientations? If possible, what are the driving factors that determine their growth characteristics, and what would the atomistic structure of the resulting 2D/2D interfaces be?” Experimentally addressing these questions, thereby, clarifying the atomistic growth mechanism of 2D vdW vertical heterostructures is technically challenging for multiple reasons. From the material growth perspective, the controlled integration of secondary 2D layers on top of pre-existing 2D layers is challenging in conventional approaches. For example, despite

some successful demonstrations, [26,83] CVD employing the simultaneous co-reactions of multiple precursors often results in the growth of distinct 2D layers either in a vertically stacked or in a horizontal stitching manner even under identical growth conditions, [18,84,85] making it difficult to establish a unified growth principle. Growths via a sequential CVD of one 2D material after the other have alternatively been explored, [21,27,38,68,86-89] which inevitably requires nontrivial microscopy investigations to visualize the atomistic 2D/2D vdW interfaces. For example, conventional cross-sectional TEM has relied on the physical/chemical milling of 2D/2D vdW interfaces down to the thickness suitable for electron transmission, which is highly sophisticated/demanding and often results in a low success yield. Accordingly, investigating statistically a large number of 2D/2D vdW interfaces in their pristine forms is difficult, thus clarifying the associated 2D growth mechanism and its governing factors remain challenging.

In this chapter, we study the CVD growth mechanism of vertically stacked 2D MoS₂/WS₂ layers and unveil the fundamental factors that dictate the vdW assembly of 2D MoS₂ layers on the basal planes of 2D WS₂ layers. We employ single-crystalline-faceted tungsten trioxide (WO₃) nanowires as a model system that offers distinct advantages over conventional approaches; 1) 2D WS₂ layers are self-assembled from the single-crystalline WO₃ nanowire surface via controlled sulfurization, yielding atomically flat 2D WS₂ basal planes with precisely controlled 2D layer numbers. These morphology-controlled 2D WS₂ layers serve as the growth template for subsequent 2D MoS₂ layers growth. 2) This nanowire-assisted growth scheme enables the direct TEM visualizations of the atomic structures of 2D MoS₂/WS₂ vdW interfaces. Moreover, it circumvents the complicated cross-sectional TEM sample preparation and its associated operation demanded in conventional approaches, thus enables the inspection of a statistically large number of samples. Benefiting from these advantages, we unveil a unique transition of the growth

characteristics in these materials, i.e., a transition from the layer-by-layer epitaxy of horizontally oriented 2D MoS_2 layers to their vertical reorientation akin to the conventional Stranski–Krastanov (SK) thin-film growths, which is driven by varying 2D layer numbers.

4.2 Results and Discussions

4.2.1 Steps in Growth Process

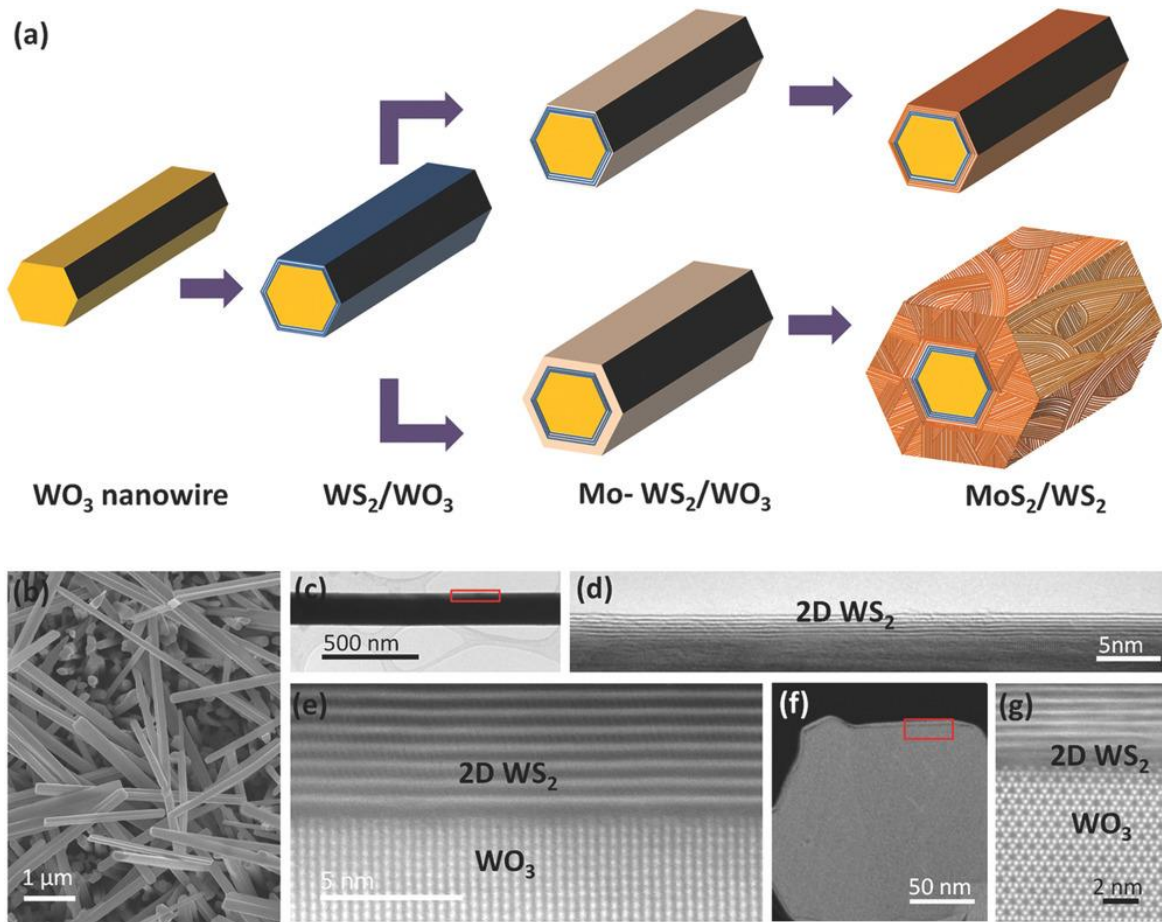


Figure 13: (a) Schematic for 2D MoS_2/WS_2 vdW vertical heterostructure growth experiments. (b) As fabricated 2D WS_2/WO_3 nanowires. (c) Low-magnification TEM image of an isolated nanowire. (d) Magnified view of the red box in (c). (e) ADF STEM image of a 2D WS_2/WO_3 interface. (f) ADF STEM image of a cross-sectioned nanowire. (g) Magnified view of the red box in (f), revealing a 2D WS_2/WO_3 interface.

Figure 13(a) illustrates the growth experiments. Highly single-crystalline hexagonal WO_3 nanowires with faceted surfaces are prepared following a previously developed method [90]. 2D MoS_2/WS_2 vdW vertical heterostructure layers are subsequently grown on the nanowire surfaces in the following sequences. The nanowires are sulfurized by reacting with vaporized sulfur (S), yielding high-crystalline 2D WS_2 layers with well-resolved 2D layers on the nanowire surface. Mo seed films of controlled thickness are subsequently deposited/sulfurized on the grown 2D WS_2 layers, achieving 2D MoS_2/WS_2 vdW vertical stacks. Distinguishable morphologies are observed in the 2D MoS_2/WS_2 vdW vertical stacks with varying 2D MoS_2 layer numbers.

4.2.2 Morphology of the as Grown 2D WS_2/WO_3 Nanowires

Figure 13(b–g) shows the morphologies of the 2D WS_2 layers grown on WO_3 nanowires obtained before the subsequent deposition/sulfurization step in figure 11(a). The scanning electron microscopy image in figure 11(b) of as-prepared 2D WS_2/WO_3 nanowires reveals well-faceted surfaces whose crystalline structures were identified by extensive TEM characterization. Figure 13(c) shows a low-magnification bright-field (BF) TEM image of an isolated 2D WS_2/WO_3 nanowire. Figure 13(d) is the higher magnification view of the red box in figure 13(c), revealing the presence of 2D WS_2 layers on the nanowire surface. The 2D WS_2 layers exhibit excellent crystallinity indicated by the well-defined layer number (5 in this case) without any broken layers throughout the entire length ($\approx 7 \mu\text{m}$). The layer number of the 2D WS_2 converted from WO_3 is highly controllable by adjusting the sulfurization conditions. The crystallinity of the 2D WS_2 layers and their interfaces were further characterized by annular dark-field (ADF) scanning TEM (STEM). Figure 13(e) shows a plane-view ADF STEM image of 2D WS_2 layers on WO_3 (different from figure 13(c and d), revealing an atomically sharp 2D WS_2/WO_3 interface and evenly spaced

2D layers. Figure 13(f) shows an ADF STEM image of a 2D WS₂/WO₃ nanowire cross-sectioned via a focused ion beam, revealing its faceted and smooth surface covered by 2D WS₂ layers throughout its entire periphery. Figure 13(g) shows a high-resolution ADF STEM image corresponding to the red box in figure 13(f), revealing uniform 2D WS₂ layers with an abrupt interface across the WO₃ surface. The image also indicates that the nanowire is oriented along the [001] axis of hexagonal WO₃ [91]. All these TEM characterizations confirm that the 2D WS₂ layers self-assembled from the single-crystalline WO₃ present excellent crystallinity in their vertical layer stacking, which is desirable for the subsequent growth of 2D MoS₂ layers on their basal planes.

4.2.3 Morphology of the MoS₂/WS₂ Heterostructure

Figure 14 compares the morphologies of the 2D MoS₂/WS₂ vdW vertical stacks grown on WO₃ by employing the secondary sulfurization of Mo (various thicknesses) shown in figure 13. Figure 14(a–e) shows the characterization of 2D MoS₂/WS₂ vdW vertical stacks achieved with the sulfurization of ≈ 3 nm thick Mo. The Raman spectroscopy profile (figure 9(a)) of as-prepared 2D MoS₂/WS₂ on WO₃ nanowires confirms the typical in-plane (E_{2g}^1) and out-of-plane (A_{1g}) vibration modes of 2D WS₂ and 2D MoS₂, [92] indicating the formation of compositionally and structurally well-defined 2D MoS₂/WS₂ layers [53]. Figure 14(b) shows an ADF STEM image of a WO₃ nanowire with 2D MoS₂/WS₂ vdW vertical stacks on its surface. The magnified image of the red box reveals distinguishable image contrasts, indicating that the newly grown material (presumably, 2D MoS₂) on 2D WS₂ layers is composed of lighter atomic elements. Figure 14(c) shows the high-resolution ADF STEM image corresponding to the blue box in figure 12(b), revealing the vertical stack of 2D MoS₂/WS₂ layers on the WO₃ surface. Figure 14(d,e) characterizes the detailed

morphologies of the 2D MoS₂/WS₂ and the 2D WS₂/WO₃ interfaces, distinguished by atomic number (Z) contrast.

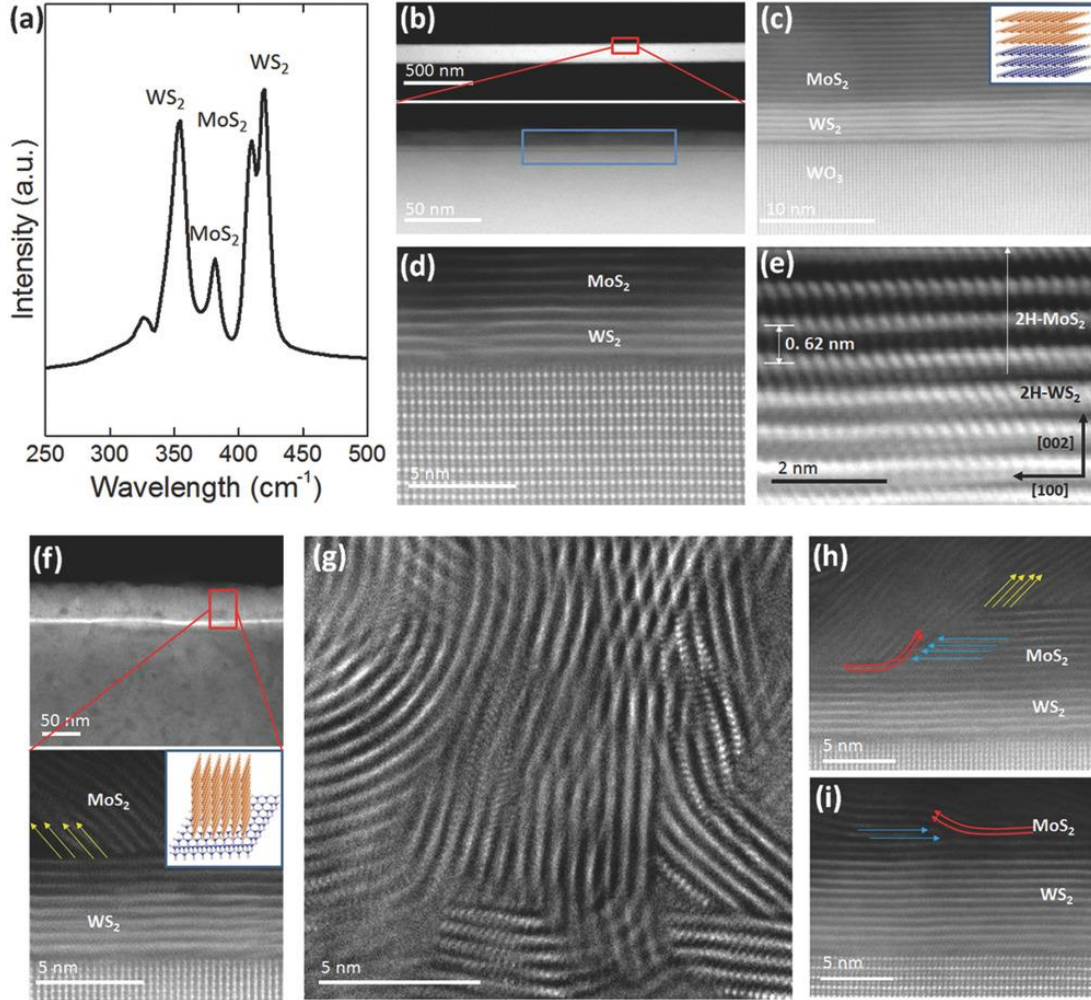


Figure 14: (a) Raman spectroscopy profile obtained from 2D MoS₂/WS₂-grown nanowires. (b–e) TEM characterization of 2D MoS₂/WS₂ vdW vertical stacks obtained by sulfurizing ≈ 3 nm Mo. (b) ADF STEM image of an isolated nanowire. (c) Magnified view of the blue box in (b), revealing 2D MoS₂/WS₂ vertical stacks. (d) ADF STEM image of a 2D MoS₂/WS₂/WO₃ interface. (e) Detailed crystalline structure of the 2D MoS₂/WS₂ interface. (f–i) TEM characterization of 2D MoS₂/WS₂ vdW vertical heterostructures obtained by sulfurizing ≈ 12 nm Mo. (f) ADF STEM image of an isolated nanowire, revealing vertically reoriented 2D MoS₂ layers. (g) Top-down plane-view of high-resolution TEM (HRTEM) image revealing the edges of vertical 2D MoS₂ layers. (h,i) Redirection of horizontal 2D MoS₂ layer orientation interfered by impeaching layers.

2D MoS₂ layers grown on the basal plane of 2D WS₂ layers present a highly uniform interlayer spacing of ≈ 0.62 nm, which well matches the hexagonal [002] planes of MoS₂. Moreover,

the sequence of the individual Mo-S-W atomic bonds, figure 14(e) reveals that both the 2D MoS₂ and 2D WS₂ preserve semiconducting 2H phases across the 2D/2D interface. The localized distribution of constituent elements in each 2D MoS₂ and 2D WS₂ was also confirmed by energy dispersive X-ray spectroscopy in STEM mode. The high crystalline quality of the 2D MoS₂ layers and their atomically sharp interfaces across 2D WS₂ layers are indicative of the vdW epitaxial growth.

4.2.4 Growth Mechanism

2D MoS₂/WS₂ vdW vertical stacks achieved by sulfurizing ≈ 12 nm thick Mo seeds exhibit contrasting growth characteristics (figure 14(f–i)). Figure 14(f) shows an ADF STEM image of 2D MoS₂/WS₂ vdW vertical stacks grown on WO₃, which reveals that 2D MoS₂ layers readjust their layer orientations with respect to those of the underlying 2D WS₂ layers. The magnified view of the red box in figure 14(f) exhibits the vertically slanted 2D MoS₂ layers on the basal planes of 2D WS₂ layers exposing their 2D edge sites on the nanowire surface. Interestingly, such vertically reoriented 2D MoS₂ layers are often observed on the horizontally oriented 2D MoS₂ layers (yellow lines in figure 14(f) grown on the basal planes of 2D WS₂ layers. This observation indicates that 2D MoS₂ layers grow from the interface of the Mo–WS₂ basal plane in a “bottom-to-top” manner under our growth conditions, and detailed growth mechanisms will be discussed in the later section. Figure 14(g) shows a high-resolution BF TEM image obtained from the nanowire surface, revealing the plane view of 2D MoS₂ vertical layers with exposed 2D edges [6]. Figure 14(h, i) shows representative TEM images, revealing a large number of 2D MoS₂ layers redirect their orientations as interfered by other layers impeaching from the opposite sides (blue and red arrows). This growth impediment of horizontal 2D MoS₂ layers and their vertical reorientation were consistently observed with 2D MoS₂/WS₂ vertical stacks obtained by the sulfurization of thick

(typically, ≥ 8 nm) Mo. It is worth mentioning that identifying this unique 2D growth characteristic benefits from our nanowire-based growth scheme as it allows for the direct visualization of 2D/2D interfaces with a large number of samples even without tedious TEM cross-section sample preparations.

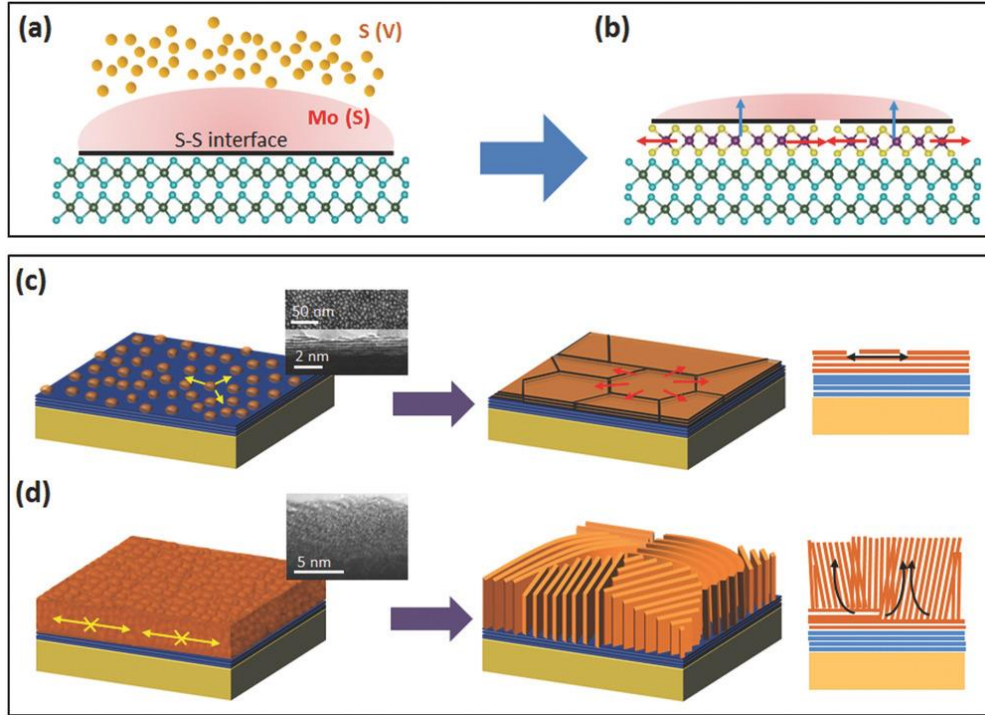


Figure 15: Schematics for the initial growth stage of 2D MoS₂ layers on 2D WS₂ layers. (a) Mo nanoparticles exposing the S–S (Mo–WS₂ basal plane) interface, which provides preferred nucleation sites. (b) Growth of a 2D MoS₂ layer on the interface, exposing another S–S interface for subsequent layer-by-layer growth. Schematics for the distinguishable growth characteristics obtained by sulfurizing Mo of different thicknesses. (c) Layer-by-layer growth of horizontal 2D MoS₂ layers on 2D WS₂ layers achieved by sulfurizing thin Mo. The insets are representative ADF STEM (top) and TEM (bottom) images to show disconnected nanoparticles on the surface of a 2D WS₂/WO₃ nanowire in a top/side view, respectively. (d) SK-like growth of vertically reoriented 2D MoS₂ layers on 2D WS₂ layers, achieved by sulfurizing thick Mo. The inset is a representative TEM image to show the side view of a continuous Mo (≈ 9 nm thickness) on the surface of a 2D WS₂/WO₃ nanowire.

Figure 15 illustrates an overview of the distinguishable growth characteristics observed in our 2D MoS₂/WS₂ vdW vertical stacks. Figure 15(a, b) depicts the initial growth stage of 2D MoS₂

layers forming on the basal planes of 2D WS₂ layers irrespective of Mo thickness. Upon reaching the growth temperature, the deposited Mo forms a droplet (presumably, solid (S) phase given its high melting temperature) on the surface of the solidus 2D WS₂ layers while vaporized (V) sulfur is being supplied. Accordingly, S–S (WS₂–Mo) and V–S (S–Mo) interfaces are newly formed, and their energetics determine the growth preference of 2D MoS₂ layers (figure 15(a)). Although the exact interfacial energy values are presently unavailable in this particular case, it has been theoretically/experimentally confirmed that S–S interfaces present higher interfacial energies over V–S interfaces providing preferred thermodynamic conditions for heterogeneous nucleation, well established in the studies of VS nanowire growths [93-95]. As a result, 2D MoS₂ layers are initiated to grow from the WS₂–Mo interfaces (black line in figure 15(a)) in a horizontal manner, which is driven to minimize the total system energy by exposing their basal planes of low surface energies. Upon their continued growth consuming deposited Mo, additional interfaces of MoS₂–Mo (black line in figure 15(b)) are exposed, offering preferred nucleation sites for subsequent growth. As a result, horizontal layer-by-layer growths of 2D MoS₂ are initially observed on top of 2D WS₂ layers irrespective of Mo thickness of figure 15(c–e) and figure 15(f, i, g), indicative of the “bottom-to-top” growth manner. Figure 15(c-d) illustrates the horizontal-to-vertical cross-over of 2D layer growth characteristics determined by varying Mo thickness. Figure 15(c) describes the growth situation when thin (typically, ≤ 3 nm) Mo is sulfurized on the basal planes of 2D WS₂ layers. Mo films of such a small thickness consist of randomly disjointed tiny Mo nanoparticles with a high density of free volume in between them (inset TEM images). Throughout sulfurization, 2D MoS₂ layers grow in the layer-by-layer manner accompanying a substantive volumetric expansion, i.e., conversion of Mo to MoS₂, which is efficiently accommodated due to the free volume. Accordingly, they continue to grow, filling in the free volume without readjusting layer

orientations. Figure 15(d) describes the growth situation when thick (typically ≥ 8 nm) Mo is sulfurized on the basal planes of 2D WS₂ layers. Depositing Mo to such a thickness results in a dense film composed of Mo nanoparticles that are continuously connected (inset TEM image). The volumetric expansion through the conversion of Mo to MoS₂ accompanies a significant accumulation of internal strain imposed by adjacently growing/impeaching 2D MoS₂ layers due to the limited free volume in between Mo. Accordingly, continuously growing 2D layers are forced to redirect layer orientations in a way to release the strain once they go beyond the initial horizontal growth stage (Figure 15(b)). This 2D growth mode transition is qualitatively understood to result from the competition of interfacial energy and lattice mismatch (strain energy) between the growing material (2D MoS₂) and its substrate (2D WS₂). The 2D MoS₂/WS₂ interface with horizontal 2D layers is expected to have a lower interfacial energy than that with vertical 2D layers owing to the very small lattice mismatch of $\approx 0.25\%$ (in-plane lattice for MoS₂ is $a = 0.3161$ nm and that for WS₂ is $a = 0.3153$ nm) [96,97]. Moreover, the horizontal/horizontal interface coherency advantage is anticipated to be small due to the weak vdW bonding present across the interface and the clean basal plane of 2D WS₂ layers without significant dangling bonds. Accordingly, the 2D MoS₂/WS₂ interface with horizontal 2D layers is thermodynamically favored over that with vertical 2D MoS₂ layers whose formation is driven by strain energy relaxation. With increasing physical confinement, the coherency of 2D MoS₂ layers with the epitaxial 2D WS₂ layer breaks down. The transition of the layer orientation in 2D MoS₂ is akin to the Stranski–Krastanov (SK) thin film growth mode in which strain energy dominates (owing to the epitaxial lattice misfit) for thicker layers [98]. Accordingly, the relaxation of the strain energy built up during 2D layers growth guides their orientation and determines the growth mode, which is dictated by the thickness of Mo (thus, 2D MoS₂ layer number), as verified below. It is noteworthy that the vertical 2D MoS₂

layers exposing dangling bonds present larger surface energy than horizontal 2D MoS₂ layers, as demonstrated by density functional theory calculations [99,100]. The horizontal-to-vertical transition of 2D layer orientations efficiently compensates for the increased surface energy by relaxing the generated strain energy, thus lowers the total system energy.

4.3 Conclusion

In conclusion, by employing single-crystalline WO₃ nanowires as a model system, we investigated the CVD growth mechanism of 2D MoS₂/WS₂ vdW vertical stacks with controlled layer orientations. We identified that their growth characteristics transit from 2D/2D layer-by-layer horizontal epitaxy to 3D-like vertical SK mode, which strongly depends on the number of 2D MoS₂ layers. This study greatly deepens our understanding of the growth principle of 2D vdW solids and has an important implication for their technological developments.

CHAPTER-5: HETEROSTRUCTURES INTEGRATION

The contents of this chapter have been published in: M. A. Islam, J. H. Kim, A. Schropp, H. Kalita, N. Choudhary, D. Weitzman, S. I. Khondaker, K. H. Oh, T. Roy, H.-S. Chung, and Y. Jung, Centimeter-Scale 2D van der Waals Vertical Heterostructures Integrated on Deformable Substrates Enabled by Gold Sacrificial Layer-Assisted Growth. Nano Letters, 2017, 17, 6157–6165.

5.1 Introduction

To broaden the scientific/technological versatilities for scaled-up flexible/stretchable technologies, there are few challenges need to be addressed for the material preparation and integration of 2D MoS₂/WS₂: (1) They should be grown on a large wafer-scale with controlled layer chemistries/morphologies, and the growth methods should be intrinsically scalable. (2) They should present mechanical flexibility either by being directly grown on flexible substrates or being transferred onto secondary flexible substrates. (3) If transferred, they should maintain the structural/chemical integrities of their original as-grown states. Accordingly, it is critically demanded to develop a reliable strategy to universally satisfy all the aforementioned growth/transfer requirements on a wafer-scale for the current microelectronics manufacturing processes. The conventional approaches to manually exfoliate/ stack up individual 2D TMD layers suffer from very small areas of transferred layers and thus remain non-scalable [26,32,83,101-108]. The CVD growths based on the co-evaporation/reaction of metal- and/or chalcogen-containing precursors generally produce materials with limited spatial coverages and nonuniform morphologies[18,22,81,84,109]. Besides unsatisfactory growths, a reliable lift-off/transfer of the as-grown 2D vdW heterostructure layers from their growth substrates (mostly

SiO₂) to secondary substrates is another major challenge. The separation of 2D TMD heterostructure layers from their SiO₂/Si growth substrates has generally involved the direct chemical etching of the SiO₂ using acid/base agents such as buffered oxide etchant (BOE) or potassium hydroxide (KOH) [87,110]. This chemical agent-based etching becomes particularly problematic when the size of the 2D TMD layers to be transferred increases as a large amount of time is demanded for the complete etching of SiO₂ by interpenetrating 2D TMD/SiO₂ interfaces. For example, ~six hours of SiO₂ etching has been reported for CVD-grown vertically stacked MoS₂/ WSe₂ of $>2 \times 2 \text{ cm}^2$ [110]. The prolonged exposure of 2D TMDs to the strong chemical agents is known to deteriorate their material properties, motivating the exploration of alternative methods [33,35,111-114]. Besides the growth/transfer challenges, it is highly desirable to directly integrate large-scale 2D layers on mechanically flexible dielectric materials (mostly thin-film oxides), as demanded in a variety of scaled-up flexible electronic devices.

In this chapter, we report a viable strategy to directly integrate centimeter-scale 2D TMD vdW heterostructures on “transferable substrates” in stacks of SiO₂/Au layers and their facile transfer to arbitrary substrates without using strong chemical agents. Motivated by the enhanced debonding nature of Au interfaced with SiO₂ inside water, we achieved a reliable lift-off and successful transfer/integration of vertically stacked, few-layer only 2D MoS₂/WS₂ vdW heterostructures on secondary substrates over an area of $>2 \times 2 \text{ cm}^2$. Furthermore, by exploring the multi functionalities of Au as sacrificial layers and growth substrates, we demonstrate a large-area photo-responsive 2D MoS₂/SWNT vertical heterojunctions on flexible substrates. This study opens a new pathway for the transfer/integration of 2D TMDs heterostructure and their flexible device applications.

5.2 Results and Discussions

5.2.1 Growth and Gold Assisted Transfer Approach

Figure 16 illustrates the sequential process for the growth and transfer/integration of 2D MoS₂/WS₂ heterostructure layers as follows: (a) On top of a cleaned SiO₂/Si substrate, thin layers of Au and SiO₂ are sequentially deposited followed by a deposition of W and Mo seed layers. (b) The prepared stack is sulfurized in a low-pressure CVD chamber, which leads to a chemical conversion of Mo/W to 2D MoS₂/WS₂ layers.

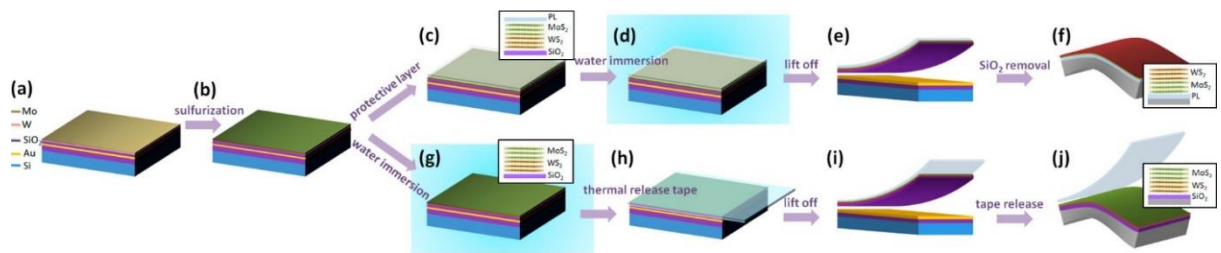


Figure 16: Illustration for the large-area growth of vertically stacked 2D MoS₂/WS₂ heterostructure layers on a SiO₂/Au-based substrate and their subsequent transfer and integration in two different ways.

Following this material growth stage, two different transfer/integration approaches can be independently pursued. In the first approach (figure 16(c-f)). (c) A thin protective layer (PL) such as PMMA or PDMS) is spin-coated on top of the 2D MoS₂/WS₂ layers. (d) The entire substrate is immersed in water, which leads to a simple lift-off of the PL/MoS₂/WS₂/SiO₂ layer-only owing to the debonding nature of Au interfaced with SiO₂ (details are to be explained below). (e) The PL/MoS₂/WS₂/SiO₂ stack is mechanically peeled off/exfoliated from the growth substrate. (f) The separated stack is transposed upside down onto a second substrate after the removal of SiO₂, where the PL functions as an adhesion material. In the second approach (figure 16(g-j)): (g) As-prepared 2D MoS₂/WS₂ layers grown on a SiO₂/Au/Si substrate are immersed in water. (h) Once removed from the water bath and air-dried, the top of the samples is covered with a thermal release tape. (i) The tape is

mechanically lifted, which leads to the separation of the 2D MoS₂/WS₂/SiO₂ layer supported by the tape.

(j) Upon the attachment of the 2D MoS₂/WS₂/SiO₂ layer onto a second substrate, the tape is released under heating at 130 °C[115]. This direct growth of 2D heterostructure layers on such transferrable substrates offers distinct advantages over conventional 2D layer transfer methods; 2D layers can retain the structural integrities of their as-grown states during the lift-off/transfer processes since the underlying growth substrate (SiO₂ layer) itself is directly transferred rather than it is etched away.

5.2.2 Morphology of the as-grown 2D MoS₂/WS₂ heterostructures

The quality of as-grown 2D MoS₂/WS₂ heterostructures was verified by extensive structural characterizations. Figure 17(a) shows a photograph of as-grown 2D MoS₂/WS₂ on the substrate, exhibiting a uniform color homogeneity over the entire substrate surface of $>2 \times 2 \text{ cm}^2$. Figure 17(b) shows the Raman spectrum collected from the same sample, exhibiting four distinct peaks associated with the in-plane E_{2g}¹ and the out-of-plane A_{1g} phonon vibration modes of individual 2D MoS₂ and 2D WS₂ layers[12,68]. The Raman spectrum does not display an indication of Mo_xW_{1-x}S₂, whose peaks are to be poised in between the peaks for individual MoS₂ and WS₂ [53,116,117], which suggests that the sample is mostly unalloyed within its thickness ($>10 \text{ nm}$). The detailed morphology of the 2D MoS₂/WS₂ heterostructure layer was characterized by TEM analysis. Figure 17(c) is a bright-field low-magnification TEM micrograph of the 2D MoS₂/WS₂ heterostructure, revealing its polycrystalline structure and continuous layer morphology. Figure 17(d) shows an HRTEM micrograph of the same sample. The image clearly reveals Moiré patterns, indicative of the vertical stacking of multiple 2D layers whose basal planes are misaligned with respect to the hexagonal [001] zone axis. Figure 17(e) is an energy-dispersive X-ray spectroscopy (EDS) elemental mapping image of the same sample characterized in a scanning TEM (STEM) mode. The image exhibits a highly uniform spatial

distribution of all constituent components of Mo, W, and S. Furthermore, the same sample was inspected by cross-sectional TEM characterizations.

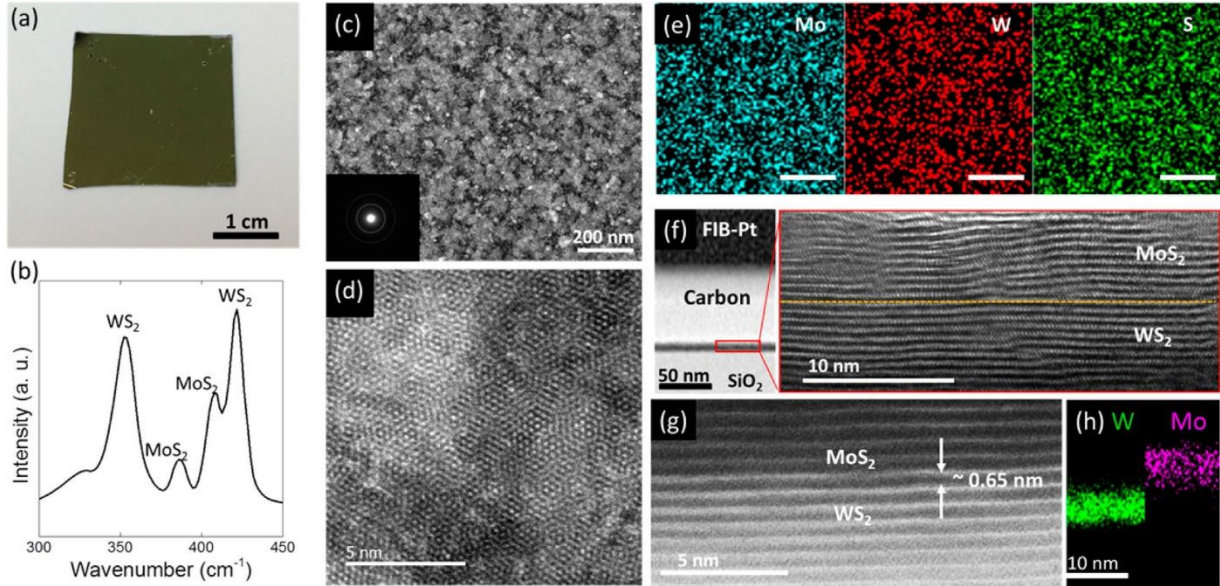


Figure 17: Morphology of the as-grown 2D MoS₂/WS₂. (a) Image of as-grown 2D MoS₂/WS₂ heterostructure layers on a SiO₂/Au/SiO₂/Si substrate. (b) Raman spectrum obtained from the sample, revealing the presence of both MoS₂ and WS₂. Low-magnification TEM (c) and a HRTEM (d) micrographs of the 2D MoS₂/WS₂ heterostructure layers in plain view. (e) STEM-EDS elemental mapping images revealing the uniform spatial distribution of constituent elements. The scale bar is 50 nm. (f) Cross-section TEM characterizations of 2D MoS₂/WS₂ heterostructure layers on a SiO₂ (left) and their detailed crystalline structures (right). (g) ADF-TEM image of the corresponding MoS₂/WS₂ interface, revealing a distinct image contrast. (h) STEM-EDS elemental map to show the spatial localization of Mo and W at the interface.

Figure 17(f) shows TEM micrographs of a cross-sectioned 2D MoS₂/WS₂ heterostructure grown on top of a SiO₂ layer (left). The HRTEM image (right) reveals the vertical stacking of 2D MoS₂ and 2D WS₂ layers, where each material consists of ~10 horizontal atomic layers with a well-defined MoS₂/WS₂ interface (yellow dotted line). Figure 17(g) shows an annular dark-field (ADF) TEM micrograph of the corresponding MoS₂/WS₂ interface. The distinct ADF image contrast between the MoS₂ and the WS₂ reflects the mass difference of constituting W and Mo. The observation is consistent with the spatial distribution of Mo and W as confirmed by the STEM-EDS elemental mapping in figure

2(h), indicating the vertical stacking of 2D MoS₂ and 2D WS₂ layers. All of these comprehensive structural/chemical characterizations evidence the successful CVD growth of large-area, vertically stacked 2D MoS₂/WS₂ heterostructure layers on top of the SiO₂ deposited Au/SiO₂/Si substrate. The direct growth of 2D MoS₂ (or, 2D WS₂) on a secondarily SiO₂ surface has previously been demonstrated via metal-organic CVD (MOCVD), which further strengthens the validity of our approach. Moreover, to ensure the lateral layer-by-layer growth of each constituent material avoiding the unwanted random vertical/slanted growth of 2D layers,[68] we performed our CVD growths with uniformly deposited metal seeds of small thickness (typically, ~4–6 nm). We also carried out the sequential growth of one material on the other via a two-step CVD process;[81,118] that is, growth of 2D WS₂ followed by 2D MoS₂ or vice-versa, and did not notice any significant distinction in the resulting morphology. Details for growth conditions can be found in the Experimental Methods section.

5.2.3 Structural and Electrical Characterizations

Figure 18(a-e) illustrates the transfer of CVD-grown vertically stacked 2D MoS₂/WS₂ heterostructure layers, which corresponds to the approach in figure 18(c-f). (a) PL (PDMS in this case)-covered 2D MoS₂/WS₂ heterostructure layers grown on a SiO₂/Au/SiO₂/Si substrate is immersed in water. (b–c) After the water immersion, the PL/MoS₂/WS₂/SiO₂ stack becomes readily detachable from the underlying Au layer and is ready for lift-off after taken out of the water bath. (d) The PL/MoS₂/WS₂/SiO₂ layer is manually peeled off from the growth substrate. (e) After the lift-off, the original growth substrate is found to be still covered with the Au layer which visibly remains intact. (f) The detached PL/MoS₂/WS₂ layer is observed to be covered with SiO₂ on its backside, indicating that the layer separation occurs at the SiO₂/Au interface. This observation suggests that the detached 2D MoS₂/WS₂ heterostructure layer retains its structural integrity as it was protected in between the PL and the SiO₂ layer during the entire lift-off process. The detached PL/MoS₂/WS₂ heterostructure layer is

highly flexible even with the SiO₂ layer attached on its backside (Figure 18(d)) and can be integrated onto secondary substrates. Figure 18(g) demonstrates the direct integration of the detached layer (on the surface of a cup following removal of the underlying SiO₂ layer). The PL (PDMS in this case) itself functions as an adhesive material that enables the sticking of the 2D WS₂/MoS₂ heterostructure layer on the foreign substrates. The dotted line in figure 18(g) indicates that the integrated layer well retains the original shape/size of its as-lifted state which corresponds to figure 18(f). Figure 18(h) demonstrates the integration of another 2D MoS₂/WS₂ heterostructure layers prepared by the transfer approach in figure 18(g-j); as-grown 2D MoS₂/WS₂ heterostructure layers on Au/SiO₂/Si substrate are separated by a thermal release tape, following the removal of SiO₂. The 2D MoS₂/WS₂ heterostructure layers supported by the tape are integrated onto a foreign substrate (PDMS in this case), followed by a release of the tape under heating. The image reveals the optical transparency of the integrated 2D heterostructure layers similar to figure 18(g). It is worth mentioning that the complete removal of the SiO₂ in these layers (figure 18(g-h)) before their integration is significantly easier/faster than the conventional SiO₂ etching-based lift-off approaches as the entire SiO₂ surface is exposed unlike that it is embedded in between 2D heterostructure layers and Si[110]. The success of this facile/reliable 2D layer separation at the SiO₂/Au interface in water is attributed to the intrinsic debonding nature of Au [119-121]. It has been known that the interfacial adhesion energy for Au interfaced with SiO₂ is lower than most of the noble metals. In air, the adhesion energy is $\sim 0.4 \text{ J/m}^2$ for Au/SiO₂, while it is $>3 \text{ J/m}^2$ for titanium (Ti), a material that has been widely used to increase the contact adhesion of Au onto SiO₂ surface. The interfacial adhesion energy is $\sim 1.3 \text{ J/m}^2$ for nickel (Ni) which is also well-known for its weak adhesion to SiO₂[120,121]. Moreover, it has been reported that water penetration drastically reduces the interfacial energies for metal/SiO₂ interfaces. For instance, $\sim 80\%$ of lower interfacial energy

has been reported for Ni/SiO₂ in water compared to in the air, and this trend is valid regardless of metals interfaced with SiO₂[120].

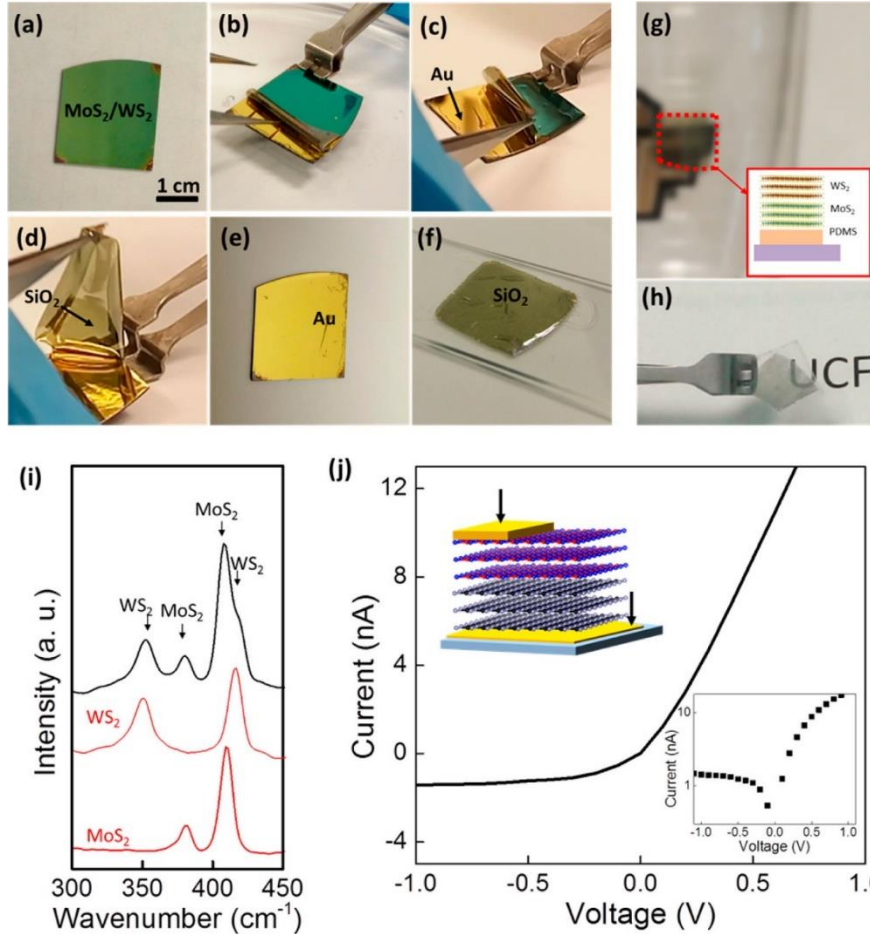


Figure 18: Sequential procedures for the transfer of 2D MoS₂/WS₂ heterostructure layers using the water-assisted Au-SiO₂ separation (a-h). (g) PDMS-coated 2D WS₂/MoS₂ heterostructure layers integrated on the surface of a cup. (h) 2D MoS₂/WS₂ heterostructure layers on a PDMS transferred from a thermal release tape. (i) Raman spectrum from 2D MoS₂/WS₂ heterostructure layers in comparison to the Raman spectra from individual 2D MoS₂ and 2D WS₂. (j) Transport characteristics of transferred 2D MoS₂/WS₂ heterostructure layers.

The structural integrities of 2D MoS₂/WS₂ heterostructure layers detached from their growth substrates were characterized and confirmed by Raman spectroscopy. The black plot in figure 18(i) shows a Raman spectrum from the separated 2D MoS₂/WS₂ heterostructure layers before the integration, figure 18(h), revealing the Raman peaks assigned to individual MoS₂ and WS₂. The Raman spectra (red

plots) obtained from individual MoS₂ and WS₂ layers grown under the same growth condition are presented for comparison. Figure 18(j) shows two-terminal carrier transport characteristics of transferred 2D MoS₂/WS₂ heterostructure layers where top/bottom metal (Au) electrodes are separately made on each material (schematic in figure 18(j), upper inset). The plot reveals a non-Ohmic rectifying transport (also, a semilogarithmic plot in figure 18(j), lower inset) confirming the presence of 2D MoS₂/WS₂ heterojunctions with band offsets, consistent with previous observations.

5.2.4 Feasibility of Gold (Au) as a Growth Substrate

In addition to the functionality as a SiO₂-sacrificial layer, we explore the feasibility of Au as a growth substrate for 2D TMD layers. To demonstrate these multi functionalities of Au, we directly grew 2D MoS₂ layers on top of Au/SiO₂/Si substrates and transfer the grown layers. Figure 19(a) illustrates the growth to- transfer procedure; 2D MoS₂ is grown on top of an Au/SiO₂/ Si substrate by the direct sulfurization of Mo, and the substrate is subsequently immersed in water. Once the substrate is removed from the water bath and is dried, a thermal release supporting tape is attached to the 2D MoS₂ layers on the substrate, and it is mechanically peeled off leading to the separation of Au-attached 2D MoS₂ from the substrate. The Au on the 2D MoS₂ can be removed resulting in 2D MoS₂ layers integrated on the tape, or the entire 2D MoS₂/Au layers can be integrated onto secondary substrates. Figure 19(b) shows an optical image of 2D MoS₂ layers directly grown on Au deposited SiO₂/Si substrates. The 2D MoS₂ layers were grown on the selected areas only where Mo films were pre-deposited, presenting different colors depending on the thickness of initial Mo (3 and 10 nm for left and right, respectively). Figure 19(c) shows Raman characteristics from the 2D MoS₂ layers directly grown on Au-deposited substrates revealing that the intensity ratio of E_{2g}¹/A_{1g} increases with decreasing the thickness of initial Mo films, consistent with previous growth studies with SiO₂/Si substrates[5]. Figure 19(d) shows a cross-sectional

ADF-TEM micrograph of a stack of 2D MoS₂/Au/SiO₂, and the zoomed-in image (red box) reveals that 2D MoS₂ (~8–10 layers) was grown on top of Au on a large area, obtained from 3 nm thick Mo deposition. Figure 17(e) is an ADF-TEM micrograph of a 2D MoS₂/Au interface, which reveals the atomically sharp MoS₂/Au interface and well-resolved 2D MoS₂ layers. STEM-EDS elemental mapping analysis does not indicate a noticeable interdiffusion of Au into the 2D MoS₂ layers.

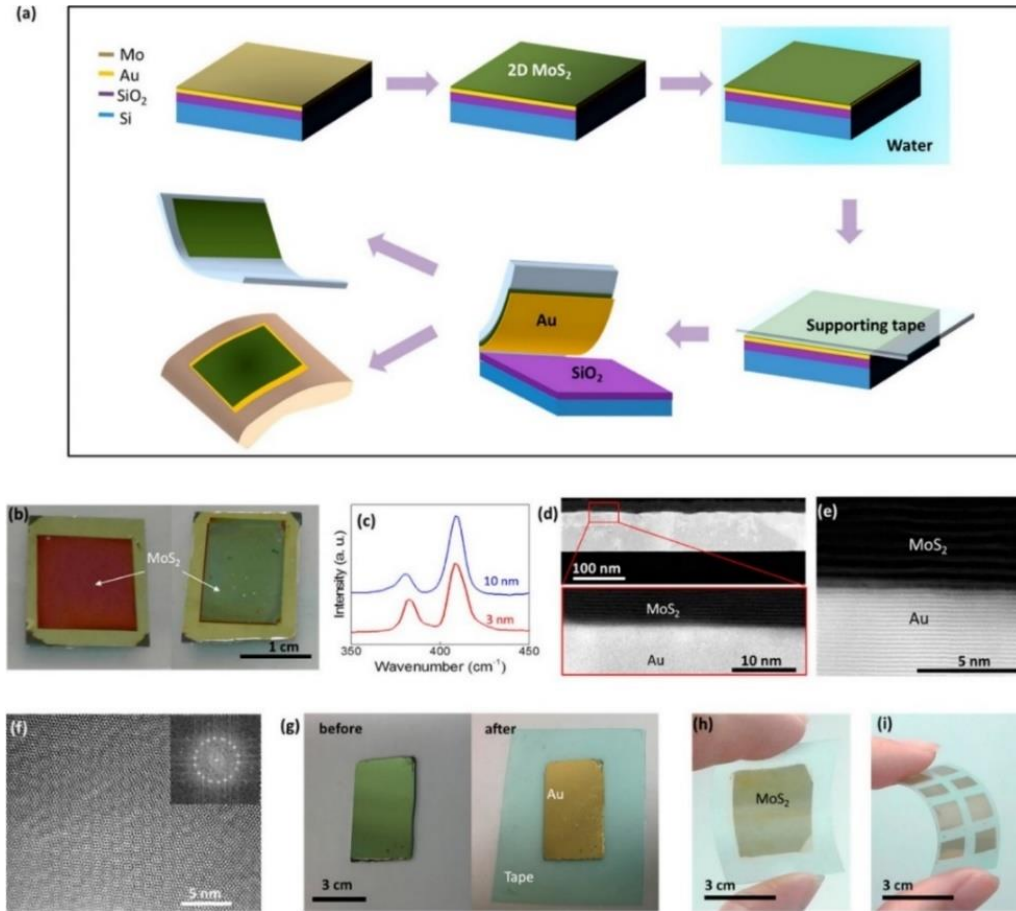


Figure 19: (a) Illustration for the direct growth of 2D MoS₂ layers on Au-deposited substrates and their subsequent transfers. (b) Images of 2D MoS₂-grown on Au/SiO₂/Si substrates. 2D MoS₂ are selectively grown with Mo of different thicknesses (left: 3 nm, right: 10 nm). (c) Raman spectrum obtained from the 2D MoS₂ layers grown on in panel b. (d) Cross-sectional ADF-TEM micrographs of 2D MoS₂ grown on an Au/SiO₂/Si substrate. The zoom-in image (red box) reveals the growth of continuous 2D MoS₂ layers. (e) ADF-TEM micrograph revealing the sharp 2D MoS₂/Au interface. (f) A plane-view of an HRTEM micrograph of few-layer 2D MoS₂ layers revealing Moiré patterns. (g) 2D MoS₂/Au before (left) and after (right) integration to a supporting tape. (h) Large-area 2D MoS₂ layers attached to a supporting tape. (i) Patterned 2D MoS₂ layers attached to a supporting tape.

Figure 19(f) shows a plane view HRTEM micrograph of 2D MoS₂ layers obtained from growth on Au-deposited SiO₂/Si substrates, different samples from figure 19(d, e). The image reveals Moiré patterns resulting from the vertical stack of multiple 2D MoS₂ layers, while the fast Fourier transform (FFT) image (inset) corresponding to the HRTEM indicates ~3–5 layers of 2D MoS₂[122]. All of these structural characterizations indicate that Au-deposited SiO₂/Si substrates function as excellent growth substrates while their potential as sacrificial layers for facile 2D layer transfers has already been proved. Figure 19(g) shows the images of as-grown 2D MoS₂ on the Au/SiO₂/Si substrate (before) and the same sample transferred/attached to a document tape (after). Figure 19(h-i) shows images of large-area (>3 cm²) and patterned 2D MoS₂ attached to supporting tapes, respectively, demonstrating their mechanical flexibility.

5.2.5 Flexible MoS₂/CNT Device Integration

To verify the versatility of the Au-assisted transfer and its applications to 2D electronics/optoelectronics, we demonstrate large-area, heterojunction devices based on vertically stacked single-walled carbon nanotube (SWNT) thin films and 2D MoS₂/Au layers. Figure 20(a) illustrates a schematic for the device fabrication; 2D MoS₂/Au layers are integrated on a secondary conductive and flexible substrate, for example, copper (Cu) foil. Subsequently, highly dispersed p-type sorted SWNTs (>99% semiconducting) are directly integrated on the surface of 2D MoS₂ layers, following the selective opening of MoS₂ via the PDMS window. As a result, large-area SWNT/2D MoS₂ vertical heterojunctions are realized where top/bottom electrodes are directly made onto the SWNT and the backside of the Cu foil, respectively, figure 20(b). Figure 20(c) shows a representative image of a large-area vertically stacked 2D MoS₂/Au layers integrated on a thin flexible Cu foil prior to the deposition of PDMS and SWNTs. The assembled SWNT/2D MoS₂ vertical heterojunctions were electrically characterized. Figure 20(d) shows the current

density (J)-voltage (V) characteristics of a representative SWNT/2D MoS₂ heterojunction on a Cu foil. Current rectification with asymmetric J–V is clearly observed (semilogarithmic plot in figure 20(d), inset), which is consistent with the recent observation with laterally stacked SWNT/2D monolayer MoS₂ p–n junction diodes[123]. The rectification ratio, that is, the ratio of forward-to-reverse current amplitude reaches ~ten, which is slightly smaller than the value reported with the micrometer-sized SWNT/2D MoS₂ lateral junction without gate voltages[123]. The vertically stacked SWNT/2D MoS₂ heterojunction devices exhibit substantive photoresponse under the illumination of white light. Figure 20(e) shows the semilogarithmic I–V characteristics of another device, different from figure 20(d) in the reverse bias regime with/without an illumination, revealing a significant photocurrent generation (i.e., $\times \sim 4\text{--}5$ increase of reverse current). We investigate the origin of the observed current rectification and photoresponse by exploring the exclusive role of the SWNT/2D MoS₂ heterojunction on carrier transport properties. Two-terminal current–voltage (I–V) characteristics of individual SWNT film and 2D MoS₂ layers without the heterojunction in the dark and under illumination are presented. The plots reveal symmetric I–V characteristics from both the materials and some photoresponse (i.e., current increase of ~ 1.3 times) in the 2D MoS₂ with a negligible current change in the SWNT. This observation confirms that the current rectification and significant photocurrent observed with the vertically stacked SWNT/2D MoS₂ device indeed originate from the vertical SWNT/2D MoS₂ heterojunction. The energy band structure of the heterojunction in figure 20(g) illustrates the underlying mechanism. The band diagram is constructed based on that the bandgap energy (E_g) of p-type pure SWNT is ~ 0.6 eV with a diameter of ~ 1.7 nm used in this study, smaller than E_g of MoS₂, which is intrinsically n-type [124]. The diagram presents a presence of type II-like band offsets responsible for relaxing the photogenerated electron-hole (e^-h^+) pairs, which subsequently diffuse across the heterojunction,

resulting in photocurrent. The recombination of charge carriers may be present caused by various mechanisms, for example, series/interfacial resistance, limiting the charge transport as reflected by the smaller rectification ratio compared to the previous lateral SWNT/2D MoS₂ heterojunction[123].

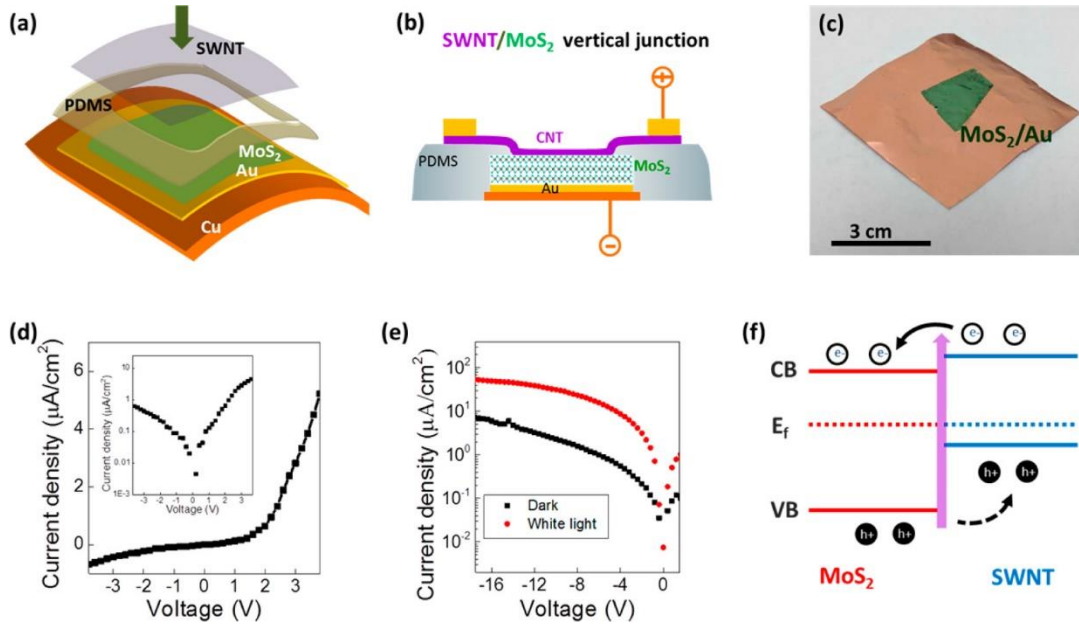


Figure 20: Flexible device integration process. (a) Schematic for the fabrication of a vertically stacked SWNT/2D MoS₂ heterojunction integrated on a flexible Cu foil. (b) Side-view illustration of a vertically stacked SWNT/2D MoS₂ heterojunction configured for electrical characterizations. (c) Image of 2D MoS₂ /Au layers integrated on a Cu foil. (d) The J–V characteristics from an SWNT/2D MoS₂ heterojunction showing current rectification and the corresponding semilogarithmic presentation (inset). (e) Photoresponse characteristics from an SWNT/2D MoS₂ heterojunction. (f) Energy band diagram of SWNT/2D MoS₂ heterojunction depicting the separation/diffusion of photocarriers generated under light illumination (purple arrow). CB, VB, and E_f represent the conduction band, valence band, and Fermi energy, respectively.

It is worth emphasizing that the SWNT/2D MoS₂ heterojunctions achieved in this study are significantly larger ($\sim\text{cm}^2$) than previous studies ($\sim\mu\text{m}^2$) and are in a vertical geometry. These attributes are more preferred for 2D optoelectronics since the diffusion length for photogenerated carriers can become very small as it corresponds to the vertical height of SNWT/2D MoS₂ layers. Further optimizations of material processing and integrations are needed to realize this advantage. Overall, all

of these demonstrations of 2D layer transfers and their applications strengthen the generality and the versatility of the Au-mediated 2D layer separation benefiting from the water-assisted debonding of Au with SiO₂. We also note that a long time (>a few hours) for water immersion often results in a more spontaneous separation of 2D MoS₂ layers from the underlying Au despite their strong adhesion properties, which offers additional advantages for the deterministic separation of 2D MoS₂ layers[125,126]. It is also worth mentioning that Au has recently drawn attention as a growth substrate for various 2D TMDs owing to its low reactivity with sulfur and low solubility with metals (Mo and W)[127]. It has been used in the forms of a foil or a deposited layer, which further strengthens the significance and the versatility of our study[111,125,127-130].

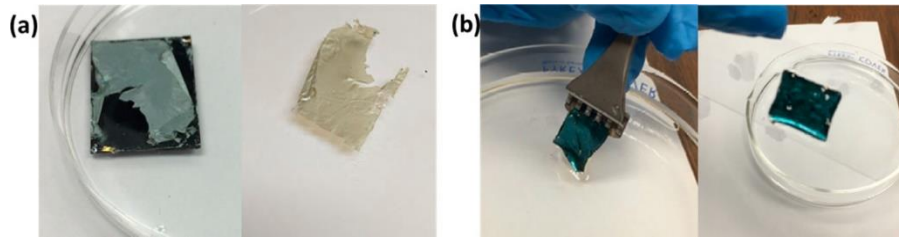


Figure 21: Comparison of growth approaches. (a) BOE-based separation of 2D MoS₂-PMMA layer, which took ~51 min (left), resulting in partially peeled-off 2D MoS₂ layers (right). (b) Water-based separation of 2D MoS₂/Au-PMMA layer, which took ~3 min (left), resulting in clean transfer (right). Both of the samples were prepared under identical experimental conditions.

Lastly, we demonstrate the comparison of the water-assisted Au-mediated transfer with the conventional BOE-based approach to verify/highlight its inherent advantage of faster and cleaner layer separation. In figure 21, we compare the transfer of 2D MoS₂ layers grown on SiO₂ (figure 21(a)) and Au (figure 21(b)) prepared under identical growth conditions (i.e., equal sample size, Mo film thickness, and growth temperature). The results show that the Au-mediated approach takes a significantly shorter time (~3 min vs. ~51 min) in separating 2D MoS₂ layers while better maintaining the structural integrity of their as-grown state.

5.3 Conclusions

In conclusion, we have demonstrated a CVD growth of vertically stacked 2D MoS₂/WS₂ vdW heterostructure layers on SiO₂/Au-based substrates and their direct transfer onto foreign substrates facilitated by the water-assisted debonding of SiO₂/ Au interfaces. This uniquely combined growth/transfer strategy is highly scalable, enabling that 2D TMD layers retain their structural integrity up to a centimeter-scale. As a proof-of-concept, large-scale SWNT/2D MoS₂ vertical heterojunctions are presented, which are difficult to achieve with conventional 2D layer stacking approaches. This study is believed to accelerate the exploration of 2D TMD heterostructure layers for device building-blocks in emerging flexible electronics and optoelectronics.

CHAPTER-6: VERTICALLY-ALIGNED 2D MoS₂ FOR HUMIDITY SENSING

The contents of this chapter have been published in: Islam, M., Kim, J., Ko, T., Noh, C., Nehate, S., Kaium, M., Ko, M., Fox, D., Zhai, L., Cho, C., Sundaram, K., Bae, T., Jung, Y., Chung, H. and Jung, Y. (2018). Three-dimensionally ordered 2D MoS₂ vertical layers integrated on flexible substrates with stretch-tunable functionality and improved sensing capability. Nanoscale, 10(37), pp.17525-17533.

6.1 Introduction

2D TMDs with vertically-aligned layers exhibit numerous atomic dangling bonds on their 2D layer edge sites, which are predominantly exposed on the surface [5,6,87,88]. As a result, they are projected to exhibit superior chemical and/or physical adsorption-driven surface reactivity offering uniquely suited advantages for a wide range of applications such as chemical and electrochemical sensing [29,131-136]. In fact, it has been experimentally verified that they present significantly improved sensitivity for detecting various chemical species compared to the 2D TMD basal planes of atomically saturated bonding [99,137]. 2D layer-orientation dependent properties and associated advantages can be further promoted as far as 2D TMDs with controlled layer orientation and structures can be integrated onto unconventional substrates of tailored functionalities. For instance, horizontally-orientated 2D TMDs and their heterostructures have been explored for a variety of flexible electronic and optoelectronic devices that benefit from the high tolerance for the mechanical deformation of 2D layers and underlying substrates [39,138]. The material properties of the 2D layers in such devices can be externally modulated *via* mechanical inputs such as bending and stretching, offering interesting

multi-functionalities [139-142]. Similar conceptual advantages are projected for 2D TMDs with vertically-aligned 2D layers with their integration onto unconventional substrates, particularly mechanically flexible ones. In this endeavor, the reliable transfer of the as-grown 2D TMD layers from the original growth substrates to the secondary substrates is a prerequisite, which should precisely maintain the 2D vertical layer orientation on a large scale. Moreover, the geometry of 2D TMDs with vertically-aligned layers should be engineered and tailored in a particular configuration to satisfy targeted functionalities demanded in projected applications. Extensive efforts have been devoted to the transfer and integration of horizontally-orientated 2D TMDs on flexible substrates for electronic and optoelectronic applications [23,101,143,144]. However, integrating 2D TMDs with vertically-aligned layers for flexible devices and their structural engineering has been largely unexplored, mainly due to the difficulty associated with their reliable transfer and integration on a large scale. Moreover, studies on their projected multi-functionalities under mechanical deformation and potential for technological applications have remained unavailable until now.

In this chapter, we report the integration of three-dimensionally ordered 2D TMDs with vertically-aligned layers onto flexible substrates and explored their technological multi-functionality and feasibility. We first demonstrate a large-area ($>2\text{ cm}^2$) CVD growth of 2D molybdenum disulfide (2D MoS₂) layers in a three-dimensionally ordered pillar form and confirm the vertical orientation of constituent 2D layers. We then transfer and integrate the entire vertically-aligned 2D MoS₂ layers onto PDMS substrates using water without involving any other chemicals. This water-assisted layer transfer precisely preserves the original structural integrity of vertically-aligned 2D MoS₂ layers, confirmed by Raman spectroscopy and electron microscopy characterization. These three-dimensionally ordered vertical 2D MoS₂ layers integrated on flexible substrates exhibit highly tunable optical absorption and surface wettability upon mechanical stretching. Moreover, they present significantly improved

sensitivity for water molecule detection compared to conventional horizontally-aligned 2D MoS₂ layers even under significant mechanical bending.

6.2 Results and Discussions

6.2.1 Growth and Water Assisted Transfer Process

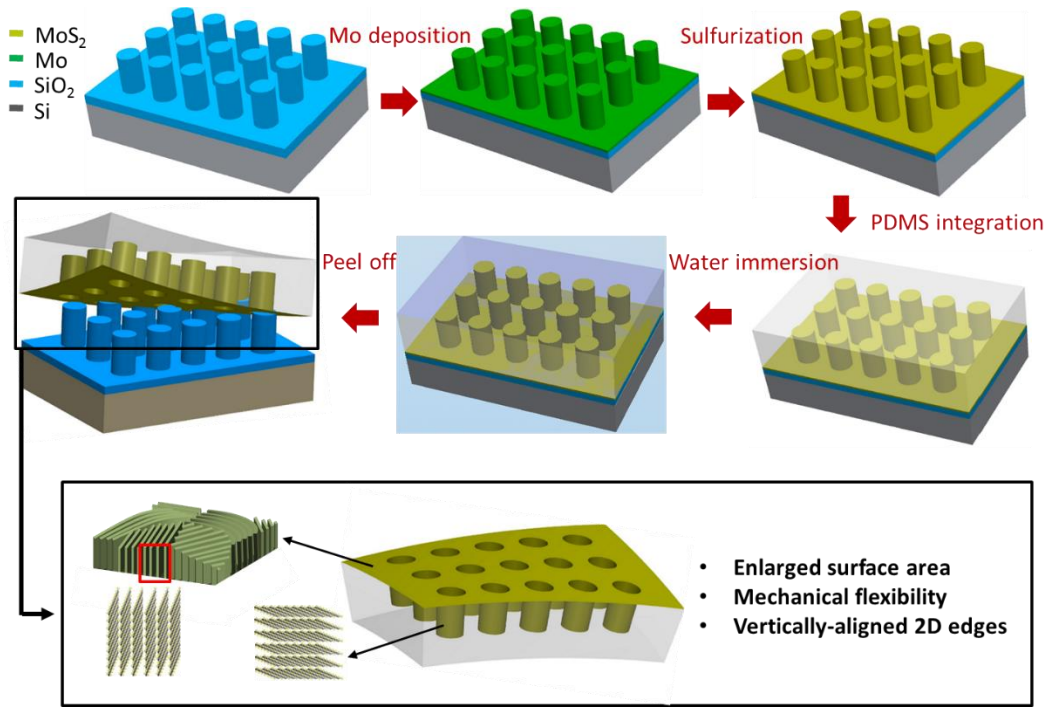


Figure 22: Schematic illustration of the large-area integration of three-dimensionally ordered 2D MoS₂ vertical layers onto a flexible PDMS substrate enabled by a water-assisted layer transfer method.

Figure 22 illustrates the fabrication process for three-dimensionally ordered vertically-aligned 2D MoS₂ layers integrated on flexible substrates. A standard optical lithography process was used to prepare an array of silicon dioxide/silicon (SiO₂/Si) pillar structures, and the prepared substrate serves as a template for 2D MoS₂ layer growth. A Mo film was then deposited on the surface of the prepared sample, followed by subsequent sulfurization in a CVD chamber. As a result, 2D MoS₂ with vertically-

aligned layers were uniformly grown on any exposed surface of the SiO₂/Si pillars, including their side-walls, as confirmed by extensive electron microscopy characterization.

A thin layer of PDMS was spin-coated on the surface of the as-prepared 2D MoS₂/SiO₂/Si pillars and was subsequently cured. The entire PDMS/2D MoS₂/SiO₂/Si substrate was then immersed in water and was manually peeled off. Before the peel-off, a corner of the PDMS/2D MoS₂/SiO₂/Si substrate was gently opened with a sharp object, which is intended to facilitate water penetration. The completely peeled 2D MoS₂/PDMS film maintains the structural integrity of the as-grown vertically-aligned 2D MoS₂ layers as well as their original pattern geometry, predominantly exposing 2D layer edge sites on the entire sample area surface. Details for material growth and transfer conditions are presented in the Experimental section. It is worth mentioning the following features to which the success of the vertically-aligned 2D MoS₂ layer growth and their water-assisted transfer is attributed: (1) vertically-aligned 2D MoS₂ layers are known to grow by the sulfurization of thick Mo films [5,145], which is attributed to the competing contribution of internal strain and volume expansion involved in the conversion of Mo to MoS₂ [25]. As 2D MoS₂ layers undergo the initial growth stages, they experience the accumulation of the internal strain exerted by the volume expansion of Mo to MoS₂ owing to the physical confinement of Mo seeds. Such dynamics lead them to redirect the 2D layer orientation vertically in a way to release the accumulating strain, as recently confirmed by TEM and simulation studies [25]. For the entire 2D MoS₂ growth experiments reported in this work, we deposited Mo films of >8 nm and sulfurized them *via* CVD. (2) Facile separation of 2D MoS₂ layers from the SiO₂ surface is attributed to their distinguishable water wettability owing to the surface energy imbalance, as previously studied [35,146-148]. SiO₂ exhibits hydrophilicity upon water adsorption while 2D MoS₂, particularly with vertically-aligned 2D layers, presents significant hydrophobicity [149-151], which is also consistent with our own observation. Accordingly, once a water droplet gets

penetrated at the interface of 2D MoS₂/SiO₂, it can create significant tension within the 2D layers, which is further promoted by the mechanical force and adhesion exerted by the PDMS.

6.2.2 Morphology of the as-grown 2D MoS₂

Before the characterization of vertically-aligned 2D MoS₂ integrated on PDMS, we first investigated the morphology of 2D MoS₂ layer-coated SiO₂/Si pillars to ensure their uniform vertical layer growth. Figure 23(a) shows an SEM image of SiO₂/Si pillars after the CVD growth of 2D MoS₂ layers on their surface. Periodically patterned pillars (height: 1 μm , pitch: 2 μm) are observed over the entire substrate area (typically, 2 cm²).

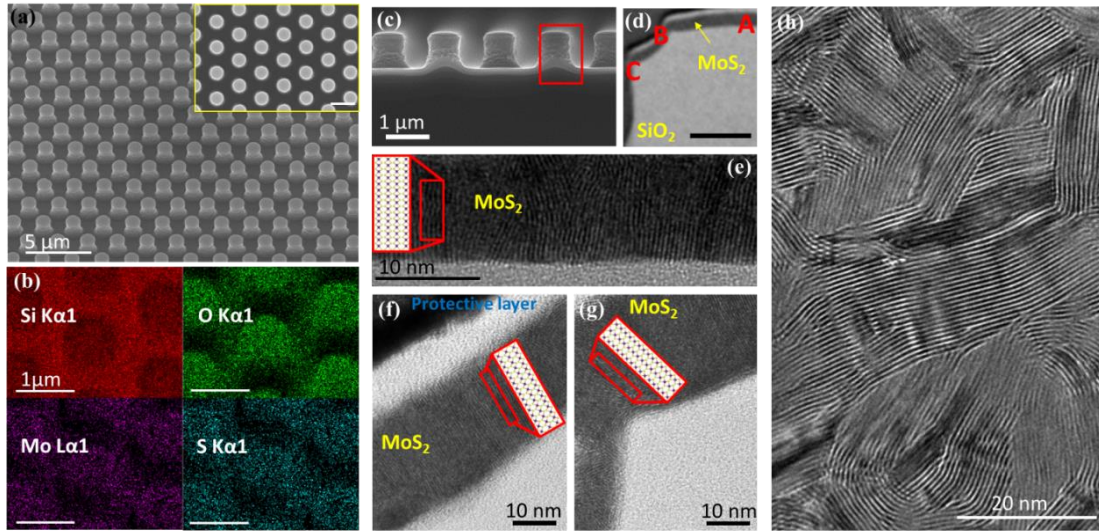


Figure 23: Growth morphology of the 2D MoS₂. (a) An SEM image of the 2D MoS₂ layer coated SiO₂/Si pillars. The scale bar in the inset is two μm . (b) SEM-EDS elemental maps showing the spatial distribution of Si, O, Mo, and S atoms in the pillars. (c) Side-view an SEM image of 2D MoS₂ layer-coated SiO₂/Si pillars. (d) Cross-sectional TEM image of the red box in (c), showing the growth of 2D MoS₂ layers on SiO₂. (e)–(g) Cross-sectional HRTEM images of the A–C regions in (d), respectively. All the images show vertically-aligned 2D MoS₂ layers irrespective of the probed locations. (h) Plane-view HRTEM image of vertically-aligned 2D MoS₂ layers revealing their 2D layer edge sites.

EDS elemental mapping images in figure 23(b) reveal the chemical compositions of the pillars, confirming the high spatial uniformity of constituents Mo, S, Si, and O. Figure 23(c) shows a side-view

of an SEM image of the same sample whose detailed morphology (red box) was further investigated by cross-sectional transmission electron microscopy (TEM). Figure 23(d) shows the corresponding cross-sectional TEM image revealing distinguishable image contrasts within the pillar, which confirms 2D MoS₂ layer growth throughout its entire periphery. The three different regions labeled A, B, and C, in figure 23(d), were further inspected by HRTEM, corresponding to figure 23 (e), (f), and (g), respectively. Figure 23(e)–(g) clearly shows that the 2D MoS₂ layers grown on the SiO₂ pillar well maintain their vertical layer orientation including its sidewall. Moreover, the vertically-aligned 2D MoS₂ layers predominantly expose open-ended 2D layer edge sites on the top surface as observed in figure 23(f). Figure 23(h) shows a plane-view HRTEM image of vertically-aligned 2D MoS₂ layers prepared by the CVD growth conditions identical to those for the pillar sample, further confirming the presence of the exposed 2D layer edge sites.

6.2.3 Structural and Optical Characterizations

Having established the successful growth of three-dimensionally ordered vertically-aligned 2D MoS₂ layers on SiO₂/Si pillar templates, we then investigated the reliability of the water-assisted layer transfer process and characterized the integrated vertical 2D MoS₂ layers/PDMS. Figure 24(a) shows an optical image of a vertically-aligned 2D MoS₂ layer-grown SiO₂/Si pillar patterned substrate. The patterned area shows a vivid visual color reflecting a significant diffraction grating effect owing to the presence of the periodically ordered pillars, as shown in the enlarged image. In figure 24(b), highly distinct colors are observed from the patterned region of the identical sample with varying the angle of the optical camera, further confirming the diffraction grating effect. Figure 24(c) shows the vertically-aligned 2D MoS₂ layers integrated on PDMS, transferred from the identical sample shown in figure 24(a). It is evident that the integrated region of 2D MoS₂ layers presents a vivid optical color similar to that observed before the transfer, indicating that the original pattern structures are well retained, as

confirmed in the enlarged image. Figure 24(d) shows an SEM image of the same sample in figure 24(c), establishing the presence of three-dimensionally ordered patterns transferred from the original pillar template. Figure 24(e) shows the corresponding SEM-EDS elemental mapping images, revealing the homogeneous spatial distribution of Mo and S which is observed throughout the entire sample area. Figure 24(f) compares the Raman spectroscopy profiles of the corresponding sample before (red line) and after (blue line) the layer transfer and integration.

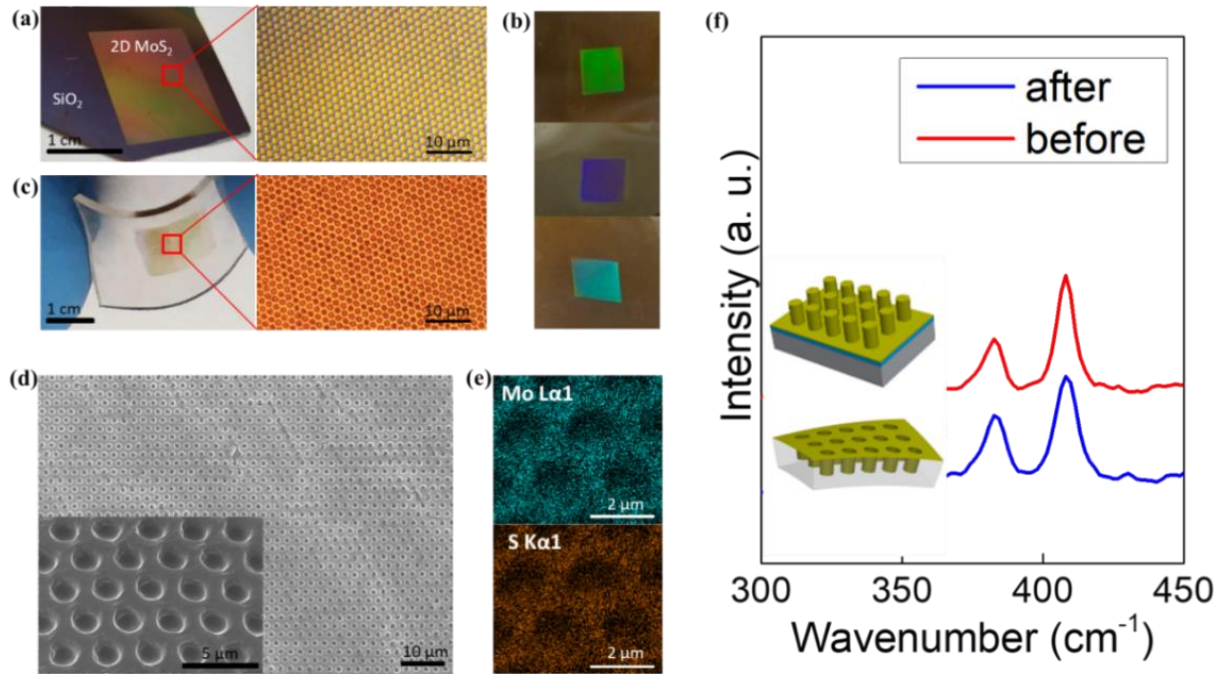


Figure 24: Optical microscopy images: (a) large-area vertical 2D MoS₂ layer-coated SiO₂/Si pillars, and (b) color variation of the corresponding pillar patterned area. (c) Optical microscopy image of vertically-aligned 2D MoS₂ layers integrated on PDMS transferred from the same sample in (a). (d) An SEM image of the corresponding vertically-aligned 2D MoS₂ layers integrated on PDMS. (e) SEM-EDS elemental map showing the spatial distribution of Mo and S in the same sample. (f) Raman spectroscopy profiles of the same sample before and after transfer.

It is evident that the vertically-aligned 2D MoS₂ layers/PDMS exhibits Raman characteristics comparable to those obtained from the as-prepared 2D MoS₂/SiO₂/Si pillars, further confirming the high reliability of the water-assisted layer transfer and integration process. We then

characterized the material properties of these three-dimensionally ordered vertical 2D MoS₂ layers/PDMS and explored their unique functionalities, which are difficult to achieve with conventional 2D MoS₂ layers. Notably, we focus on the tunability of their optical, structural, and electrical properties driven by mechanical deformation. Figure 25(a) and (b) show the images of vertically-aligned 2D MoS₂ layers/PDMS at uniaxial strain levels of 0% and 30%, respectively. The images clearly show that the sample is highly stretchable, retaining its structural integrity upon reversible and repeated stretching, as shown in the corresponding enlarged images. The sample was confirmed to keep well-resolved 2D MoS₂ characteristic Raman peaks even after 30% stretching repeated 100 times with a visibly insignificant structural change inspected by optical microscopy. We first characterized the optical properties of the sample by performing ultraviolet-visible (UV-Vis) spectroscopy characterization at a systematically varying tensile stretch level. Figure 25(c) shows that the optical absorbance monotonically decreases with increasing stretching, which reflects the reduction in the surface–volume-ratio in the given area of the sample. Two optical absorbance peaks are observed in the spectral range of 600–700 nm, which correspond to A and B excitonic peaks from the K point of the Brillouin zone in 2D MoS₂ layers, respectively. The observation of these optical absorbance characteristics is entirely consistent with previous studies on 2D MoS₂ layers, which further confirms the large-area reliable transfer and integration of high-quality 2D MoS₂ layers onto PDMS [51,52,54,152,153]. We note that these excitonic peaks systematically exhibit a slight redshift with increasing stretch, as manifested by the A excitonic peak energy shift shown in figure 25(d). Strain induced shifts of excitonic peak energies in 2D MoS₂ layers have been previously reported, [59,154,155] while the extent of the energy shift observed in our sample is not as pronounced as those found in horizontally-oriented 2D MoS₂ mono-to-few layers [154]. Concerning the experimentally observed optical absorption and

excitonic peak characteristic change, the exclusive role of the interatomic layer distance change in 2D MoS₂ layers should be considered as previously studied [156-158]. The strain-driven change of Mo–Mo, Mo–S, and S–S bond length distances has been suggested to be responsible for the bandgap energy and excitonic peak shifts resulting from orbital hybridization [157]. Although it is unambiguous that the contribution of the interatomic layer distance change cannot be ruled out, it is challenging to precisely decouple this intrinsic effect from the extrinsic participation driven by the surface-to-volume ratio change.

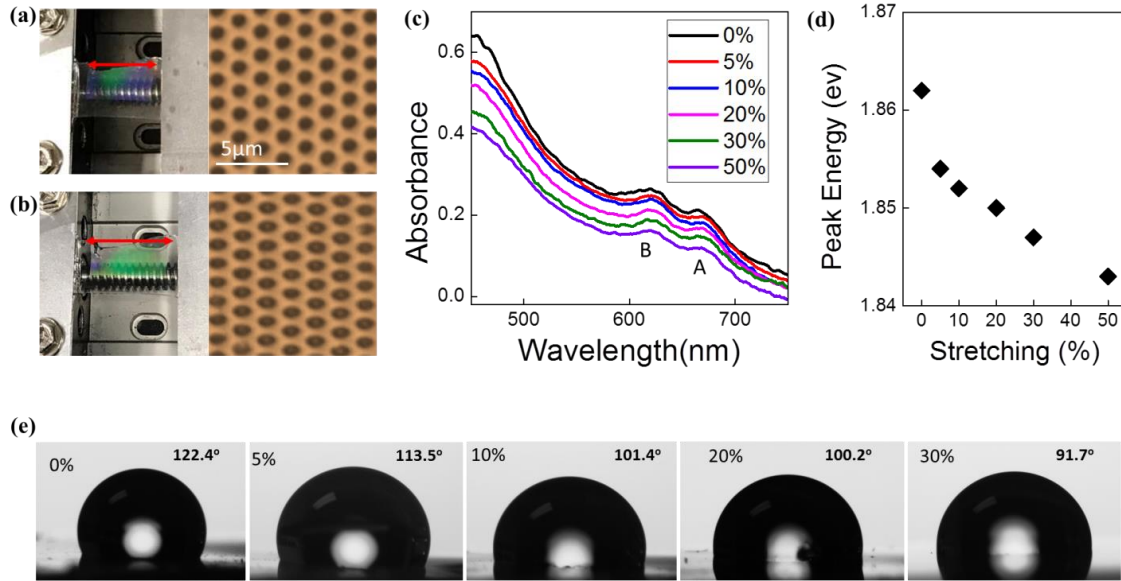


Figure 25: Camera and optical microscope images of vertically-aligned 2D MoS₂ layers/PDMS under uniaxial tensile strains of (a) 0% and (b) 30%. (c) Optical absorbance of the same sample with varying strain levels. (d) Variation of A excitonic peak energy with varying strain levels. (e) Optical images of the water contact angle (WCA) with varying strain levels from 0% to 30% strain, exhibiting decreasing water contact angle with increasing surface roughness owing to the flattening of the sample substrate by applying tensile strain.

The most serious difficulty stems from our materials possessing unique and unconventional geometries, *i.e.*, 2D layers are vertically-aligned while uniformly wrapping around 3D post-structures-which complicates the definition of “in-plane” and “out-of-plane” strain unlike previous studies [158].

6.2.4 Stretch-Tunable Mechanical Properties

In addition to demonstrating the tunable optical properties, we studied the stretch-driven controllability of the structural properties of vertical 2D MoS₂ layers/PDMS by characterizing their surface wettability through water contact angle (WCA) measurements. Figure 25(e) shows the trend of the WCA value change with varying stretch levels in the range of 0%–30%. The as-prepared material at 0% strain presents a significantly high WCA of $>120^\circ$, thus exhibiting an excellent hydrophobicity. With increasing stretch levels, the WCA gradually decreases, yielding a large degree of tunability of over $>30^\circ$, with an applied tensile stretch of 30%. To better clarify the reason for the stretch-driven change of the WCA values, we applied the Wenzel equation [159] and observed that the prediction from the Wenzel equation only could not fully explain the experimental results. This observation indicates the presence of additional factors in governing the surface wettability beyond the diminished roughness effect driven by the flattening of the structured PDMS. We note that the WCA values of 2D MoS₂ layers can be strongly affected by their geographical orientation, which can often realize significantly larger surface wettability beyond the numerical prediction from the Wenzel equation. For instance, Choi *et al.* [150] reported that the WCA values of vertically-aligned 2D MoS₂ layers on stretchable substrates gradually decrease as the substrates become flatter (less textured), achieving surface wettability comparable to our cases.

6.2.5 Flexible Humidity Sensing Properties

Lastly, we study the electrical properties of the three-dimensionally ordered vertical 2D MoS₂ layers/PDMS and explore their practical application aspects. We particularly focus on their electrical characterization upon vaporized water molecule adsorption, assessing feasibility for humidity sensing. The justification for the electrical humidity sensing application is as follows: the material

presents (1) an enlarged surface-to-volume ratio owing to the three-dimensional geometry, (2) numerous dangling bonds on the surface-exposed 2D layer edges, and (3) high mechanical flexibility promoted by the underlying flexible PDMS. Figure 26(a) shows the current-voltage (I - V) characteristics of three-dimensionally ordered vertical 2D MoS₂ layers/PDMS exposed to vaporized water molecules at a controlled humidity level. The current monotonically decreases with increasing relative humidity in the tested range of 30% to 90%, which is consistent with the previous observations with horizontally-oriented 2D MoS₂ layers [160,161]. All the I - V plots show nearly linear isotropy indicating that the Ohmic contact of electrodes was well maintained irrespective of the varying level of water molecules introduced. Values for the relative change of resistance, R/R_0 , are obtained at each humidity level (black plot), where R_0 denotes the reference resistance value at 30% humidity. For comparison, two different control samples of (a) vertically-aligned 2D MoS₂ layers without patterns (blue plot) and (b) horizontally-aligned 2D MoS₂ layers without patterns (pink plot) are presented. We note that the exposure of 2D layer edges in the vertically-aligned layers presents a significant improvement in sensitivity; for example, ~400% over ~200% at the same relative humidity of 90%. This improvement is attributed to the significantly higher phys- and/or chem-adsorption capability of 2D edges owing to their numerous Mo/S dangling bonds compared to chemically-inert 2D basal planes, which is consistent with recent theoretical prediction [132,135] and experimental verifications [99]. We then compare the R/R_0 values for vertically-aligned layers with three-dimensionally patterned structures (black plot) and without any patterns (blue plot). We note that the patterned sample exhibits significantly enhanced (~7 times) sensitivity over the one without patterns, which is attributed to its increased surface-to-volume ratio. We indeed calculated that having the three-dimensionally ordered pillar structures (figure 26(a)) enlarges the surface area >5 times over non-patterned samples, drastically increasing the area of the active sites for water molecule capture. We further tested the sensitivity of the

vertically-aligned 2D MoS₂ layers/PDMS upon mechanical bending (red plot) and did not observe any significant degradation up to a bending radius of ~6 mm. Accordingly, the significantly improved sensitivity shown in the red and black plots is attributed to the combined results of the increased surface-to-volume ratio and exposed 2D dangling bonds, while precisely decoupling these two distinct effects for better clarification needs further investigation. The observed current decrease with increasing relative humidity is consistent with the literature [60,134,160,161] and can be understood as follows; 2D MoS₂ layers are intrinsically n-type semiconductors and tend to donate free electrons upon interacting with water molecules adsorbed on their layer edge sites. As a result, the free electrons are transferred from the vertically-aligned 2D MoS₂ layers which become charge-depleted, resulting in a decrease of current as illustrated in figure 26(c). Furthermore, we have investigated the long-term stability of our 2D MoS₂-based humidity sensors by repeatedly measuring their electrical resistances with varying humidity. We have confirmed that they show well-maintained sensitivity even for a month, suggesting the structural robustness of the vertically-aligned 2D MoS₂ layers whose end surfaces are strongly bound to the chemically cured PDMS. In order to quantitatively verify how the orientation of 2D MoS₂ layers affects the sensing capability, we adopted density functional theory (DFT) and calculated the adsorption energies of water molecules with varying layer orientation (figure 26(d-f)). The DFT calculation results confirm that water molecules are more strongly adsorbed onto the edge sites than the basal planes of 2D MoS₂ layers; the adsorption energy of one water molecule on the basal plane is calculated to be -0.166 eV while those on the Mo and S edges are -1.094 eV and -0.278 eV, respectively. The adsorption energy, E_{ads} , of a water molecule on 2D MoS₂ layers was calculated as $E_{\text{ads}} = E_{\text{tot}} - (E_{\text{MoS}} + E_{\text{wat}})$, where E_{tot} is the energy of 2D MoS₂ layers with an adsorbed water molecule, and E_{MoS} and E_{wat} are the energies of 2D MoS₂ layers and a water molecule, respectively. The much larger adsorption energy on the Mo edge over the S edge is because Mo, a transition metal, is

more prone to form additional atomic bonds over S. The schematic illustration supports this claim in figure 26(e), which depicts that the oxygen of a water molecule is directed to the exposed Mo edge-opposite to the case of the S edge (figure 26(f)). Although all 2D MoS₂ layer edges do not expose Mo sites only, it is evident that vertically-aligned 2D MoS₂ layers exhibit significantly enriched dangling bonds compared to horizontal 2D layers, which guarantees improved reactivity upon water molecule adsorption.

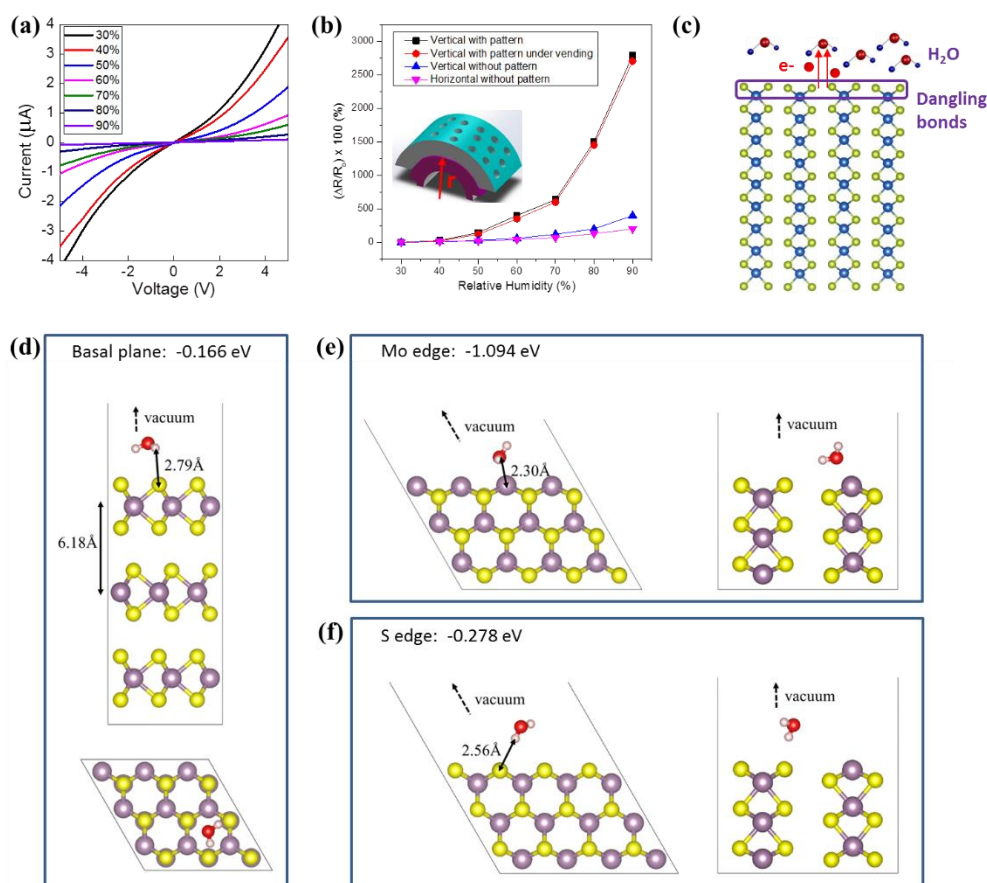


Figure 26: (a) I–V characteristics of patterned vertically-aligned 2D MoS₂ layers/PDMS upon water molecule absorption in the relative humidity range of 30% to 90%. (b) Comparison of the relative resistance change with varying relative humidity for patterned vertical 2D MoS₂/PDMS (black), patterned vertical 2D MoS₂/PDMS under bending (red), vertical 2D MoS₂/PDMS without patterns (blue), and horizontal 2D MoS₂/PDMS without patterns (pink). (c) Schematic illustration of electron transfer in vertically-aligned 2D MoS₂ layers upon water molecule absorption. (d)–(f) DFT calculation snapshots of adsorbed water molecules on the (d) basal plane, (e) Mo edge, and (f) S edge in 2D MoS₂ layers.

6.3 Conclusions

In conclusion, we demonstrate a novel approach to grow, transfer, and integrate three-dimensionally ordered 2D MoS₂ with vertically-aligned layers on flexible substrates on a centimeter scale. A water-assisted 2D layer separation process precisely preserves the structural integrity of the configured 2D MoS₂ layers initially in a three-dimensional form upon their integration, which is enabled without involving any undesired chemical etchants. This new form of 2D materials presents a unique combination of enhanced surface area, mechanical flexibility, and surface-exposed 2D edge layer sites. Moreover, they exhibit the intriguing stretch-driven tunability of a variety of material properties and high potential for humidity sensing applications.

CHAPTER-7: VERTICALLY-ALIGNED 2D MoS₂ FOR STRETCHABLE GAS SENSOR

7.1 Introduction

In recent years, a large number of studies have been demonstrated for efficient gas sensing performances. For instance, the conventional metal oxide-based chemiresistive sensors exhibit reduced sensitivity and selectivity as they require an elevated operating temperature ($\sim 300^{\circ}\text{C}$) and a complex fabrication process[162,163]. As an alternative to this strategy, UV light was used to remove oxygen ions from the sensor surface, thereby enhancing the removal rate of gas molecules[164]. Therefore, these methods are required excessive energy consumption, which is safety concerns and reliability issues. 2D MoS₂ has been attracting substantial attention over the past few years owing to its high adsorption coefficient, enhanced surface-to-volume ratio, tunable bandgap, and promising physical, electronic, and optical properties [7,162,163,165-168]. The simple transfer/integration process on the flexible substrates, charge transport characteristics, and bio-compatibility make 2D MoS₂ an excellent candidate for high-performance stretchable gas sensing applications[169-171]. However, previously studies 2D MoS₂ based sensors suffer a lack of room-temperature response, recovery, and significant oxygen adsorption in air. Moreover, their unreliable stretchability and lack of robust body-attachable capability make them impractical for sensing applications[167,172-175]. Nitrogen dioxide(NO₂) is one of the most dangerous contaminants which can cause eye and lung irritation and respiratory infections[176].

As mentioned in the previous chapters, the vertically-aligned 2D MoS₂ layers exposed their edges with higher adsorption energy, which contain very high-density d-orbital electrons. These

electrons have strong binding interactions with outside environment for sensing gas/biological molecules[88,99,177,178]. For instance, Cho et al. reported enhanced gas adsorption properties of vertically-aligned 2D MoS₂ layers and compared their performance with horizontal layers[99]. This sensor exhibits a very low sensitivity at lower gas concentrations. Moreover, mechanical-tunable functionalities are unexplored in this study. In another study, a low-temperature (200 °C) synthesis of 2D MoS₂ is presented to demonstrate a flexible gas sensor at room temperature[179]. However, this sensor cannot explain higher mechanical stretchability at lower NO₂ gas concentrations.

Therefore, it is desirable to develop a highly stretchable NO₂ gas sensor to leverage the intrinsically high adsorption capability of vertically-oriented 2D MoS₂ layers. Moreover, this particular property advantage of 2D MoS₂ layers can be further promoted as far as we can integrate them into the human body or any wearable device. Furthermore, excessive mechanical durability of 2D MoS₂ is required to incorporate them into wearable devices. This attribute is beyond the intrinsic stretchability limits of the atomically-thin 2D MoS₂ layer. Moreover, the obstruction of room temperature response and recovery, repeatability, and reliability issues observed from the metal-oxide based and graphene sensors are need to be addressed [180,181].

In this chapter, we demonstrate a stretchable room-temperature NO₂ gas sensor with the water-assisted integration of vertically-aligned 2D MoS₂ layers on the PMMA substrate. To enhance the stretchability of the gas sensor, we designed a unique horseshoe-like serpentine pattern of the 2D MoS₂/PMMA. This vertically-aligned 2D MoS₂/ PMMA preserves the material quality with controlled morphologies/chemistries, which are verified by their extensive Raman spectroscopy, X-ray photoelectron spectroscopy (XPS), and HRTEM analyses. Moreover, upon applying tensile strain from 0% to 40%, this sensor exhibits electrical, Raman, and photoresponse

properties without any noticeable performance degradation. Furthermore, a sensitivity of ~470% was obtained from the NO₂ gas sensing measurements (0 to 30 ppm). The sensor device exhibits gas sensing properties without any performance degradation under the high tensile strain (40%).

7.2 Results and Discussions

7.2.1 Sensor Fabrication Steps

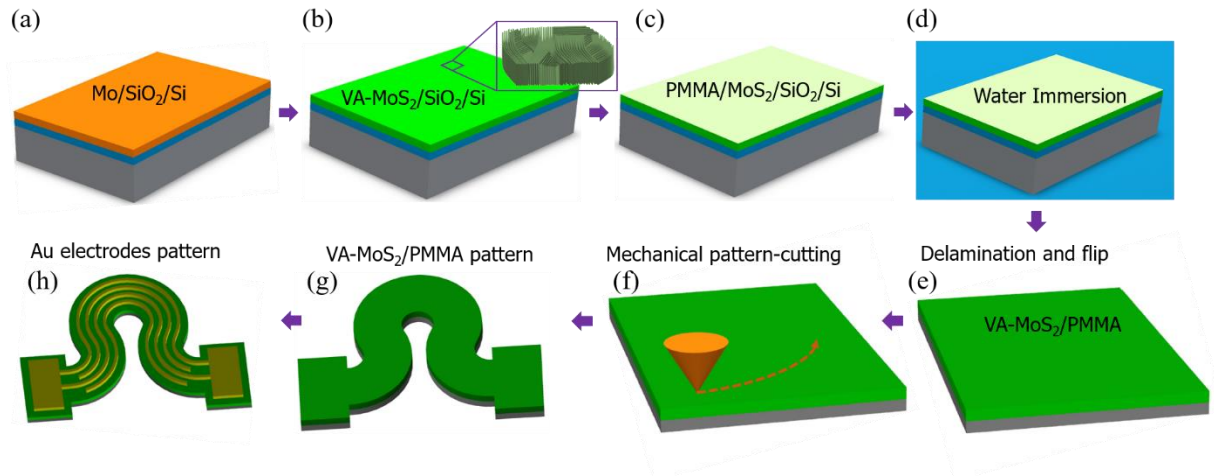


Figure 27: Schematic diagram of the stretchable gas sensor fabrication process. (a) Metal Mo deposition. (b) Thermal sulfurization. (c) Spin-coating with PMMA. (d-e) Water immersion and lift-off. (f-g) Mechanically cut the serpentine pattern and remove the extraneous/un-patterned area. (h) Gold electrode deposition with a shadow mask.

Figure 27 is the schematic illustration of the sequential growth and transfer process of the horseshoe-like a serpentine pattern of 2D MoS₂ layers. In the beginning, Mo film was deposited on cleaned silicon dioxide/silicon (SiO₂/Si) substrate employing the electron-beam evaporation method. Subsequently, the deposited film is sulfurized in a chemical vapor deposition furnace, as in figure 27(a-b). Therefore, MoS₂ films with vertically-aligned 2D layers are grown on the SiO₂/Si substrate, which is confirmed by transmission electron microscopic characterization.

A sub-micrometer-thick PMMA was spin-coated on the as-grown 2D MoS₂ and immersed in water, followed by manually peeling off with the water transfer method explained in our previous studies, in figure 27(c-e) [31]. The MoS₂/PMMA film is then carved into a horseshoe-like a serpentine pattern with a benchtop programmable mechanical cutter plotter, as depicted in figure 27(f-g). The geometry (width: 6 mm, arc angle: 125 degrees) of the serpentine structured 2D MoS₂/PMMA was chosen based on theoretical simulation results to obtain stretchability ~50%, compatible with stretchable/wearable sensor devices. This water-assisted transfer and integration approach attributed unique features over traditional non-scalable wet chemical etching and mechanical exfoliation methods; 2D layers can transfer without involving any chemical etchant [31]. A shadow mask was designed for making gold (Au) electrodes with a modified interdigitated structure, as shown in figure 27(h). This water-assisted integration of 2D MoS₂/PMMA can retain the structural integrity similar to their as-grown states. As-fabricated, a horse-shoe-like serpentine pattern can be transferred on to any arbitrary substrate or any part of the human body regardless of its curvature/bendability. This serpentine geometrical pattern has distinct advantages in terms of mechanical durability; (i) longer length than if it was straight, (ii) more twisting upon stretching, and (iii) can completely deform in-plane; therefore it can accommodate larger pre-strain and is compliant to higher stretchability to survive many deformation cycles [182-186]. For electrochemical or chemical sensing, the orientation of the 2D MoS₂ layer is the crucial factor that can be directly observed from the HRTEM analysis. Figure 28(a) depicts an HRTEM micrographs of the vertically-aligned 2D MoS₂ layers. It is clear that the as-grown and transferred 2D MoS₂ films composed of predominantly exposed 2D edges, which can uniformly cover an entire surface area. To estimate the thickness of the as transferred 2D MoS₂ layers, atomic force microscopy (AFM) was used to analyze the topography of the area near the border of the MoS₂-PMMA interface, as in figure

28(b). The thickness of the MoS₂ layers were obtained ~16 nm from the AFM height measurement. The optical transmittance of the 2D MoS₂/PMMA substrate was measured using an ultraviolet-visible spectrophotometer over an area of 2 cm × 2 cm, as in figure 28(c). A transmittance of ~70% was obtained from the MoS₂/PMMA sample and 97% from the bare PMMA within the wavelength range of 400 to 800 nm. Owing to the additional light absorption by the 2D MoS₂ layers, the observed transmittance values were lower in the vertically-aligned 2D MoS₂, which are consistent with previous studies [88,187-189].

7.2.2 Chemical/Structural Morphology

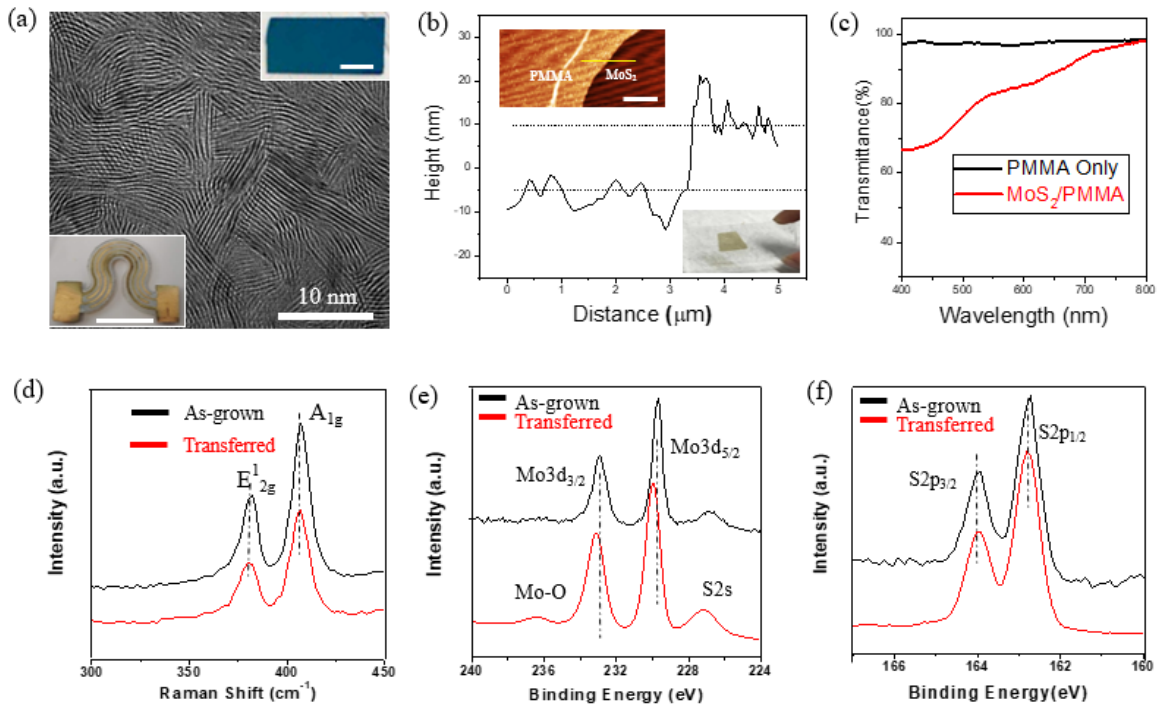


Figure 28: Optical, structural, and chemical morphology of the vertically-aligned 2D MoS₂ stretchable sensor by AFM, Transmittance, Raman, and XPS analysis. (a) The HRTEM image is exhibiting all vertically-aligned 2D MoS₂ layers of the entire sample. (b) AFM height profile measurement of the 2D MoS₂/PMMA. (c) Optical transmittance spectra of bare PMMA and MoS₂/PMMA. (d) Raman spectra obtained from as-grown and transferred 2D MoS₂ layers. (e-f) The XPS scans for the Mo and S binding energies of the 2D MoS₂ layers. (e) The XPS spectra (Mo3d core level) of the as-grown 2D MoS₂/SiO₂/Si (black) substrate and transferred MoS₂ film on the PMMA (red) substrate. (f) XPS spectra of the S2p core level of the as-grown and transferred sample

Raman spectroscopy is a versatile technique to determine the structural fingerprint of the crystalline structure using quantum mechanical vibration of the molecule. The Raman spectra in figure 28(d) indicates a typical in-plane (E_{2g}^1) and out-of-plane (A_{1g}) phonon modes of as-grown and transferred 2D MoS₂ films obtained at a 532 nm laser line. The Raman spectra reveal strong signatures of both in-plane and out-of-plane vibrational modes at 381 cm⁻¹ and 407 cm⁻¹, respectively, a clear indication of well-defined growth of 2D MoS₂ layers. The intensity ratio (E_{2g}^1/A_{1g}) is ~0.5, which implies a dominating out-of-plane (A_{1g}) vibration mode than in-plane owing to the pronounced exposure of the 2D edge sites of the vertically-aligned layers [6,31,68].

To investigate the stoichiometry and the chemical states of the 2D MoS₂ films, we used an XPS analysis. Figure 28(b-c) depicted the XPS spectra for the binding energies of the Mo3*d* and S2*p* orbitals of the as-grown and transferred 2D MoS₂ samples. Two distinct peaks attributed to the doublet Mo 3d_{5/2} and Mo 3d_{3/2} from the spin-orbit split of the Mo3*d* core levels, which are located at 229.68 and 232.88 eV binding energies. Moreover, the other two peaks, corresponding to the S 2p_{3/2} and S 2p_{1/2} orbital of divalent sulfide ions (S²⁻), which are observed at 162.79 eV and 163.97 eV binding energies. These results indicate the existence of Mo and S, with an estimated atomic composition ratio is ~1:2.17, usually obtained from p-type MoS₂ from sulfur-rich or molybdenum-deficient environment [190]. Moreover, the absence of the peak at 236.2 eV corresponding to Mo-O bonds of the as-grown states indicates the absence of molybdenum oxides in our CVD system. However, there is a very negligible (~0.15 eV) increase in binding energy observed from the as transferred sample, which might occur due to the water transfer process of 2D MoS₂ layers and the presence of negligibly small oxidation states, as shown from the as-transferred sample. These moieties can act as a trap state for charge carriers passing through the MoS₂ layer. Furthermore, the negligible peak intensity of the binding energy of the Mo orbital

indicates the entirety of the Mo atoms have been sulfurized to form a crystalline 2D MoS₂ structure. All these structural and chemical analyses revealed that the transferred 2D MoS₂ layers on the PMMA substrate well-maintained their structural quality identical to the as-grown states.

7.2.3 Mechanically Stretchable Functionalities

To confirm the mechanical stretchability and electrical reliability of the 2D MoS₂ layers serpentine structures, we first analyzed their electrical properties under systematically applied strain from 0 to 50% with a home build motorized linear stretcher. Figure 29(b) depicts the two-terminal current (I)–voltage (V) electrical transport characteristics from a horseshoe-like patterned 2D MoS₂/PMMA layers. We observed a minimal decrease of current with an increased in stretching, indicates that the patterned 2D MoS₂ layers well-retained their electrical reliability even up to 50% strain.

Having understood the electrical transport properties of the 2D MoS₂, we studied Raman analysis under strain. Figure 29(c) shows the Raman spectra of the 2D MoS₂ layers at 40% uniaxial strains along with its as-transferred 2D MoS₂ layers for comparison. Two distinct peaks corresponding to intralayer vibrations are observed from the Raman analysis. We found that the interlayer in-plane(E_{2g}^1) and the out-of-plane (A_{1g}) vibration modes are identical before and after transfer. We did not observe any peak splitting (at 40% strain), which is found if strain modifies the hexagonal lattice and breaking the symmetry [56,155,191,192]. Moreover, a negligible peak shift was found in the in-plane(E_{2g}^1) mode under 40% strain, while there was no effect of their out-of-plane (A_{1g}). This observation further strengthened the structural integrity and mechanical tolerability of the serpentine structured 2D MoS₂ layers at a 40% strain. It is noticeable that this study focused on precisely defined large area (>2 cm²) 2D MoS₂ layer for stretchable sensor. remarkably promoting over the previous studies owing to its synergistic effect of layer orientation

control, enhance optical, electrical, and mechanical properties, and excellent stretchable sensing capability.

7.2.4 Stretchable Gas Sensing

To explore the practical device application, we demonstrated the NO₂ gas sensing performance with the as-fabricated stretchable sensor. The NO₂ gas was introduced to the sensor inside a synchrotron acrylic vacuum chamber. A commercial NO₂ gas-sensor was placed inside the vacuum chamber to monitor precise gas concentration; details are explained in the experimental section. The real-time current change of the sensor was monitored from the current (I) vs. time (T) measurement (figure 29(d)) by applying a constant voltage of 7V. The current changes dramatically with the time by introducing precisely controlled NO₂ gas concentrations from 0 to 30 ppm. We observed that the current gradually increases with increasing NO₂ gas concentration from 5 ppm to 30 ppm, consistent with the previous observation of the 2D MoS₂ on flexible PET substrate[179]. The sensitivity of the sensor is defined as Sensitivity (S) %=(I_g-I₀)/I₀×100%=(ΔI/I₀)×100%, where I₀ and I_g indicate the currents of the sensor under air and analyte gas, respectively. By applying the NO₂ gas concentration from 0 to 30 ppm, the sensor exhibited a very high response of approximately 470%, as shown in figure 29(d). This significantly improved sensitivity attributed to the combined effect of the higher surface-to-volume ratio and exposed 2D dangling bonds owing to the vertically orientated 2D MoS₂ layers grown in our CVD system.

To demonstrate stretchable sensing performances, we further tested gas sensing properties of the vertically-aligned 2D MoS₂ layers/PMMA upon uniaxial strain 40% at a constant gas concentration (5 ppm in this case). We did not observe any degradation of the current after carefully compare with the unstrained device under identical gas concentrations (figure 29(e)). The repeatable response to a periodical introduction of a particular gas concentration (5 ppm in this

case) indicates that the sensor well-maintain gas sensing performance. This excellent response is attributed to the combination of edge exposed vertically grown 2D MoS₂ and the serpentine geometry, which further validates structural robustness of the sensor where 2D layers are firmly attached to the underlying PMMA substrate. The justification for the enhanced stretchable gas sensing properties is as follows: (i) vertically-aligned 2D MoS₂ layers exhibited higher surface to-volume-ratio, (ii) enriched set of dangling bonds on the surface-exposed 2D layer edges, and (iii) very high mechanical stretchability owing to the serpentine pattern geometry. The gas response was increased by injecting higher gas concentration owing to the increased adsorption between analytes and edges of the 2D MoS₂ layers.

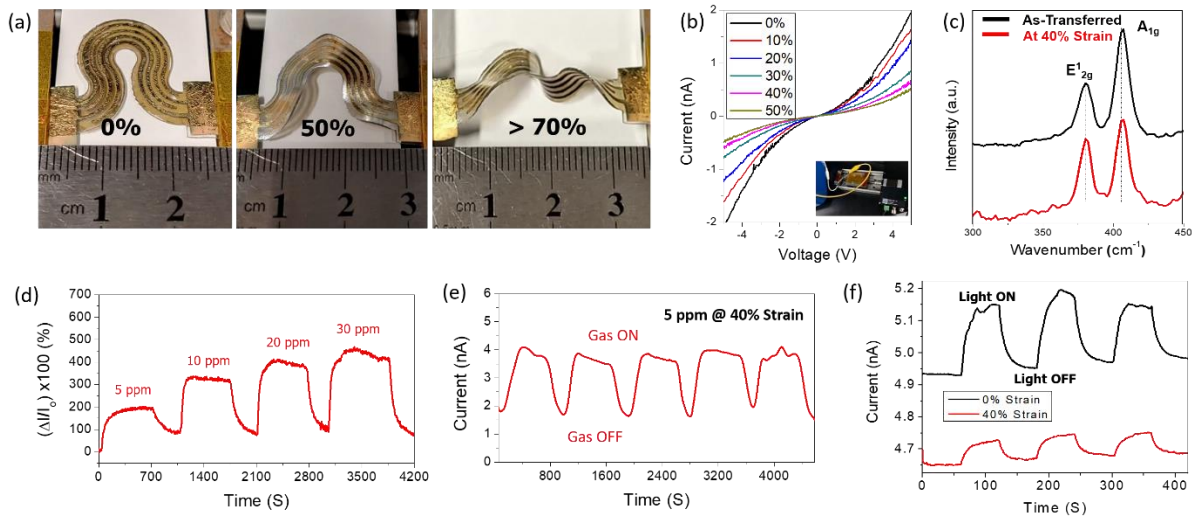


Figure 29: Mechanically stretchable performance of the device, (a) Camera image under stretching from 0 to 70%. (b) Two-terminal electrical (I-V) characterization of the sensor from 0 to 50% strain. (c, f) Raman-strain and photocurrent measurement from 0 to 40% strain. (d-e) The real-time gas response at 5 ppm, 10 ppm, 20 ppm, and 30 ppm and gas sensing performance at 40% strain.

The principle of the gas sensing mechanism depends on the charge transfer method. In this method, 2D material act as a charge acceptor or donor, therefore the conductance of the device changes upon inducing analytes. The gas molecules are adsorbed on the surface of 2D materials

by the electrostatic forces. The direction of electron charge transfer is determined by the type of reactive gas, either reducing or oxidizing. This is likely because the gas molecules are adsorbed on the edge sites of the 2D MoS₂ layers owing to its intrinsically higher adsorption energy compared to their chemically inert terrace sites of the horizontal layers[31]. The stretchable sensor based on 2D MoS₂ exhibits gas response, which usually observed from the p-type device, as explained in the previously reported 2D MoS₂ and WS₂ based gas sensor. [167,193]. Furthermore, we observed the photoresponse characteristics before and after 40% strain without significant performance degradation (figure 29 (f)).

7.3 Conclusion

A facile water-assisted transfer of vertically-aligned 2D MoS₂ layers with a non-conventional serpentine pattern was used to demonstrate a stretchable NO₂ gas sensor. The resulted sensor exhibited a high sensitivity of ~470% from 5 ppm to 30 ppm NO₂ gas concentration. The presented sensor shows NO₂ gas sensing without any performance degradation at a 40% tensile strain. The combined effect of the vertically-aligned 2D MoS₂ for enhancing gas sensing and serpentine structure for increased stretchability can be extended to study other gas or biological molecule sensing performances.

CHAPTER-8: SUMMARY AND FUTURE PERSPECTIVES

In this dissertation, I have studied a CVD growth mechanism of 2D MoS₂/WS₂ heterostructure with controlled layer orientations and their direct transfer approach onto elastomeric substrates. I then advanced my study and demonstrated a vertically-aligned 2D layer separation method with their stretch-driven tunability and a high potential for stretchable humidity and gas sensing applications. This dissertation work indicates that the transition from horizontal-to-vertical growth direction strongly depends on the initial metal (Mo) thickness, and internal strain developed during 2D layers growth dictates the growth mode variation. I also demonstrated a direct transfer and integration of 2D MoS₂/WS₂ vdW heterostructure layers on SiO₂/Au-based substrates with the aid of water-assisted debonding of SiO₂/Au interfaces. Moreover, I integrated the vertically-aligned 2D MoS₂ layers pattern on a flexible substrate with a water-assisted 2D layer separation process without involving any undesired chemical etchants. This new form of 2D materials presents a unique combination of enhanced surface area, mechanical flexibility, and surface-exposed 2D layer edges. Moreover, they offer the intriguing stretch-driven tunability for a variety of material properties and high potential for humidity sensing applications. Furthermore, I demonstrated a vertically-aligned 2D MoS₂ layer serpentine pattern for stretchable NO₂ gas sensing applications.

This study will play a vital role in the development of the 2D MoS₂ and its heterostructure for its scalable fabrication of stretchable optoelectronics devices and sensors. Therefore, this study significantly reduces gaps in the existing research study, opening up exciting new challenges and opportunities for academic inquiry.



There has been a rapid surge of interest and unprecedented progress of the 2D TMDs and their heterostructure in the past few years. Additional efforts are needed to develop a scalable method to precisely controlled chemical composition, physical dimensions (lateral size and vertical thickness), relative orientation, and interfacial contact. A complete understanding of the various combination of the 2D heterostructure and their devices are yet to be developed to unlock their full potentials. The combination of increasing edge density (3D-pillar structure) and stretchability (serpentine pattern) can be used to design a high-performance, versatile sensor. These pave the way for developing a high-performance multifunctional sensor for the stretchable and wearable device applications.






APPENDIX: COPYRIGHT PERMISSIONS


Figure 2

11/8/2019

Rightslink® by Copyright Clearance Center

 Home
  Help
  Live Chat
  Sign in
  Create Account



Metal Seed Layer Thickness-Induced Transition From Vertical to Horizontal Growth of MoS₂ and WS₂
 Author: Yeonwoong Jung, Jie Shen, Yanhui Liu, et al
 Publication: Nano Letters
 Publisher: American Chemical Society
 Date: Dec 1, 2014
 Copyright © 2014, American Chemical Society

PERMISSION/LICENSE IS GRANTED FOR YOUR ORDER AT NO CHARGE

This type of permission/license, instead of the standard Terms & Conditions, is sent to you because no fee is being charged for your order. Please note the following:

- Permission is granted for your request in both print and electronic formats, and translations.
- If figures and/or tables were requested, they may be adapted or used in part.
- Please print this page for your records and send a copy of it to your publisher/graduate school.
- Appropriate credit for the requested material should be given as follows: "Reprinted (adapted) with permission from (COMPLETE REFERENCE CITATION). Copyright (YEAR) American Chemical Society." Insert appropriate information in place of the capitalized words.
- One-time permission is granted only for the use specified in your request. No additional uses are granted (such as derivative works or other editions). For any other uses, please submit a new request.



If credit is given to another source for the material you requested, permission must be obtained from that source.





BACK CLOSE WINDOW


© 2019 Copyright - All Rights Reserved | Copyright Clearance Center, Inc. | [Privacy statement](#) | [Terms and Conditions](#) Comments? We would like to hear from you. E-mail us at customer@copyright.com

11/8/2019

Rightslink® by Copyright Clearance Center

 Home
  Help
  Live Chat
  Md Ashraful Islam



Noble metal-coated MoS₂ nanofilms with vertically-aligned 2D layers for visible light-driven photocatalytic degradation of emerging water contaminants
 Author: Md Ashraful Islam et al
 Publication: Scientific Reports
 Publisher: Springer Nature
 Date: Nov 2, 2017
 Copyright © 2017, Springer Nature

Creative Commons

This is an open access article distributed under the terms of the [Creative Commons CC BY](#) license, which permits unrestricted use, distribution, and reproduction in any medium, provided the original work is properly cited.

You are not required to obtain permission to reuse this article.


To request permission for a type of use not listed, please contact [Springer Nature](#)





© 2019 Copyright - All Rights Reserved | Copyright Clearance Center, Inc. | [Privacy statement](#) | [Terms and Conditions](#) Comments? We would like to hear from you. E-mail us at customer@copyright.com


Figure-3

11/8/2019

Rightslink® by Copyright Clearance Center

 Home
  Help
  Live Chat
  Sign in
  Create Account



Metal Seed Layer Thickness-Induced Transition From Vertical to Horizontal Growth of MoS₂ and WS₂
Author: Yeonwoong Jung, Jie Shen, Yanhui Liu, et al
Publication: Nano Letters
Publisher: American Chemical Society
Date: Dec 1, 2014
Copyright © 2014, American Chemical Society

PERMISSION/LICENSE IS GRANTED FOR YOUR ORDER AT NO CHARGE

This type of permission/license, instead of the standard Terms & Conditions, is sent to you because no fee is being charged for your order. Please note the following:

- Permission is granted for your request in both print and electronic formats, and translations.
- If figures and/or tables were requested, they may be adapted or used in part.
- Please print this page for your records and send a copy of it to your publisher/graduate school.
- Appropriate credit for the requested material should be given as follows: "Reprinted (adapted) with permission from (COMPLETE REFERENCE CITATION). Copyright (YEAR) American Chemical Society." Insert appropriate information in place of the capitalized words.
- One-time permission is granted only for the use specified in your request. No additional uses are granted (such as derivative works or other editions). For any other uses, please submit a new request.

If credit is given to another source for the material you requested, permission must be obtained from that source.



BACK CLOSE WINDOW






© 2019 Copyright - All Rights Reserved | Copyright Clearance Center, Inc. | [Privacy statement](#) | [Terms and Conditions](#) Comments? We would like to hear from you. E-mail us at customer@copyright.com


Figure-4

10/29/2019

Rightslink® by Copyright Clearance Center

 Home
  Help
  Email Support
  Sign in
  Create Account



The chemistry of two-dimensional layered transition metal dichalcogenide nanosheets
Author: Manish Chhowalla, Hyeon Suk Shin, Goki Eda, Lain-Jong Li, Kian Ping Loh et al.
Publication: Nature Chemistry
Publisher: Springer Nature
Date: Mar 20, 2013
Copyright © 2013, Springer Nature

Quick Price Estimate

This service provides permission for reuse only.
If you do not have a copy of the article you are using, you may copy and paste the content and reuse according to the terms of your agreement. Please be advised that obtaining the content you license is a separate transaction not involving RightsLink.

This reuse request is free of charge although you are required to obtain a license through RightsLink and comply with the license terms and conditions. You will not be charged for this order. Please select the Continue button and place an order for this reuse.

Adaptations/modifications - Springer Nature allows adaptation of figures for style and formatting purposes under this license under the condition that this does not alter the meaning of the content.

I would like to...
I am a/an...
My format is...
I would like to use...
Number of figures/tables
High-res required

reuse in a dissertation/thesis
academic/university or research
electronic
figures/tables/illustrations
1
no

Circulation/distribution
Are you the author of this Springer Nature content?
I will be translating...
My currency is...
Quick Price

50000 or greater
no
no
USD - \$
0.00 USD

QUICK PRICE
CONTINUE

© 2019 Copyright - All Rights Reserved | [Copyright Clearance Center, Inc.](#) | [Privacy statement](#) | [Terms and Conditions](#) Comments? We would like to hear from you. E-mail us at customer@copyright.com

Figure-5

10/29/2019

Rightslink® by Copyright Clearance Center



RightsLink®



Chemical Vapor Deposition Growth and Applications of Two-Dimensional Materials and Their Heterostructures

Author: Zhengyang Cai, Bilu Liu, Xiaolong Zou, et al

Publication: Chemical Reviews

Publisher: American Chemical Society

Date: Jul 1, 2018

Copyright © 2018, American Chemical Society

PERMISSION/LICENSE IS GRANTED FOR YOUR ORDER AT NO CHARGE

This type of permission/license, instead of the standard Terms & Conditions, is sent to you because no fee is being charged for your order. Please note the following:

- Permission is granted for your request in both print and electronic formats, and translations.
 - If figures and/or tables were requested, they may be adapted or used in part.
 - Please print this page for your records and send a copy of it to your publisher/graduate school.
 - Appropriate credit for the requested material should be given as follows: "Reprinted (adapted) with permission from (COMPLETE REFERENCE CITATION). Copyright (YEAR) American Chemical Society." Insert appropriate information in place of the capitalized words.
 - One-time permission is granted only for the use specified in your request. No additional uses are granted (such as derivative works or other editions). For any other uses, please submit a new request.
- If credit is given to another source for the material you requested, permission must be obtained from that source.

[BACK](#)

[CLOSE WINDOW](#)

© 2019 Copyright - All Rights Reserved | [Copyright Clearance Center, Inc.](#) | [Privacy statement](#) | [Terms and Conditions](#)
 Comments? We would like to hear from you. E-mail us at customercare@copyright.com

Figure-6

11/8/2019

Rightslink® by Copyright Clearance Center



RightsLink®



Home



Help



Live Chat



Sign in



Create Account



Environmental Applications of 2D Molybdenum Disulfide (MoS₂) Nanosheets

Author: Zhongying Wang, Baoxia Mi

Publication: Environmental Science & Technology

Publisher: American Chemical Society

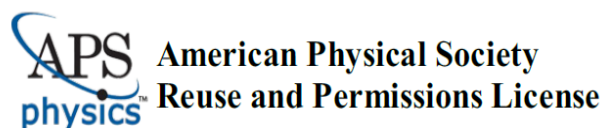
Date: Aug 1, 2017

Copyright © 2017, American Chemical Society

PERMISSION/LICENSE IS GRANTED FOR YOUR ORDER AT NO CHARGE

This type of permission/license, instead of the standard Terms & Conditions, is sent to you because no fee is being charged for your order. Please note the following:

Figure-7



08-Nov-2019

This license agreement between the American Physical Society ("APS") and Md Ashraful Islam ("You") consists of your license details and the terms and conditions provided by the American Physical Society and SciPris.

Licensed Content Information

License Number:	RNP/19/NOV/020139
License date:	08-Nov-2019
DOI:	10.1103/PhysRevLett.105.136805
Title:	Atomically Thin MoS_2 : A New Direct-Gap Semiconductor
Author:	Kin Fai Mak et al.
Publication:	Physical Review Letters
Publisher:	American Physical Society
Cost:	USD \$ 0.00

Request Details

Does your reuse require significant modifications: No

Specify intended distribution locations: United States

Reuse Category: Reuse in a thesis/dissertation

Requestor Type: Student

Items for Reuse: Figures/Tables

Number of Figure/Tables: 1

Figure/Tables Details: Lattice structure of MoS_2 in both the in- and out-of-plane directions and simplified band structure of bulk MoS_2 , showing the lowest conduction band c_1 and the highest split valence band

Format for Reuse: Electronic

Information about New Publication:

University/Publisher: University of Central Florida

Title of dissertation/thesis: CHEMICAL VAPOR DEPOSITION GROWTH OF LARGE AREA 2D MoS_2 LAYERS: LAYER ORIENTATION CONTROL, HETEROSTRUCTURE INTEGRATION, AND APPLICATIONS FOR STRETCHABLE SENSORS

Author(s): Md Ashraful Islam

Expected completion date: Nov. 2019

License Requestor Information

Name:	Md Ashraful Islam
Affiliation:	Individual
Email Id:	ashraf.diu@gmail.com
Country:	United States





TERMS AND CONDITIONS






The American Physical Society (APS) is pleased to grant the Requestor of this license a non-exclusive, non-transferable permission, limited to Electronic format, provided all criteria outlined below are followed.


1. You must also obtain permission from at least one of the lead authors for each separate work, if you haven't done so already. The author's name and affiliation can be found on the first page of the published Article.
2. For electronic format permissions, Requestor agrees to provide a hyperlink from the reprinted APS material using the source material's DOI on the web page where the work appears. The hyperlink should use the standard DOI resolution URL, <http://dx.doi.org/{DOI}>. The hyperlink may be embedded in the copyright credit line.
3. For print format permissions, Requestor agrees to print the required copyright credit line on the first page where the material appears: "Reprinted (abstract/excerpt/figure) with permission from [(FULL REFERENCE CITATION) as follows: Author's Names, APS Journal Title, Volume Number, Page Number and Year of Publication.] Copyright (YEAR) by the American Physical Society."
4. Permission granted in this license is for a one-time use and does not include permission for any future editions, updates, databases, formats or other matters. Permission must be sought for any additional use.
5. Use of the material does not and must not imply any endorsement by APS.
6. APS does not imply, purport or intend to grant permission to reuse materials to which it does not hold copyright. It is the requestor's sole responsibility to ensure the licensed material is original to APS and does not contain the copyright of another entity, and that the copyright notice of the figure, photograph, cover or table does not indicate it was reprinted by APS with permission from another source.
7. The permission granted herein is personal to the Requestor for the use specified and is not transferable or assignable without express written permission of APS. This license may not be amended except in writing by APS.
8. You may not alter, edit or modify the material in any manner.
9. You may translate the materials only when translation rights have been granted.
10. APS is not responsible for any errors or omissions due to translation.
11. You may not use the material for promotional, sales, advertising or marketing purposes.
12. The foregoing license shall not take effect unless and until APS or its agent, Aptara, receives payment in full in accordance with Aptara Billing and Payment Terms and Conditions, which are incorporated herein by reference.
13. Should the terms of this license be violated at any time, APS or Aptara may revoke the license with no refund to you and seek relief to the fullest extent of the laws of the USA. Official written notice will be made using the contact information provided with the permission request. Failure to receive such notice will not nullify revocation of the permission.
14. APS reserves all rights not specifically granted herein.
15. This document, including the Aptara Billing and Payment Terms and Conditions, shall be the entire agreement between the parties relating to the subject matter hereof.

Figure-8

11/8/2019 Rightslink® by Copyright Clearance Center

 Home
  Help
  Live Chat
  Sign In
  Create Account



Emerging Photoluminescence in Monolayer MoS₂
 Author: Andrea Splendiani, Liang Sun, Yuanbo Zhang, et al
 Publication: Nano Letters
 Publisher: American Chemical Society
 Date: Apr 1, 2010
Copyright © 2010, American Chemical Society

PERMISSION/LICENSE IS GRANTED FOR YOUR ORDER AT NO CHARGE

This type of permission/license, instead of the standard Terms & Conditions, is sent to you because no fee is being charged for your order. Please note the following:

- Permission is granted for your request in both print and electronic formats, and translations.
- If figures and/or tables were requested, they may be adapted or used in part.
- Please print this page for your records and send a copy of it to your publisher/graduate school.
- Appropriate credit for the requested material should be given as follows: "Reprinted (adapted) with permission from (COMPLETE REFERENCE CITATION). Copyright (YEAR) American Chemical Society." Insert appropriate information in place of the capitalized words.
- One-time permission is granted only for the use specified in your request. No additional uses are granted (such as derivative works or other editions). For any other uses, please submit a new request.



If credit is given to another source for the material you requested, permission must be obtained from that source.





BACK CLOSE WINDOW


© 2019 Copyright - All Rights Reserved | Copyright Clearance Center, Inc. | Privacy statement | Terms and Conditions
 Comments? We would like to hear from you. E-mail us at customer-care@copyright.com

Figure-9

11/8/2019 Rightslink® by Copyright Clearance Center

 Home
  Help
  Live Chat
  Md Ashraful Islam ▾



Ultrasensitive photodetectors based on monolayer MoS₂
 Author: Oriol Lopez Sanchez, Dominik Lembke, Metin Kayci, Aleksandra Radenovic, Andras Kis
 Publication: Nature Nanotechnology
 Publisher: Springer Nature
 Date: Jun 9, 2013
Copyright © 2013, Springer Nature

Order Completed

Thank you for your order.

This Agreement between University of Central Florida -- Md Ashraful Islam ("You") and Springer Nature ("Springer Nature") consists of your license details and the terms and conditions provided by Springer Nature and Copyright Clearance Center.

Your confirmation email will contain your order number for future reference.

License Number	4704290382054	Printable Details
License date	Nov 08, 2019	

11/8/2019

Rightslink® by Copyright Clearance Center

Licensed Content		Order Details	
Licensed Content Publisher	Springer Nature	Type of Use	Thesis/Dissertation
Licensed Content Publication	Nature Nanotechnology	Requestor type	non-commercial (non-profit)
Licensed Content Title	Ultrasensitive photodetectors based on monolayer MoS2	Format	electronic
Licensed Content Author	Oriol Lopez-Sanchez, Dominik Lembke, Metin Kayci, Aleksandra Radenovic, Andras Kis	Portion	figures/tables/illustrations
Licensed Content Date	Jun 9, 2013	Number of figures/tables/illustrations	1
Licensed Content Volume	8	High-res required	no
Licensed Content Issue	7	Will you be translating?	no
		Circulation/distribution	1 - 29
		Author of this Springer Nature content	no
About Your Work		Additional Data	
Title	CHEMICAL VAPOR DEPOSITION GROWTH OF LARGE AREA 2D MoS2 LAYERS: LAYER ORIENTATION CONTROL, HETEROSTRUCTURE INTEGRATION, AND APPLICATIONS FOR STRETCHABLE SENSORS	Order reference number	00000
Institution name	University of Central Florida	Portions	1(a)
Expected presentation date	Nov 2019		
Requestor Location		Tax Details	
Requestor Location	University of Central Florida 3028 Southern Pine Trail 3028s ORLANDO, FL 32826 United States Attn: University of Central Florida		
\$ Price			
Total	0.00 USD		
		Total: 0.00 USD	
CLOSE WINDOW		ORDER MORE	



Home



Help



Email Support



Sign In



Create Account



Synthetic approaches to two-dimensional transition metal dichalcogenide nanosheets

Author: Jack R. Brent, Nicky Savjani, Paul O'Brien

Publication: Progress in Materials Science

Publisher: Elsevier

Date: August 2017

Copyright © 2017, Elsevier

Creative Commons

This is an open access article distributed under the terms of the [Creative Commons CC-BY](#) license, which permits unrestricted use, distribution, and reproduction in any medium, provided the original work is properly cited.

You are not required to obtain permission to reuse this article.

To request permission for a type of use not listed, please contact [Elsevier](#) Global Rights Department.

Are you the [author](#) of this Elsevier journal article?

© 2019 Copyright - All Rights Reserved | [Copyright Clearance Center, Inc.](#) | [Privacy statement](#) | [Terms and Conditions](#)
Comments? We would like to hear from you. E-mail us at customer care@copyright.com

Strain-Driven and Layer-Number-Dependent Crossover of Growth Mode in van der Waals Heterostructures: 2D/2D Layer-By-Layer Horizontal Epitaxy to 2D/3D Vertical Reorientation

JOHN WILEY AND SONS LICENSE TERMS AND CONDITIONS

Nov 08, 2019

This Agreement between University of Central Florida -- Md Ashraf Islam ("You") and John Wiley and Sons ("John Wiley and Sons") consists of your license details and the terms and conditions provided by John Wiley and Sons and Copyright Clearance Center.

License Number	4704360265498
License date	Nov 08, 2019
Licensed Content Publisher	John Wiley and Sons
Licensed Content Publication	Advanced Materials Interfaces
Licensed Content Title	Strain-Driven and Layer-Number-Dependent Crossover of Growth Mode in van der Waals Heterostructures: 2D/2D Layer-By-Layer Horizontal Epitaxy to 2D/3D Vertical Reorientation
Licensed Content Author	Nitin Choudhary, Hee-Suk Chung, Jung Han Kim, et al
Licensed Content Date	May 17, 2018
Licensed Content Volume	5
Licensed Content Issue	14
Licensed Content Pages	9

Type of Use	Dissertation/Thesis
Requestor type	Author of this Wiley article
Format	Electronic
Portion	Full article
Will you be translating?	No
Title of your thesis / dissertation	CHEMICAL VAPOR DEPOSITION GROWTH OF LARGE AREA 2D MoS2 LAYERS: LAYER ORIENTATION CONTROL, HETEROSTRUCTURE INTEGRATION, AND APPLICATIONS FOR STRETCHABLE SENSORS
Expected completion date	Nov 2019
Expected size (number of pages)	1
Requestor Location	University of Central Florida 3028 Southern Pine Trail ORLANDO, FL 32826 United States Attn: University of Central Florida
Publisher Tax ID	EU826007151
Total	0.00 USD
Terms and Conditions	

TERMS AND CONDITIONS

This copyrighted material is owned by or exclusively licensed to John Wiley & Sons, Inc. or one of its group companies (each a "Wiley Company") or handled on behalf of a society with which a Wiley Company has exclusive publishing rights in relation to a particular work (collectively "WILEY"). By clicking "accept" in connection with completing this licensing transaction, you agree that the following terms and conditions apply to this transaction (along with the billing and payment terms and conditions established by the Copyright Clearance Center Inc., ("CCC's Billing and Payment terms and conditions"), at the time that you opened your RightsLink account (these are available at any time at <http://myaccount.copyright.com>).

Terms and Conditions

<https://s100.copyright.com/MyAccount/web/jsp/viewprintablelicensefrommyorders.jsp?ref=030804a8-8814-4fe9-83f0-88515e30cf4d&email=>

1/4

11/8/2019

RightsLink - Your Account

- The materials you have requested permission to reproduce or reuse (the "Wiley Materials") are protected by copyright.
- You are hereby granted a personal, non-exclusive, non-sub licensable (on a stand-alone basis), non-transferable, worldwide, limited license to reproduce the Wiley Materials for the purpose specified in the licensing process. This license, and any **CONTENT (PDF or image file) purchased as part of your order**, is for a one-time use only and limited to any maximum distribution number specified in the license. The first instance of republication or reuse granted by this license must be completed within two years of the date of the grant of this license (although copies prepared before the end date may be distributed thereafter). The Wiley Materials shall not be used in any other manner or for any other purpose, beyond what is granted in the license. Permission is granted subject to an appropriate acknowledgement given to the author, title of the material/book/journal and the publisher. You shall also duplicate the copyright notice that appears in the Wiley publication in your use of the Wiley Material. Permission is also granted on the understanding that nowhere in the text is a previously published source acknowledged for all or part of this Wiley Material. Any third party content is expressly excluded from this permission.
- With respect to the Wiley Materials, all rights are reserved. Except as expressly granted by the terms of the license, no part of the Wiley Materials may be copied, modified, adapted (except for minor reformatting required by the new Publication), translated, reproduced, transferred or distributed, in any form or by any means, and no derivative works may be made based on the Wiley Materials without the prior permission of the respective copyright owner. **For STM Signatory Publishers clearing permission under the terms of the STM Permissions Guidelines only, the terms of the license are extended to include subsequent editions and for editions in other languages, provided such editions are for the work as a**

whole in situ and does not involve the separate exploitation of the permitted figures or extracts, You may not alter, remove or suppress in any manner any copyright, trademark or other notices displayed by the Wiley Materials. You may not license, rent, sell, loan, lease, pledge, offer as security, transfer or assign the Wiley Materials on a stand-alone basis, or any of the rights granted to you hereunder to any other person.

- The Wiley Materials and all of the intellectual property rights therein shall at all times remain the exclusive property of John Wiley & Sons Inc, the Wiley Companies, or their respective licensors, and your interest therein is only that of having possession of and the right to reproduce the Wiley Materials pursuant to Section 2 herein during the continuance of this Agreement. You agree that you own no right, title or interest in or to the Wiley Materials or any of the intellectual property rights therein. You shall have no rights hereunder other than the license as provided for above in Section 2. No right, license or interest to any trademark, trade name, service mark or other branding ("Marks") of WILEY or its licensors is granted hereunder, and you agree that you shall not assert any such right, license or interest with respect thereto
- NEITHER WILEY NOR ITS LICENSORS MAKES ANY WARRANTY OR REPRESENTATION OF ANY KIND TO YOU OR ANY THIRD PARTY, EXPRESS, IMPLIED OR STATUTORY, WITH RESPECT TO THE MATERIALS OR THE ACCURACY OF ANY INFORMATION CONTAINED IN THE MATERIALS, INCLUDING, WITHOUT LIMITATION, ANY IMPLIED WARRANTY OF MERCHANTABILITY, ACCURACY, SATISFACTORY QUALITY, FITNESS FOR A PARTICULAR PURPOSE, USABILITY, INTEGRATION OR NON-INFRINGEMENT AND ALL SUCH WARRANTIES ARE HEREBY EXCLUDED BY WILEY AND ITS LICENSORS AND WAIVED BY YOU.
- WILEY shall have the right to terminate this Agreement immediately upon breach of this Agreement by you.
- You shall indemnify, defend and hold harmless WILEY, its Licensors and their respective directors, officers, agents and employees, from and against any actual or threatened claims, demands, causes of action or proceedings arising from any breach of this Agreement by you.
- IN NO EVENT SHALL WILEY OR ITS LICENSORS BE LIABLE TO YOU OR ANY OTHER PARTY OR ANY OTHER PERSON OR ENTITY FOR ANY SPECIAL, CONSEQUENTIAL, INCIDENTAL, INDIRECT, EXEMPLARY OR PUNITIVE DAMAGES, HOWEVER CAUSED, ARISING OUT OF OR IN CONNECTION WITH THE DOWNLOADING, PROVISIONING, VIEWING OR USE OF THE MATERIALS REGARDLESS OF THE FORM OF ACTION, WHETHER FOR BREACH OF CONTRACT, BREACH OF WARRANTY, TORT, NEGLIGENCE, INFRINGEMENT OR OTHERWISE (INCLUDING, WITHOUT LIMITATION, DAMAGES BASED ON LOSS OF PROFITS, DATA, FILES, USE, BUSINESS OPPORTUNITY OR CLAIMS OF THIRD PARTIES), AND WHETHER OR NOT THE PARTY HAS BEEN ADVISED OF THE POSSIBILITY OF SUCH DAMAGES. THIS LIMITATION SHALL APPLY NOTWITHSTANDING ANY FAILURE OF ESSENTIAL PURPOSE OF ANY LIMITED REMEDY PROVIDED HEREIN.
- Should any provision of this Agreement be held by a court of competent jurisdiction to be illegal, invalid, or unenforceable, that provision shall be deemed amended to achieve as nearly as possible the same economic effect as the original provision, and the legality, validity and enforceability of the remaining provisions of this Agreement shall not be affected or impaired thereby.

<https://s100.copyright.com/MyAccount/web/jsp/viewprintablelicensefrommyorders.jsp?ref=0308c4a8-6814-4fe9-83f6-88515e30cf4d&email=>

2/4

11/8/2019

RightsLink - Your Account

- The failure of either party to enforce any term or condition of this Agreement shall not constitute a waiver of either party's right to enforce each and every term and condition of this Agreement. No breach under this agreement shall be deemed waived or excused by either party unless such waiver or consent is in writing signed by the party granting such waiver or consent. The waiver by or consent of a party to a breach of any provision of this Agreement shall not operate or be construed as a waiver of or consent to any other or subsequent breach by such other party.
- This Agreement may not be assigned (including by operation of law or otherwise) by you without WILEY's prior written consent.
- Any fee required for this permission shall be non-refundable after thirty (30) days from receipt by the CCC.
- These terms and conditions together with CCC's Billing and Payment terms and conditions (which are incorporated herein) form the entire agreement between you and WILEY concerning this licensing transaction and (in the absence of fraud) supersedes all prior agreements and representations of the parties, oral or written. This Agreement may not be amended except in writing signed by both parties. This Agreement shall be binding upon and inure to the benefit of the parties' successors, legal representatives, and authorized assigns.
- In the event of any conflict between your obligations established by these terms and conditions and those established by CCC's Billing and Payment terms and conditions, these terms and conditions shall prevail.

- In the event of any conflict between your obligations established by these terms and conditions and those established by CCC's Billing and Payment terms and conditions, these terms and conditions shall prevail.
- WILEY expressly reserves all rights not specifically granted in the combination of (i) the license details provided by you and accepted in the course of this licensing transaction, (ii) these terms and conditions and (iii) CCC's Billing and Payment terms and conditions.
- This Agreement will be void if the Type of Use, Format, Circulation, or Requestor Type was misrepresented during the licensing process.
- This Agreement shall be governed by and construed in accordance with the laws of the State of New York, USA, without regards to such state's conflict of law rules. Any legal action, suit or proceeding arising out of or relating to these Terms and Conditions or the breach thereof shall be instituted in a court of competent jurisdiction in New York County in the State of New York in the United States of America and each party hereby consents and submits to the personal jurisdiction of such court, waives any objection to venue in such court and consents to service of process by registered or certified mail, return receipt requested, at the last known address of such party.

WILEY OPEN ACCESS TERMS AND CONDITIONS

Wiley Publishes Open Access Articles in fully Open Access Journals and in Subscription journals offering Online Open. Although most of the fully Open Access journals publish open access articles under the terms of the Creative Commons Attribution (CC BY) License only, the subscription journals and a few of the Open Access Journals offer a choice of Creative Commons Licenses. The license type is clearly identified on the article.

The Creative Commons Attribution License

The [Creative Commons Attribution License \(CC-BY\)](#) allows users to copy, distribute and transmit an article, adapt the article and make commercial use of the article. The CC-BY license permits commercial and non-

Creative Commons Attribution Non-Commercial License

The [Creative Commons Attribution Non-Commercial \(CC-BY-NC\) License](#) permits use, distribution and reproduction in any medium, provided the original work is properly cited and is not used for commercial purposes.(see below)

Creative Commons Attribution-Non-Commercial-NoDerivs License

The [Creative Commons Attribution Non-Commercial-NoDerivs License \(CC-BY-NC-ND\)](#) permits use, distribution and reproduction in any medium, provided the original work is properly cited, is not used for commercial purposes and no modifications or adaptations are made. (see below)

Use by commercial "for-profit" organizations

Use of Wiley Open Access articles for commercial, promotional, or marketing purposes requires further explicit permission from Wiley and will be subject to a fee.

Further details can be found on Wiley Online Library <http://olabout.wiley.com/WileyCDA/Section/id-410895.html>

Other Terms and Conditions:

<https://s100.copyright.com/MyAccount/web/jsp/viewprintablelicensefrommyorders.jsp?ref=0308c4a8-6814-4fe9-83f6-88515e30cf4d&email=>

3/4

11/8/2019

RightsLink - Your Account

v1.10 Last updated September 2015

Questions? customer@copyright.com or +1-855-239-3415 (toll free in the US) or +1-978-646-2777.

11/8/2019

RightsLink - Your Account

- The failure of either party to enforce any term or condition of this Agreement shall not constitute a waiver of either party's right to enforce each and every term and condition of this Agreement. No breach under this agreement shall be deemed waived or excused by either party unless such waiver or consent is in writing signed by the party granting such waiver or consent. The waiver by or consent of a party to a breach of any provision of this Agreement shall not operate or be construed as a waiver of or consent to any other or subsequent breach by such other party.
- This Agreement may not be assigned (including by operation of law or otherwise) by you without WILEY's prior written consent.
- Any fee required for this permission shall be non-refundable after thirty (30) days from receipt by the CCC.
- These terms and conditions together with CCC's Billing and Payment terms and conditions (which are incorporated herein) form the entire agreement between you and WILEY concerning this licensing transaction and (in the absence of fraud) supersedes all prior agreements and representations of the parties, oral or written. This Agreement may not be amended except in writing signed by both parties. This Agreement shall be binding upon and inure to the benefit of the parties' successors, legal representatives, and authorized assigns.

Centimeter-Scale 2D van der Waals Vertical Heterostructures Integrated on Deformable Substrates Enabled by Gold Sacrificial Layer-Assisted Growth

9/9/2019

Rightslink® by Copyright Clearance Center



RightsLink®

Home

Create Account

Help



ACS Publications
Most Trusted. Most Cited. Most Read.

Title: Centimeter-Scale 2D van der Waals Vertical Heterostructures Integrated on Deformable Substrates Enabled by Gold Sacrificial Layer-Assisted Growth

Author: Md Ashraful Islam, Jung Han Kim, Anthony Schropp, et al

Publication: Nano Letters

Publisher: American Chemical Society

Date: Oct 1, 2017

Copyright © 2017, American Chemical Society

LOGIN

If you're a [copyright.com](#) user, you can login to RightsLink using your [copyright.com](#) credentials. Already a RightsLink user or want to [learn more?](#)

Quick Price Estimate

Permission for this particular request is granted for print and electronic formats, and translations, at no charge. Figures and tables may be modified. Appropriate credit should be given. Please print this page for your records and provide a copy to your publisher. Requests for up to 4 figures require only this record. Five or more figures will generate a printout of additional terms and conditions. Appropriate credit should read: "Reprinted with permission from {COMPLETE REFERENCE CITATION}. Copyright {YEAR} American Chemical Society." Insert appropriate information in place of the capitalized words.

I would like to... ?

reuse in a Thesis/Dissertation ▼

Requestor Type ?

Author (original work) ▼

Portion ?

Full article ▼

Format ?

Print ▼

Will you be translating? ?

make a selection ▼

Select your currency

USD - \$ ▼

This service provides permission for reuse only. If you do not have a copy of the article you are using, you may copy and paste the content and reuse according to the terms of your agreement. Please be advised that obtaining the content you license is a separate transaction not involving Rightslink.

Will you be translating? ?

make a selection ▼

Select your currency

USD - \$ ▼

Quick Price

Click Quick Price

QUICK PRICE

CONTINUE

To request permission for a type of use not listed, please contact [the publisher](#) directly.

Copyright © 2019 [Copyright Clearance Center, Inc.](#) All Rights Reserved. [Privacy statement](#). [Terms and Conditions](#). Comments? We would like to hear from you. E-mail us at [customerservice@copyright.com](#)

Three dimensionally-ordered 2D MoS₂ vertical layers integrated on flexible substrates with stretch-tunable functionality and improved sensing capability.

11/8/2019

Manage Account



Marketplace™

Special Requests > Special Request Details

[Cancel Request](#)

Nanoscale

Article Three dimensionally-ordered 2D MoS₂ vertical layers integrated on flexible substrates with str...

GENERAL INFORMATION

Request ID	Request Date
600001182	08 Nov 2019
Request Status	
Pending	

ALL DETAILS

ISSN:	2040-3364
Type of Use:	Republish in a thesis/dissertation
Publisher:	RSC Pub
Portion:	Chapter/article

LICENSED CONTENT

Publication Title	Nanoscale	Rightholder	Royal Society of Chemistry
Article Title	Three dimensionally-ordered 2D MoS ₂ vertical layers integrated on flexible substrates with stretch-tunable functionality and improved sensing capability.	Publication Type	Journal
		Start Page	17525
		Issue	37
		Volume	10
Author/Editor	Guo jia na mi ke xue zhong xin (China), Royal Society of Chemistry (Great Britain)		
Date	01/01/2009		
Language	English		

https://marketplace.copyright.com/rs-ui-web/manage_account/special-requests/details/4d98b9df-21ed-4503-b47c-b529491bd728

1/3

11/8/2019

Manage Account

Country	United Kingdom of Great Britain and Northern Ireland
---------	--

REQUEST DETAILS

Portion Type	Chapter/article	Rights Requested	Main product
Page range(s)	17525-17533	Distribution	Worldwide
Total number of pages	9	Translation	Original language of publication
Format (select all that apply)	Electronic	Copies for the disabled?	No
Who will republish the	Publisher, not-for-profit		

Duration of Use	Current edition and up to 5 years	privileges?	
Lifetime Unit Quantity	Up to 499	Incidental promotional use?	No
		Currency	USD

NEW WORK DETAILS

Title	CHEMICAL VAPOR DEPOSITION GROWTH OF LARGE AREA 2D MoS2 LAYERS: LAYER ORIENTATION CONTROL, HETEROSTRUCTURE INTEGRATION, AND APPLICATIONS FOR STRETCHABLE SENSORS	Institution name	University of Central Florida
		Expected presentation date	2019-11-08
Instructor name	Dr. Yeonwoong Jung		

ADDITIONAL DETAILS

The requesting person / organization to appear on the license	Md Ashraful Islam
---	-------------------

REUSE CONTENT DETAILS

Title, description or numeric reference of the portion(s)	Three dimensionally-ordered 2D MoS2 vertical layers integrated on flexible substrates with stretch-tunable functionality and improved sensing capability.	Title of the article/chapter the portion is from	Three dimensionally-ordered 2D MoS2 vertical layers integrated on flexible substrates with stretch-tunable functionality and improved sensing capability.
---	---	--	---

https://marketplace.copyright.com/rs-ui-web/manage_account/special-requests/details/4d96b9df-21ed-4503-b47c-b529491bd728


2/3

11/8/2019

Manage Account

Editor of portion(s)	Zhai, Lei; Sundaram, Kalpathy B.; Noh, Chanwoo; Nehate, Shraddha; Ko, Tae-Jun; Ko, Minjee; Kim, Jung Han; Kaium, Md Golam; Jung, YounJoon; Jung, Yeonwoong; Islam, Md Ashraful; Fox, David; Chung, Hee-Suk; Cho, Chang-Hee; Bae, Tae Sung	Author of portion(s)	Zhai, Lei; Sundaram, Kalpathy B.; Noh, Chanwoo; Nehate, Shraddha; Ko, Tae-Jun; Ko, Minjee; Kim, Jung Han; Kaium, Md Golam; Jung, YounJoon; Jung, Yeonwoong; Islam, Md Ashraful; Fox, David; Chung, Hee-Suk; Cho, Chang-Hee; Bae, Tae Sung
Volume of serial or monograph	10	Issue, if republishing an article from a serial	37
Page or page range of portion	17525-17533	Publication date of portion	2018-01-01

COMMENTS

 Add Comment / Attachment

LIST OF REFERENCES

- [1] Bhimanapati G R, Lin Z, Meunier V, Jung Y, Cha J, Das S, Xiao D, Son Y, Strano M S, Cooper V R, *et al.* 2015 Recent Advances in Two-Dimensional Materials beyond Graphene *ACS Nano* **9** 11509-39
- [2] Cai Z, Liu B, Zou X and Cheng H-M 2018 Chemical Vapor Deposition Growth and Applications of Two-Dimensional Materials and Their Heterostructures *Chemical Reviews* **118** 6091-133
- [3] Chhowalla M, Shin H S, Eda G, Li L-J, Loh K P and Zhang H 2013 The chemistry of two-dimensional layered transition metal dichalcogenide nanosheets *Nature Chemistry* **5** 263
- [4] Venkata Subbaiah Y, Saji K and Tiwari A 2016 Atomically thin MoS₂: A versatile nongraphene 2D material *Advanced Functional Materials* **26** 2046-69
- [5] Jung Y, Shen J, Liu Y, Woods J M, Sun Y and Cha J J 2014 Metal Seed Layer Thickness-Induced Transition From Vertical to Horizontal Growth of MoS₂ and WS₂ *Nano Letters* **14** 6842-9
- [6] Islam M A, Church J, Han C, Chung H-S, Ji E, Kim J H, Choudhary N, Lee G-H, Lee W H and Jung Y 2017 Noble metal-coated MoS₂ nanofilms with vertically-aligned 2D layers for visible light-driven photocatalytic degradation of emerging water contaminants *Scientific reports* **7** 14944
- [7] Lee E, Yoon Y S and Kim D-J 2018 Two-dimensional transition metal dichalcogenides and metal oxide hybrids for gas sensing *ACS sensors* **3** 2045-60
- [8] Shang S-L, Lindwall G, Wang Y, Redwing J M, Anderson T, and Liu Z-K 2016 Lateral Versus Vertical Growth of Two-Dimensional Layered Transition-Metal Dichalcogenides: Thermodynamic Insight into MoS₂ *Nano Letters* **16** 5742-50
- [9] Cao Q, Zhao L, Wang A, Yang L, Lai L, Wang Z-L, Kim J, Zhou W, Yamauchi Y and Lin J 2019 Tailored synthesis of Zn–N co-doped porous MoC nanosheets towards efficient hydrogen evolution *Nanoscale* **11** 1700-9

- [10] Anantharaj S, Valappil M O, Karthick K, Pillai V K, Alwarappan S, and Kundu S 2019 Electrochemically chopped WS₂ quantum dots as an efficient and stable electrocatalyst for water reduction *Catalysis Science & Technology* **9** 223-31
- [11] Yin F, Gu B, Lin Y, Panwar N, Tjin S C, Qu J, Lau S P, and Yong K-T 2017 Functionalized 2D nanomaterials for gene delivery applications *Coordination Chemistry Reviews* **347** 77-97
- [12] Woods J M, Jung Y, Xie Y, Liu W, Liu Y, Wang H and Cha J J 2016 One-Step Synthesis of MoS₂/WS₂ Layered Heterostructures and Catalytic Activity of Defective Transition Metal Dichalcogenide Films *ACS Nano* **10** 2004-9
- [13] Geim A K and Grigorieva I V 2013 Van der Waals heterostructures *Nature* **499** 419
- [14] Wang H, Liu F, Fu W, Fang Z, Zhou W, and Liu Z 2014 Two-dimensional heterostructures: fabrication, characterization, and application *Nanoscale* **6** 12250-72
- [15] Liu Y, Weiss N O, Duan X, Cheng H-C, Huang Y, and Duan X 2016 Van der Waals heterostructures and devices *Nature Reviews Materials* **1** 16042
- [16] Wei W, Dai Y, Sun Q, Yin N, Han S, Huang B and Jacob T 2015 Electronic structures of in-plane two-dimensional transition-metal dichalcogenide heterostructures *Physical Chemistry Chemical Physics* **17** 29380-6
- [17] Duan X, Wang C, Shaw J C, Cheng R, Chen Y, Li H, Wu X, Tang Y, Zhang Q and Pan A 2014 Lateral epitaxial growth of two-dimensional layered semiconductor heterojunctions *Nature nanotechnology* **9** 1024
- [18] Gong Y, Lin J, Wang X, Shi G, Lei S, Lin Z, Zou X, Ye G, Vajtai R, and Yakobson B I 2014 Vertical and in-plane heterostructures from WS₂/MoS₂ monolayers *Nature materials* **13** 1135
- [19] Yan A, Velasco Jr J, Kahn S, Watanabe K, Taniguchi T, Wang F, Crommie M F and Zettl A 2015 Direct growth of single-and few-layer MoS₂ on h-BN with preferred relative rotation angles *Nano letters* **15** 6324-31

- [20] Geim A K and Grigorieva I V 2013 Van der Waals heterostructures *Nature* **499** 419-25
- [21] Wang S, Wang X and Warner J H 2015 All chemical vapor deposition growth of MoS₂: h-BN vertical van der Waals heterostructures *ACS nano* **9** 5246-54
- [22] Lin Y-C, Ghosh R K, Addou R, Lu N, Eichfeld S M, Zhu H, Li M-Y, Peng X, Kim M J and Li L-J 2015 Atomically thin resonant tunnel diodes built from synthetic van der Waals heterostructures *Nature communications* **6** 7311
- [23] Islam M A, Kim J H, Schropp A, Kalita H, Choudhary N, Weitzman D, Khondaker S I, Oh K H, Roy T, Chung H-S, *et al.* 2017 Centimeter-Scale 2D van der Waals Vertical Heterostructures Integrated on Deformable Substrates Enabled by Gold Sacrificial Layer-Assisted Growth *Nano Letters* **17** 6157-65
- [24] Samad L, Bladow S M, Ding Q, Zhuo J, Jacobberger R M, Arnold M S and Jin S 2016 Layer-controlled chemical vapor deposition growth of MoS₂ vertical heterostructures via van der Waals epitaxy *ACS nano* **10** 7039-46
- [25] Choudhary N, Chung H S, Kim J H, Noh C, Islam M A, Oh K H, Coffey K, Jung Y, and Jung Y 2018 Strain-Driven and Layer-Number-Dependent Crossover of Growth Mode in van der Waals Heterostructures: 2D/2D Layer-By-Layer Horizontal Epitaxy to 2D/3D Vertical Reorientation *Advanced Materials Interfaces* **5** 1800382
- [26] Fang H, Battaglia C, Carraro C, Nemsak S, Ozdol B, Kang J S, Bechtel H A, Desai S B, Kronast F, and Unal A A 2014 Strong interlayer coupling in van der Waals heterostructures built from single-layer chalcogenides *Proceedings of the National Academy of Sciences* **111** 6198-202
- [27] Zhang X, Meng F, Christianson J R, Arroyo-Torres C, Lukowski M A, Liang D, Schmidt J R and Jin S 2014 Vertical heterostructures of layered metal chalcogenides by van der Waals epitaxy *Nano letters* **14** 3047-54

- [28] Choi W, Choudhary N, Han G H, Park J, Akinwande D and Lee Y H 2017 Recent development of two-dimensional transition metal dichalcogenides and their applications *Materials Today* **20** 116-30
- [29] Gao L 2017 Flexible device applications of 2D semiconductors *Small* **13** 1603994
- [30] Yu H, Liao M, Zhao W, Liu G, Zhou X J, Wei Z, Xu X, Liu K, Hu Z, Deng K, *et al.* 2017 Wafer-Scale Growth and Transfer of Highly-Oriented Monolayer MoS₂ Continuous Films *ACS Nano* **11** 12001-7
- [31] Islam M A, Kim J H, Ko T-J, Noh C, Nehate S, Kaium M G, Ko M, Fox D, Zhai L, Cho C-H, *et al.* 2018 Three dimensionally-ordered 2D MoS₂ vertical layers integrated on flexible substrates with stretch-tunable functionality and improved sensing capability *Nanoscale* **10** 17525-33
- [32] Ma D, Shi J, Ji Q, Chen K, Yin J, Lin Y, Zhang Y, Liu M, Feng Q, Song X, *et al.* 2015 A universal etching-free transfer of MoS₂ films for applications in photodetectors *Nano Research* **8** 3662-72
- [33] Van Ngoc H, Qian Y, Han S K and Kang D J 2016 PMMA-Etching-Free Transfer of Wafer-scale Chemical Vapor Deposition Two-dimensional Atomic Crystal by a Water Soluble Polyvinyl Alcohol Polymer Method *Scientific Reports* **6** 33096
- [34] Castellanos-Gomez A, Buscema M, Molenaar R, Singh V, Janssen L, van der Zant H S J and Steele G A 2014 Deterministic transfer of two-dimensional materials by all-dry viscoelastic stamping *2D Materials* **1** 011002
- [35] Gurarslan A, Yu Y, Su L, Yu Y, Suarez F, Yao S, Zhu Y, Ozturk M, Zhang Y, and Cao L 2014 Surface-Energy-Assisted Perfect Transfer of Centimeter-Scale Monolayer and Few-Layer MoS₂ Films onto Arbitrary Substrates *ACS Nano* **8** 11522-8
- [36] Kim J H, Ko T-J, Okogbue E, Han S S, Shawkat M S, Kaium M G, Oh K H, Chung H-S and Jung Y 2019 Centimeter-scale Green Integration of Layer-by-Layer 2D TMD vdW Heterostructures on Arbitrary Substrates by Water-Assisted Layer Transfer *Scientific Reports* **9** 1641

- [37] Ma X, Liu Q, Xu D, Zhu Y, Kim S, Cui Y, Zhong L and Liu M 2017 Capillary-Force-Assisted Clean-Stamp Transfer of Two-Dimensional Materials *Nano Letters* **17** 6961-7
- [38] Islam M A, Kim J H, Schropp A, Kalita H, Choudhary N, Weitzman D, Khondaker S I, Oh K H, Roy T and Chung H-S 2017 Centimeter-scale 2D van der Waals vertical heterostructures integrated on deformable substrates enabled by gold sacrificial layer-assisted growth *Nano letters* **17** 6157-65
- [39] Yu K J, Yan Z, Han M, and Rogers J A 2017 Inorganic semiconducting materials for flexible and stretchable electronics *npj Flexible Electronics* **1** 4
- [40] Rogers J A, Someya T, and Huang Y 2010 Materials and mechanics for stretchable electronics *science* **327** 1603-7
- [41] Rogers J 2009 Materials and mechanics for stretchable electronics-from electronic eye cameras to conformal brain monitors: IEEE) p 1602-3
- [42] Song J 2015 Mechanics of stretchable electronics *Current Opinion in Solid State and Materials Science* **19** 160-70
- [43] Su Y, Liu Z, Kim S, Wu J, Huang Y and Rogers J A 2012 Mechanics of stretchable electronics with high fill factors *International Journal of Solids and Structures* **49** 3416-21
- [44] Wang Y, Li Z, and Xiao J 2016 Stretchable thin film materials: fabrication, application, and mechanics *Journal of Electronic Packaging* **138** 020801
- [45] Wang Z and Mi B 2017 Environmental applications of 2D molybdenum disulfide (MoS₂) nanosheets *Environmental science & technology* **51** 8229-44
- [46] Chhowalla M, Shin H S, Eda G, Li L-J, Loh K P and Zhang H 2013 The chemistry of two-dimensional layered transition metal dichalcogenide nanosheets *Nature chemistry* **5** 263

- [47] Zhu C, Wang G, Liu B, Marie X, Qiao X, Zhang X, Wu X, Fan H, Tan P and Amand T 2013 Strain tuning of optical emission energy and polarization in monolayer and bilayer MoS₂ *Physical Review B* **88** 121301
- [48] Mak K F, Lee C, Hone J, Shan J and Heinz T F 2010 Atomically thin MoS₂: a new direct-gap semiconductor *Physical review letters* **105** 136805
- [49] Splendiani A, Sun L, Zhang Y, Li T, Kim J, Chim C-Y, Galli G, and Wang F 2010 Emerging photoluminescence in monolayer MoS₂ *Nano letters* **10** 1271-5
- [50] Dhakal K P, Duong D L, Lee J, Nam H, Kim M, Kan M, Lee Y H and Kim J 2014 Confocal absorption spectral imaging of MoS₂: optical transitions depending on the atomic thickness of intrinsic and chemically doped MoS₂ *Nanoscale* **6** 13028-35
- [51] Tonndorf P, Schmidt R, Böttger P, Zhang X, Börner J, Liebig A, Albrecht M, Kloc C, Gordan O and Zahn D R 2013 Photoluminescence emission and Raman response of monolayer MoS₂, MoSe₂, and WSe₂ *Optics express* **21** 4908-16
- [52] Eda G, Yamaguchi H, Voiry D, Fujita T, Chen M and Chhowalla M 2011 Photoluminescence from Chemically Exfoliated MoS₂ *Nano Letters* **11** 5111-6
- [53] Chen Y, Xi J, Dumcenco D O, Liu Z, Suenaga K, Wang D, Shuai Z, Huang Y-S and Xie L 2013 Tunable band gap photoluminescence from atomically thin transition-metal dichalcogenide alloys *Acs Nano* **7** 4610-6
- [54] Castellanos-Gomez A, Roldán R, Cappelluti E, Buscema M, Guinea F, van der Zant H S J and Steele G A 2013 Local Strain Engineering in Atomically Thin MoS₂ *Nano Letters* **13** 5361-6
- [55] Li W, Zhang G, Guo M and Zhang Y-W 2014 Strain-tunable electronic and transport properties of MoS₂ nanotubes *Nano Research* **7** 518-27
- [56] Kukucska G and Koltai J 2017 Theoretical Investigation of Strain and Doping on the Raman Spectra of Monolayer MoS₂ *physica status solidi (b)* **254** 1700184

- [57] Johari P and Shenoy V B 2012 Tuning the Electronic Properties of Semiconducting Transition Metal Dichalcogenides by Applying Mechanical Strains *ACS Nano* **6** 5449-56
- [58] Bertolazzi S, Brivio J and Kis A 2011 Stretching and breaking of ultrathin MoS₂ *ACS nano* **5** 9703-9
- [59] He K, Poole C, Mak K F and Shan J 2013 Experimental Demonstration of Continuous Electronic Structure Tuning via Strain in Atomically Thin MoS₂ *Nano Letters* **13** 2931-6
- [60] Late D J, Huang Y-K, Liu B, Acharya J, Shirodkar S N, Luo J, Yan A, Charles D, Waghmare U V, David V P, *et al.* 2013 Sensing Behavior of Atomically Thin-Layered MoS₂ Transistors *ACS Nano* **7** 4879-91
- [61] Bertolazzi S, Gobbi M, Zhao Y, Backes C, and Samorì P 2018 Molecular chemistry approaches for tuning the properties of two-dimensional transition metal dichalcogenides *Chemical Society Reviews* **47** 6845-88
- [62] Anichini C, Czepa W, Pakulski D, Aliprandi A, Ciesielski A, and Samorì P 2018 Chemical sensing with 2D materials *Chemical Society Reviews* **47** 4860-908
- [63] Lopez-Sanchez O, Lembke D, Kayci M, Radenovic A and Kis A 2013 Ultrasensitive photodetectors based on monolayer MoS₂ *Nature nanotechnology* **8** 497
- [64] Brent J R, Savjani N and O'Brien P 2017 Synthetic approaches to two-dimensional transition metal dichalcogenide nanosheets *Progress in Materials Science* **89** 411-78
- [65] Lin Z, McCreary A, Briggs N, Subramanian S, Zhang K, Sun Y, Li X, Borys N J, Yuan H, and Fullerton-Shirey S K 2016 2D materials advances: from large scale synthesis and controlled heterostructures to improved characterization techniques, defects and applications *2D Materials* **3** 042001

- [66] Das S, Robinson J A, Dubey M, Terrones H and Terrones M 2015 Beyond graphene: progress in novel two-dimensional materials and van der Waals solids *Annual Review of Materials Research* **45** 1-27
- [67] Woo Y, Hong W, Yang S Y, Kim H J, Cha J H, Lee J E, Lee K J, Kang T and Choi S Y 2018 Large-Area CVD-Grown MoS₂ Driver Circuit Array for Flexible Organic Light-Emitting Diode Display *Advanced Electronic Materials* **4** 1800251
- [68] Choudhary N, Park J, Hwang J Y, Chung H-S, Dumas K H, Khondaker S I, Choi W and Jung Y 2016 Centimeter scale patterned growth of vertically stacked few layers only 2D MoS₂/WS₂ van der Waals heterostructure *Scientific reports* **6** 25456
- [69] Choudhary N, Park J, Hwang J Y and Choi W 2014 Growth of Large-Scale and Thickness-Modulated MoS₂ Nanosheets *ACS Applied Materials & Interfaces* **6** 21215-22
- [70] Grimme S, Antony J, Ehrlich S and Krieg H 2010 A consistent and accurate ab initio parametrization of density functional dispersion correction (DFT-D) for the 94 elements H-Pu *The Journal of chemical physics* **132** 154104
- [71] Kresse G and Joubert D 1999 From ultrasoft pseudopotentials to the projector augmented-wave method *Physical Review B* **59** 1758
- [72] Perdew J P, Burke K, and Ernzerhof M 1996 Generalized gradient approximation made simple *Physical review letters* **77** 3865
- [73] Perdew J P, Burke K, and Ernzerhof M 1997 Generalized Gradient Approximation Made Simple [Phys. Rev. Lett. 77, 3865 (1996)] *Physical Review Letters* **78** 1396-
- [74] Li H, Li Y, Aljarb A, Shi Y and Li L-J 2018 Epitaxial Growth of Two-Dimensional Layered Transition-Metal Dichalcogenides: Growth Mechanism, Controllability, and Scalability *Chemical Reviews* **118** 6134-50

- [75] Li M-Y, Shi Y, Cheng C-C, Lu L-S, Lin Y-C, Tang H-L, Tsai M-L, Chu C-W, Wei K-H and He J-H 2015 Epitaxial growth of a monolayer WSe₂-MoS₂ lateral pn junction with an atomically sharp interface *Science* **349** 524-8
- [76] Utama M I B, Zhang Q, Zhang J, Yuan Y, Belarre F J, Arbiol J and Xiong Q 2013 Recent developments and future directions in the growth of nanostructures by van der Waals epitaxy *Nanoscale* **5** 3570-88
- [77] Lin Y-C, Lu N, Perea-Lopez N, Li J, Lin Z, Peng X, Lee C H, Sun C, Calderin L and Browning P N 2014 Direct synthesis of van der Waals solids *Acs Nano* **8** 3715-23
- [78] Novoselov K, Mishchenko A, Carvalho A and Neto A C 2016 Ph m teri ls nd vn der ls heterostru tures *Science* **353** 461
- [79] Tan C, Lai Z and Zhang H 2017 Ultrathin two-dimensional multinary layered metal chalcogenide nanomaterials *Advanced Materials* **29** 1701392
- [80] Voiry D, Yang J and Chhowalla M 2016 Recent strategies for improving the catalytic activity of 2D TMD nanosheets toward the hydrogen evolution reaction *Advanced Materials* **28** 6197-206
- [81] Xue Y, Zhang Y, Liu Y, Liu H, Song J, Sophia J, Liu J, Xu Z, Xu Q, and Wang Z 2015 Scalable production of a few-layer MoS₂/WS₂ vertical heterojunction array and its application for photodetectors *Acs Nano* **10** 573-80
- [82] Qian X, Wang Y, Li W, Lu J and Li J 2015 Modelling of stacked 2D materials and devices *2D Materials* **2** 032003
- [83] Lee C-H, Lee G-H, Van Der Zande A M, Chen W, Li Y, Han M, Cui X, Arefe G, Nuckolls C and Heinz T F 2014 Atomically thin p-n junctions with van der Waals heterointerfaces *Nature nanotechnology* **9** 676

- [84] Heo H, Sung J H, Jin G, Ahn J H, Kim K, Lee M J, Cha S, Choi H and Jo M H 2015 Rotation-Misfit-Free Heteroepitaxial Stacking and Stitching Growth of Hexagonal Transition-Metal Dichalcogenide Monolayers by Nucleation Kinetics Controls *Advanced Materials* **27** 3803-10
- [85] Zhang J, Wang J, Chen P, Sun Y, Wu S, Jia Z, Lu X, Yu H, Chen W and Zhu J 2016 Observation of strong interlayer coupling in MoS₂/WS₂ heterostructures *Advanced Materials* **28** 1950-6
- [86] Haigh S, Gholinia A, Jalil R, Romani S, Britnell L, Elias D, Novoselov K, Ponomarenko L, Geim A and Gorbachev R 2012 Cross-sectional imaging of individual layers and buried interfaces of graphene-based heterostructures and superlattices *Nature materials* **11** 764
- [87] Jung Y, Shen J, Sun Y, and Cha J J 2014 Chemically synthesized heterostructures of two-dimensional molybdenum/tungsten-based dichalcogenides with vertically aligned layers *ACS nano* **8** 9550-7
- [88] Kong D, Wang H, Cha J J, Pasta M, Koski K J, Yao J and Cui Y 2013 Synthesis of MoS₂ and MoSe₂ Films with Vertically Aligned Layers *Nano Letters* **13** 1341-7
- [89] Yu Y, Hu S, Su L, Huang L, Liu Y, Jin Z, Purezky A A, Geohegan D B, Kim K W, and Zhang Y 2014 Equally efficient interlayer exciton relaxation and improved absorption in epitaxial and nonepitaxial MoS₂/WS₂ heterostructures *Nano letters* **15** 486-91
- [90] Choudhary N, Li C, Chung H-S, Moore J, Thomas J and Jung Y 2016 High-performance one-body core/shell nanowire supercapacitor enabled by conformal growth of capacitive 2D WS₂ layers *ACS nano* **10** 10726-35
- [91] Devan R S, Patil R A, Lin J H and Ma Y R 2012 One-dimensional metal-oxide nanostructures: recent developments in synthesis, characterization, and applications *Advanced Functional Materials* **22** 3326-70
- [92] Zhang Q, Xiao X, Zhao R, Lv D, Xu G, Lu Z, Sun L, Lin S, Gao X and Zhou J 2015 Two-Dimensional Layered Heterostructures Synthesized from Core–Shell Nanowires *Angewandte Chemie International Edition* **54** 8957-60

- [93] Cai Y, Chan S K, Sou I K, Chan Y F, Su D S and Wang N 2006 The Size-Dependent Growth Direction of ZnSe Nanowires *Advanced Materials* **18** 109-14
- [94] Nebol'sin V A and Shchetinin A A 2003 Role of Surface Energy in the Vapor–Liquid–Solid Growth of Silicon *Inorganic Materials* **39** 899-903
- [95] Wacaser B A, Dick K A, Johansson J, Borgström M T, Deppert K, and Samuelson L 2009 Preferential interface nucleation: an expansion of the VLS growth mechanism for nanowires *Advanced Materials* **21** 153-65
- [96] Schutte W, De Boer J and Jellinek F 1987 Crystal structures of tungsten disulfide and diselenide *Journal of Solid State Chemistry* **70** 207-9
- [97] Wakabayashi N, Smith H and Nicklow R 1975 Lattice dynamics of hexagonal Mo S₂ studied by neutron scattering *Physical Review B* **12** 659
- [98] Baskaran A and Smereka P 2012 Mechanisms of stranski-krastanov growth *Journal of Applied Physics* **111** 044321
- [99] Cho S-Y, Kim S J, Lee Y, Kim J-S, Jung W-B, Yoo H-W, Kim J, and Jung H-T 2015 Highly enhanced gas adsorption properties in vertically aligned MoS₂ layers *ACS nano* **9** 9314-21
- [100] Fei L, Lei S, Zhang W-B, Lu W, Lin Z, Lam C H, Chai Y and Wang Y 2016 Direct TEM observations of growth mechanisms of two-dimensional MoS₂ flakes *Nature communications* **7** 12206
- [101] Castellanos-Gomez A, Buscema M, Molenaar R, Singh V, Janssen L, Van Der Zant H S and Steele G A 2014 Deterministic transfer of two-dimensional materials by all-dry viscoelastic stamping *2D Materials* **1** 011002
- [102] Furchi M M, Pospischil A, Libisch F, Burgdörfer J and Mueller T 2014 Photovoltaic effect in an electrically tunable van der Waals heterojunction *Nano letters* **14** 4785-91

- [103] Chiu M-H, Zhang C, Shiu H-W, Chuu C-P, Chen C-H, Chang C-Y S, Chen C-H, Chou M-Y, Shih C-K and Li L-J 2015 Determination of band alignment in the single-layer MoS₂/WSe₂ heterojunction *Nature communications* **6** 7666
- [104] Hong X, Kim J, Shi S-F, Zhang Y, Jin C, Sun Y, Tongay S, Wu J, Zhang Y, and Wang F 2014 Ultrafast charge transfer in atomically thin MoS₂/WS₂ heterostructures *Nature nanotechnology* **9** 682
- [105] Tongay S, Fan W, Kang J, Park J, Koldemir U, Suh J, Narang D S, Liu K, Ji J, and Li J 2014 Tuning interlayer coupling in large-area heterostructures with CVD-grown MoS₂ and WS₂ monolayers *Nano letters* **14** 3185-90
- [106] Ceballos F, Bellus M Z, Chiu H-Y and Zhao H 2014 Ultrafast charge separation and indirect exciton formation in a MoS₂–MoSe₂ van der Waals heterostructure *ACS nano* **8** 12717-24
- [107] Rivera P, Schaibley J R, Jones A M, Ross J S, Wu S, Aivazian G, Klement P, Seyler K, Clark G and Ghimire N J 2015 Observation of long-lived interlayer excitons in monolayer MoSe₂–WSe₂ heterostructures *Nature communications* **6** 6242
- [108] Nourbakhsh A, Zubair A, Dresselhaus M S and Palacios T s 2016 Transport properties of a MoS₂/WSe₂ heterojunction transistor and its potential for application *Nano letters* **16** 1359-66
- [109] Gong Y, Lei S, Ye G, Li B, He Y, Keyshar K, Zhang X, Wang Q, Lou J and Liu Z 2015 Two-step growth of two-dimensional WSe₂/MoSe₂ heterostructures *Nano letters* **15** 6135-41
- [110] Yu J H, Lee H R, Hong S S, Kong D, Lee H-W, Wang H, Xiong F, Wang S and Cui Y 2015 Vertical heterostructure of two-dimensional MoS₂ and WSe₂ with vertically aligned layers *Nano letters* **15** 1031-5
- [111] Yun S J, Chae S H, Kim H, Park J C, Park J-H, Han G H, Lee J S, Kim S M, Oh H M and Seok J 2015 Synthesis of centimeter-scale monolayer tungsten disulfide film on gold foils *ACS nano* **9** 5510-9

- [112] Lu Z, Sun L, Xu G, Zheng J, Zhang Q, Wang J and Jiao L 2016 Universal transfer and stacking of chemical vapor deposition grown two-dimensional atomic layers with water-soluble polymer mediator *ACS nano* **10** 5237-42
- [113] Li H, Wu J, Huang X, Yin Z, Liu J and Zhang H 2014 A universal, rapid method for clean transfer of nanostructures onto various substrates *ACS nano* **8** 6563-70
- [114] Phan H D, Kim Y, Lee J, Liu R, Choi Y, Cho J H, and Lee C 2017 Ultraclean and Direct Transfer of a Wafer-Scale MoS₂ Thin Film onto a Plastic Substrate *Advanced Materials* **29** 1603928
- [115] Lin Z, Zhao Y, Zhou C, Zhong R, Wang X, Tsang Y H and Chai Y 2015 Controllable Growth of Large-Size Crystalline MoS₂ and Resist-Free Transfer Assisted with a Cu Thin Film *Scientific Reports* **5** 18596
- [116] Lui C H, Malard L M, Kim S, Lantz G, Laverge F E, Saito R and Heinz T F 2012 Observation of layer-breathing mode vibrations in few-layer graphene through combination Raman scattering *Nano letters* **12** 5539-44
- [117] Zhang M, Wu J, Zhu Y, Dumcenco D O, Hong J, Mao N, Deng S, Chen Y, Yang Y and Jin C 2014 Two-dimensional molybdenum tungsten diselenide alloys: photoluminescence, Raman scattering, and electrical transport *ACS nano* **8** 7130-7
- [118] Wu C-R, Chang X-R, Chu T-W, Chen H-A, Wu C-H and Lin S-Y 2016 Establishment of 2D crystal heterostructures by sulfurization of sequential transition metal depositions: preparation, characterization, and selective growth *Nano letters* **16** 7093-7
- [119] Zhao J, Guo Y, Cai L, Li H, Wang K X, Cho I S, Lee C H, Fan S and Zheng X 2016 High-Performance Ultrathin BiVO₄ Photoanode on Textured Polydimethylsiloxane Substrates for Solar Water Splitting *ACS Energy Letters* **1** 68-75
- [120] Lee C H, Kim J-H, Zou C, Cho I S, Weisse J M, Nemeth W, Wang Q, Van Duin A C, Kim T-S and Zheng X 2013 Peel-and-stick: mechanism study for efficient fabrication of flexible/transparent thin-film electronics *Scientific reports* **3** 2917

- [121] Kennedy M, Moody N, Adams D, Clift M and Bahr D 2008 Environmental influence on interface interactions and adhesion of Au/SiO₂ *Materials Science and Engineering: A* **493** 299-304
- [122] Jeon J, Jang S K, Jeon S M, Yoo G, Jang Y H, Park J-H and Lee S 2015 Layer-controlled CVD growth of large-area two-dimensional MoS₂ films *Nanoscale* **7** 1688-95
- [123] Jariwala D, Sangwan V K, Wu C-C, Prabhumirashi P L, Geier M L, Marks T J, Lauhon L J and Hersam M C 2013 Gate-tunable carbon nanotube–MoS₂ heterojunction pn diode *Proceedings of the National Academy of Sciences* **110** 18076-80
- [124] Shekhar S, Stokes P and Khondaker S I 2011 Ultrahigh density alignment of carbon nanotube arrays by dielectrophoresis *ACS nano* **5** 1739-46
- [125] Desai S B, Madhvapathy S R, Amani M, Kiriya D, Hettick M, Tosun M, Zhou Y, Dubey M, Ager III J W and Chrzan D 2016 Gold-mediated exfoliation of ultralarge optoelectronically-perfect monolayers *Advanced Materials* **28** 4053-8
- [126] Chang J, Lin Z, Zhu H, Isikgor F H, Xu Q-H, Zhang C, Hao Y and Ouyang J 2016 Enhancing the photovoltaic performance of planar heterojunction perovskite solar cells by doping the perovskite layer with alkali metal ions *Journal of Materials Chemistry A* **4** 16546-52
- [127] Gao Y, Liu Z, Sun D-M, Huang L, Ma L-P, Yin L-C, Ma T, Zhang Z, Ma X-L and Peng L-M 2015 Large-area synthesis of high-quality and uniform monolayer WS₂ on reusable Au foils *Nature communications* **6** 8569
- [128] Grønborg S S, Ulstrup S, Bianchi M, Dendzik M, Sanders C E, Lauritsen J V, Hofmann P and Miwa J A 2015 Synthesis of epitaxial single-layer MoS₂ on Au (111) *Langmuir* **31** 9700-6
- [129] Bradley A J, M. Ugeda M, da Jornada F H, Qiu D Y, Ruan W, Zhang Y, Wickenburg S, Riss A, Lu J and Mo S-K 2015 Probing the role of interlayer coupling and coulomb interactions on electronic structure in few-layer MoSe₂ nanostructures *Nano letters* **15** 2594-9

- [130] Shi J, Ma D, Han G-F, Zhang Y, Ji Q, Gao T, Sun J, Song X, Li C, and Zhang Y 2014 Controllable growth and transfer of monolayer MoS₂ on Au foil and its potential application in hydrogen evolution reaction *ACS nano* **8** 10196-204
- [131] Kibsgaard J, Chen Z, Reinecke B N and Jaramillo T F 2012 Engineering the surface structure of MoS₂ to preferentially expose active edge sites for electrocatalysis *Nature Materials* **11** 963
- [132] Ni B and Wang X 2015 Face the edges: catalytic active sites of nanomaterials *Advanced Science* **2** 1500085
- [133] Rao C, Gopalakrishnan K and Maitra U 2015 Comparative study of potential applications of graphene, MoS₂, and other two-dimensional materials in energy devices, sensors, and related areas *ACS applied materials & interfaces* **7** 7809-32
- [134] Tan Y, Yu K, Yang T, Zhang Q, Cong W, Yin H, Zhang Z, Chen Y and Zhu Z 2014 The combinations of hollow MoS₂ micro@ nano-spheres: one-step synthesis, excellent photocatalytic and humidity sensing properties *Journal of Materials Chemistry C* **2** 5422-30
- [135] Tsai C, Chan K, Abild-Pedersen F and Nørskov J K 2014 Active edge sites in MoSe₂ and WSe₂ catalysts for the hydrogen evolution reaction: a density functional study *Physical Chemistry Chemical Physics* **16** 13156-64
- [136] Wang H, Zhang Q, Yao H, Liang Z, Lee H-W, Hsu P-C, Zheng G and Cui Y 2014 High Electrochemical Selectivity of Edge versus Terrace Sites in Two-Dimensional Layered MoS₂ Materials *Nano Letters* **14** 7138-44
- [137] Deokar G, Rajput N, Vancsó P, Ravaux F, Jouiad M, Vignaud D, Cecchet F and Colomer J-F 2017 Large area growth of vertically aligned luminescent MoS₂ nanosheets *Nanoscale* **9** 277-87
- [138] Jang S, Kim S J, Koh H J, Jang D H, Cho S Y, and Jung H T 2017 Highly periodic metal dichalcogenide nanostructures with complex shapes, high resolution, and high aspect ratios *Advanced Functional Materials* **27** 1703842

- [139] Bissett M A, Tsuji M and Ago H 2014 Strain engineering the properties of graphene and other two-dimensional crystals *Physical Chemistry Chemical Physics* **16** 11124-38
- [140] He X, Li H, Zhu Z, Dai Z, Yang Y, Yang P, Zhang Q, Li P, Schwingenschlogl U and Zhang X 2016 Strain engineering in monolayer WS₂, MoS₂, and the WS₂/MoS₂ heterostructure *Applied Physics Letters* **109** 173105
- [141] Tang D-M, Kvashnin D G, Najmaei S, Bando Y, Kimoto K, Koskinen P, Ajayan P M, Yakobson B I, Sorokin P B and Lou J 2014 Nanomechanical cleavage of molybdenum disulphide atomic layers *Nature communications* **5** 3631
- [142] Yang Y, Yang X, Tan Y and Yuan Q 2017 Recent progress in flexible and wearable bio-electronics based on nanomaterials *Nano Research* **10** 1560-83
- [143] Ma D, Shi J, Ji Q, Chen K, Yin J, Lin Y, Zhang Y, Liu M, Feng Q and Song X 2015 A universal etching-free transfer of MoS₂ films for applications in photodetectors *Nano Research* **8** 3662-72
- [144] Zhao J, Yu H, Chen W, Yang R, Zhu J, Liao M, Shi D and Zhang G 2016 Patterned Peeling 2D MoS₂ off the Substrate *ACS Applied Materials & Interfaces* **8** 16546-50
- [145] Shokhen V, Miroshnikov Y, Gershinsky G, Gotlib N, Stern C, Naveh D and Zitoun D 2017 On the impact of Vertical Alignment of MoS₂ for Efficient Lithium Storage *Scientific Reports* **7** 3280
- [146] Gurarlan A, Jiao S, Li T D, Li G, Yu Y, Gao Y, Riedo E, Xu Z, and Cao L 2016 Van der waals force isolation of monolayer MoS₂ *Advanced Materials* **28** 10055-60
- [147] Kumar P and Viswanath B 2017 Horizontally and vertically aligned growth of strained MoS₂ layers with dissimilar wetting and catalytic behaviors *CrystEngComm* **19** 5068-78
- [148] Lai S, Jeon J, Song Y-J and Lee S 2016 Water-penetration-assisted mechanical transfer of large-scale molybdenum disulfide onto arbitrary substrates *RSC Advances* **6** 57497-501

- [149] Bhimanapati G R, Hankins T, Lei Y, Vilá R A, Fuller I, Terrones M and Robinson J A 2016 Growth and Tunable Surface Wettability of Vertical MoS₂ Layers for Improved Hydrogen Evolution Reactions *ACS Applied Materials & Interfaces* **8** 22190-5
- [150] Choi J, Mun J, Wang M C, Ashraf A, Kang S-W, and Nam S 2017 Hierarchical, Dual-Scale Structures of Atomically Thin MoS₂ for Tunable Wetting *Nano Letters* **17** 1756-61
- [151] Kumar P and Viswanath B 2017 Horizontally and vertically aligned growth of strained MoS₂ layers with dissimilar wetting and catalytic behaviors *CrystEngComm* **19** 5068-78
- [152] Dong N, Li Y, Feng Y, Zhang S, Zhang X, Chang C, Fan J, Zhang L, and Wang J 2015 Optical Limiting and Theoretical Modelling of Layered Transition Metal Dichalcogenide Nanosheets *Scientific Reports* **5** 14646
- [153] Li H, Contryman A W, Qian X, Ardakani S M, Gong Y, Wang X, Weisse J M, Lee C H, Zhao J, Ajayan P M, *et al.* 2015 Optoelectronic crystal of artificial atoms in strain-textured molybdenum disulphide *Nature Communications* **6** 7381
- [154] Frisenda R, Drüppel M, Schmidt R, Michaelis de Vasconcellos S, Perez de Lara D, Bratschitsch R, Rohlfing M and Castellanos-Gomez A 2017 Biaxial strain tuning of the optical properties of single-layer transition metal dichalcogenides *npj 2D Materials and Applications* **1** 10
- [155] Yang R, Lee J, Ghosh S, Tang H, Sankaran R M, Zorman C A and Feng P X L 2017 Tuning Optical Signatures of Single- and Few-Layer MoS₂ by Blown-Bubble Bulge Straining up to Fracture *Nano Letters* **17** 4568-75
- [156] Scalise E, Houssa M, Pourtois G, Afanas'ev V and Stesmans A 2012 Strain-induced semiconductor to metal transition in the two-dimensional honeycomb structure of MoS₂ *Nano Research* **5** 43-8
- [157] Tsai M-Y, Tarasov A, Hesabi Z R, Taghinejad H, Campbell P M, Joiner C A, Adibi A and Vogel E M 2015 Flexible MoS₂ Field-Effect Transistors for Gate-Tunable Piezoresistive Strain Sensors *ACS Applied Materials & Interfaces* **7** 12850-5

- [158] Yang L, Cui X, Zhang J, Wang K, Shen M, Zeng S, Dayeh S A, Feng L and Xiang B 2014 Lattice strain effects on the optical properties of MoS₂ nanosheets *Scientific Reports* **4** 5649
- [159] Kozbial A, Gong X, Liu H and Li L 2015 Understanding the Intrinsic Water Wettability of Molybdenum Disulfide (MoS₂) *Langmuir* **31** 8429-35
- [160] Ahn C, Lee J, Kim H U, Bark H, Jeon M, Ryu G H, Lee Z, Yeom G Y, Kim K and Jung J 2015 Low-temperature synthesis of large-scale molybdenum disulfide thin films directly on a plastic substrate using plasma-enhanced chemical vapor deposition *Advanced Materials* **27** 5223-9
- [161] Zhao J, Li N, Yu H, Wei Z, Liao M, Chen P, Wang S, Shi D, Sun Q, and Zhang G 2017 Highly sensitive MoS₂ humidity sensors array for noncontact sensation *Advanced Materials* **29** 1702076
- [162] Guo S, Yang D, Zhang S, Dong Q, Li B, Tran N, Li Z, Xiong Y and Zaghoul M E 2019 Development of a Cloud-Based Epidermal MoSe₂ Device for Hazardous Gas Sensing *Advanced Functional Materials* **29** 1900138
- [163] Pham T, Li G, Bekyarova E, Itkis M E and Mulchandani A 2019 MoS₂-Based Optoelectronic Gas Sensor with Sub-parts-per-billion Limit of NO₂ Gas Detection *ACS nano* **13** 3196-205
- [164] Kumar R, Goel N and Kumar M 2017 UV-Activated MoS₂ Based Fast and Reversible NO₂ Sensor at Room Temperature *ACS Sensors* **2** 1744-52
- [165] Perkins F K, Friedman A L, Cobas E, Campbell P, Jernigan G and Jonker B T 2013 Chemical vapor sensing with monolayer MoS₂ *Nano letters* **13** 668-73
- [166] Liu X, Ma T, Pinna N, and Zhang J 2017 Two-dimensional nanostructured materials for gas sensing *Advanced Functional Materials* **27** 1702168
- [167] Guo H, Lan C, Zhou Z, Sun P, Wei D and Li C 2017 Transparent, flexible, and stretchable WS₂ based humidity sensors for electronic skin *Nanoscale* **9** 6246-53

- [168] Kang Y, Pyo S, Jo E and Kim J 2019 Light-assisted recovery of reacted MoS₂ for reversible NO₂ sensing at room temperature *Nanotechnology* **30** 355504
- [169] Kaur J, Singh M, Dell'Aversana C, Benedetti R, Giardina P, Rossi M, Valadan M, Vergara A, Cutarelli A, and Montone A M I 2018 Biological interactions of biocompatible and water-dispersed MoS₂ nanosheets with bacteria and human cells *Scientific reports* **8** 16386
- [170] Shah P, Narayanan T N, Li C-Z and Alwarappan S 2015 Probing the biocompatibility of MoS₂ nanosheets by cytotoxicity assay and electrical impedance spectroscopy *Nanotechnology* **26** 315102
- [171] Velusamy D B, Kim R H, Cha S, Huh J, Khazaeinezhad R, Kassani S H, Song G, Cho S M, Cho S H, and Hwang I 2015 Flexible transition metal dichalcogenide nanosheets for band-selective photodetection *Nature communications* **6** 8063
- [172] Donarelli M and Ottaviano L 2018 2D materials for gas sensing applications: A review on graphene oxide, MoS₂, WS₂ and phosphorene *Sensors* **18** 3638
- [173] Yoon J, Park W, Bae G Y, Kim Y, Jang H S, Hyun Y, Lim S K, Kahng Y H, Hong W K, and Lee B H 2013 Highly flexible and transparent multilayer MoS₂ transistors with graphene electrodes *Small* **9** 3295-300
- [174] Yan H, Zhong M, Lv Z and Wan P 2017 Stretchable electronic sensors of nanocomposite network films for ultrasensitive chemical vapor sensing *Small* **13** 1701697
- [175] Yang Y and Deng Z D 2019 Stretchable sensors for environmental monitoring *Applied Physics Reviews* **6** 011309
- [176] Wetchakun K, Samerjai T, Tamaekong N, Liewhiran C, Siri Wong C, Kruefu V, Wisitsoraat A, Tuantranont A and Phanichphant S 2011 Semiconducting metal oxides as sensors for environmentally hazardous gases *Sensors and Actuators B: Chemical* **160** 580-91

- [177] Zhao S, Wang G, Liao J, Lv S, Zhu Z, and Li Z 2018 Vertically aligned MoS₂/ZnO nanowires nanostructures with highly enhanced NO₂ sensing activities *Applied Surface Science* **456** 808-16
- [178] Yang Y, Fei H, Ruan G, Xiang C and Tour J M 2014 Edge-Oriented MoS₂ Nanoporous Films as Flexible Electrodes for Hydrogen Evolution Reactions and Supercapacitor Devices *Advanced materials* **26** 8163-8
- [179] Zhao Y, Song J-G, Ryu G H, Ko K Y, Woo W J, Kim Y, Kim D, Lim J H, Lee S and Lee Z 2018 Low-temperature synthesis of 2D MoS₂ on a plastic substrate for a flexible gas sensor *Nanoscale* **10** 9338-45
- [180] He Q, Zeng Z, Yin Z, Li H, Wu S, Huang X and Zhang H 2012 Fabrication of flexible MoS₂ thin-film transistor arrays for practical gas-sensing applications *Small* **8** 2994-9
- [181] Kumar R, Goel N, Agrawal A V, Raliya R, Rajamani S, Gupta G, Biswas P, Kumar M and Kumar M 2019 Boosting Sensing Performance of Vacancy-Containing Vertically Aligned MoS₂ using rGO Particles *IEEE Sensors Journal*
- [182] Hocheng H and Chen C-M 2014 Design, fabrication and failure analysis of stretchable electrical routings *Sensors* **14** 11855-77
- [183] Sim K, Li Y, Song J and Yu C 2019 Biaxially Stretchable Ultrathin Si Enabled by Serpentine Structures on Prestrained Elastomers *Advanced Materials Technologies* **4** 1800489
- [184] Matsuhisa N, Chen X, Bao Z, and Someya T 2019 Materials and structural designs of stretchable conductors *Chemical Society Reviews* **48** 2946-66
- [185] Trung T Q and Lee N-E 2017 Materials and devices for transparent stretchable electronics *Journal of Materials Chemistry C* **5** 2202-22
- [186] Kabiri Ameri S, Ho R, Jang H, Tao L, Wang Y, Wang L, Schnyer D M, Akinwande D, and Lu N 2017 Graphene electronic tattoo sensors *ACS nano* **11** 7634-41

- [187] Park M, Park Y J, Chen X, Park Y K, Kim M S and Ahn J H 2016 MoS₂-based tactile sensor for electronic skin applications *Advanced Materials* **28** 2556-62
- [188] Kim T-Y, Ha J, Cho K, Pak J, Seo J, Park J, Kim J-K, Chung S, Hong Y and Lee T 2017 Transparent Large-Area MoS₂ Phototransistors with Inkjet-Printed Components on Flexible Platforms *ACS nano* **11** 10273-80
- [189] Lee Y, Lee J, Bark H, Oh I-K, Ryu G H, Lee Z, Kim H, Cho J H, Ahn J-H and Lee C 2014 Synthesis of wafer-scale uniform molybdenum disulfide films with control over the layer number using a gas phase sulfur precursor *Nanoscale* **6** 2821-6
- [190] McDonnell S, Addou R, Buie C, Wallace R M, and Hinkle C L 2014 Defect-Dominated Doping and Contact Resistance in MoS₂ *ACS Nano* **8** 2880-8
- [191] Lee J-U, Woo S, Park J, Park H C, Son Y-W and Cheong H 2017 Strain-shear coupling in bilayer MoS₂ *Nature Communications* **8** 1370
- [192] Conley H J, Wang B, Ziegler J I, Haglund Jr R F, Pantelides S T, and Bolotin K I 2013 Bandgap engineering of strained monolayer and bilayer MoS₂ *Nano letters* **13** 3626-30
- [193] Jha R K and Guha P K 2016 Liquid exfoliated pristine WS₂ nanosheets for ultrasensitive and highly stable chemiresistive humidity sensors *Nanotechnology* **27** 475503